Università degli Studi del Piemonte Orientale

"Amedeo Avogadro"

Dipartimento di Dipartimento di Scienze e Innovazione Tecnologica

Dottorato di Ricerca in Chemistry&Biology

XXIX ciclo 2013-2016

THERMODYNAMIC, KINETIC AND NMR RELAXOMETRIC STUDIES OF Mn(II) COMPLEXES AS MRI PROBES

Attila Forgács

Supervised by Prof. Mauro Botta

PhD program coordinator: Prof. Domenico Osella

Table of Contents Page

Chapter 1

Introduction

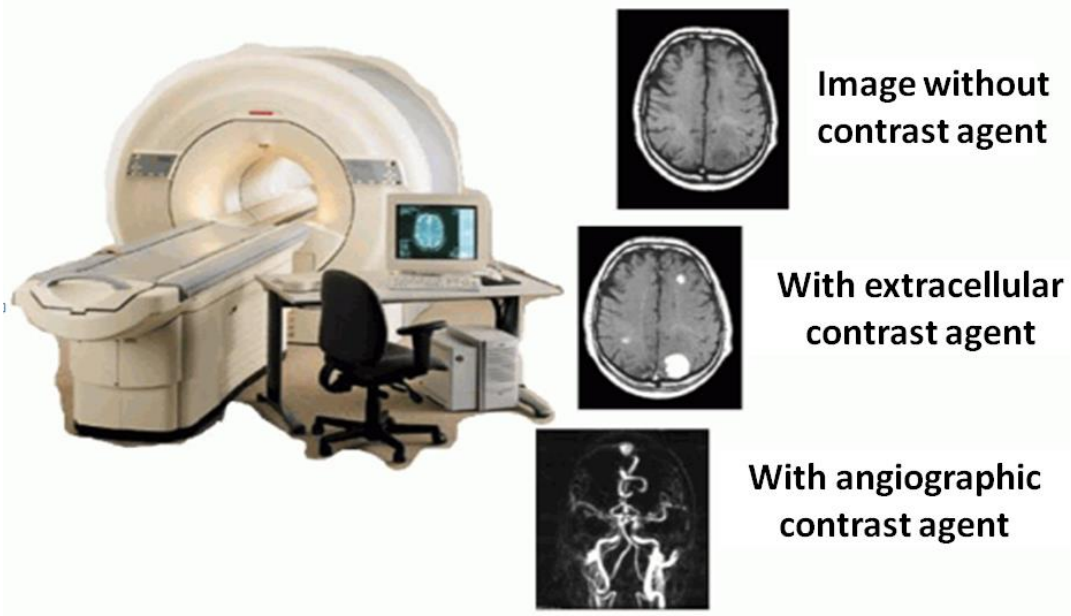

Magnetic Resonance Imaging (MRI) is one of the most successful and powerful non-invasive diagnostic methods among the several in vivo imaging techniques available in clinical diagnostic and biomedical research. MRI has severeal advantages as an imaging modality, which also explains its gain and very rapid development. These are: lack of ionizing radiation for image acquisition, noninvasiveness with a high patient acceptability, excellent delineation of anatomic systems that arises from a high level of inherent contrast, outstanding temporal and spatial resolution, ability of application to virtually every part of the body.[1] The use of contrast agents (CA) has become really important in improving the low intrinsic sensitivity of this method.[2] Traditionally, the imaging procedures have been combined with the use of dedicated contrast media, to further enhance the visualization of morphology and physiology. This combination of imaging hardware and contrast media was of high importance for the development of modern clinical radiology. MRI is no different in this respect, and the contrast media used are based largely on complexes of *f*-elements. The complexes need to be endowed with high stability to avoid the in vivo release of toxic free metal ions.

Even though inherent contrast in MRI can be manipulated to a much greater extent than in other imaging techniques, certain diagnostic questions cannot be answered easily and require the application of CAs. The contrast in an MR image is the result of a complex interplay of several factors, including instrumental parameters, proton density and the relative T_1 and T_2 relaxation times of the imaged tissues. Because it is nearly impossible to change the water content of tissues, CAs on the market or in clinical or pre-clinical trials focus upon $T_{1,2}$ changes. Generally, the purpose is to reduce T_1 in order to obtain an intense signal in short times and a better signal-to-noise ratio. These paramagnetic probes are essentially complexes of Gd (or Mn) due to the combination of high magnetic moment and favourable properties in terms of electronic relaxation. Well over 200 million patients have been dosed so far and the world market is estimated to be of the order of 1.2 billion/y. The solid-state structure, *in vitro* and *in vivo* properties of a large number of Gd^{3+}-complexes have been investigated intensively in the last 20-25 years.

Timeline of MRI imaging:

The history of MRI imaging can be dated back in the late 19th century when Nikola Tesla discovered the Rotating Magnetic Field in Budapest, Hungary (1882). This was a radical discovery in physics. In 1946, two scientists in the United States, independently of each other, described a physico-chemical phenomenon, which was based upon the magnetic properties of certain nuclei in the periodic system. This was Nuclear Magnetic Resonance, for short NMR.

The two scientists, Edward M. Purcell and Felix Bloch, were awarded the Nobel Prize in Physics in 1952.

In 1955, Erik Odeblad and Gunnar Lindström from Stockholm published their NMR studies, with relaxation time measurements of living cells and excised animal tissue.

In 1971 Raymond Damadian, a physician and experimenter working at Brooklyn's Downstate Medical Center reported that discovered that tumors and normal tissue can be distinguished *in vivo* by nuclear magnetic resonance because of the differences in the relaxation times. One of the greatest pioneers in the history of NMR is Paul Lauterbur. In March 1973, he published the first images of two tubes of water in Nature.

In 1977-78, Raymond Damadian built the first MRI scanner, assisted by his two post-doctoral students, Michael Goldsmith and Larry Minkoff, at New York's Downstate Medical Center. He recorded the first MRI scan of a healthy human body in 1977 and of a human body with cancer in 1978.

In 1987, real time MR imaging of heart becomes its development. In 1991, Filler and colleagues describe imaging of axonal transport of superparamagnetic metal oxide particles, a technique that later becomes important in imaging of neural tracts. In 1993, functional MRI of the brain is introduced. In 1994, the first intraoperative MR unit developed by GE and Harvard is installed at the Brigham and Women's Hospital in Boston. In the 1990's, in addition to research centers and large hospitals, small distant hospitals and imaging centers started to exploit MRI principally for neuroimaging and locomotor system imaging.

The use of contrast agents also started in the early 1980's. Paul C. Lauterbur described the concept of using paramagnetic metal ions to enhance the contrast (and reduce acquisition times) of structures, in 1978. After injecting a manganese salt solution as contrast agent, he imaged five dogs with myocardial infarctions and was able to highlight them.

In October 1983, Lauterbur's group published a major overview of paramagnetic contrast agents in MRI, addressing problems and questions involved in the development of CAs.

The patent application for Gd-DTPA dimeglumine was submitted in July 1981. In 1984, Dennis H. Carr and Wolfgang Schörner reported the first images in men. In 1988, Gd-DTPA (Magnevist) became commercially available, followed shortly afterwards in 1989 by the macrocyclic Gd-DOTA (Dotarem) from Guerbet (France). A number of other agents entered the marketplace during the 1990s.[3,4]

Over the last decades, more than 800 potential MR contrast agents have been described in the literature or have been patented, but only a dozen are available on the market for clinical use.

Nowadays there are more than 60 million experiments are carried out in every year, and MRI is still the most rapidly developing diagnostic method.

Classes of Contrast Agents:

MRI contrast agents can be conveniently classified into five different classes:
T_1 agents, T_2/T_2* agents, CEST agents, ^{19}F-based agents and hyperpolarized probes.

T_1 agents:

T_1 agents are mainly represented by complexes of paramagnetic metal ions [Gd(III) or Mn(II)] that enhance the MR water signal intensity. These are also called positive CAs because they provide brighter images in T_{1w} scans. The main benefits using T_1 agents arise from the high versatility of this contrast mechanism that is affected by a large number of factors related to either structural and dynamic characteristics of the agent and biological aspects like the intra-voxel distribution of the probe (e.g., intra/extra-vascular, intra/extra-cellular).[5,6,7] All Gd-based CAs have a low molecular mass of about 500 Da, are extremely hydrophilic complexes and are excreted unmetabolised in the urine. They have similar pharmacokinetic properties with similar plasma half-lives, and, due to their small size, extracellular Gd-based CAs are excreted almost exclusively by passive glomerular filtration through the kidneys with neither secretion nor reabsorption. However, protein binding GBCAs are also excreted to varying degrees by the hepatobiliary route.

T_2/T_2* agents:

T_2/T_2* agents are chemicals, mostly superparamagnetic nanoparticles made of iron oxides, capable to shorten the T_2/T_2* of water protons much more than T_1. These complexes can be identified by the following molecular formula: $Fe_2^{III}O_3M^{II}O$, where M^{II} can be: Fe^{2+}, Mn^{2+}, Ni^{2+}, Co^{2+}, Mg^{2+}. In solution, these complexes are assumed to be spherically symmetric solvated superparamagnetic iron-oxides (SPIO) nanoparticles. They can be classified into four groups based on their diameter. Oral-SPIO: 300 nm; Standard SPIO (SSPIO): 60-150 nm; Ultrasmall-SPIO (USPIO): 5 to 30 nm; and monocrystalline iron-oxide nanoparticles (MION): smaller than 10 nm. They are also referred to as negative CA because they decrease signal intensity, which results in darker images. Such nanoparticles possess a higher sensitivity than T_1 agents that justifies their widespread use in MR-molecular imaging methods, particularly for cellular imaging.[8] An obvious disadvantage is that the signal loss is

not desirable, particularly when the target site has an intrinsically low signal (e.g., lungs, hemorrhages).

CEST agents:

The family of CEST agents is constantly growing; the peculiarities of these systems could open new and interesting future perspectives for MRI agents in pharmacology research. The diamagnetic metal-free systems can eliminate the risks associated with the use of metal-based contrast agents. The acronym CEST stands for *Chemical Exchange Saturation* Transfer and identifies those chemicals that generate a MRI contrast via the transfer, transmitted by chemical exchange, of saturated (i.e., after irradiation with a frequency specified RF pulse) protons from the donor pool (CEST agent) to the acceptor pool (bulk water). The most important advantage of using CEST agents is that the rate of the contrast is only dependent on the concentration of the contrast agent and their mobile protons exchange rate. A good CEST agent should be characterized by:

- fast proton exchange in physiological pH and temperature
- high chemical shift difference ($\Delta\omega$) among the mobile protons and the water protons
- small toxicity, good solubility and small osmolality

Endogenous metabolites with exchangeable protons including many endogenous proteins with amide protons, glycosaminoglycans, glycogen, myo-inositol, glutamate, creatine and several others have been identified as potential *in vivo* endogenous CEST agents.

Paramagnetic lanthanide ions that induce large hyperfine shifted resonances in close protons are particularly useful for CEST contrast because high $\Delta\omega$ values allow access to a wider variety of faster exchanging chemical systems. Lanthanide-based agents of this type are referred to as PARACEST agents.[6]

Heteronuclear agents:

CEST agents share the frequency-encoded contrast property with those agents containing MRI detectable nuclei different from protons. Among them, two classes deserve to be mentioned here because they comprise compounds already approved for use in humans or in advanced clinical trials: ^{19}F agents and hyperpolarized probes.

^{19}F agents:

^{19}F nuclei are the most sensitive nuclear spins after protons and hence can be detected by MRI without isotopic enrichment. The detection sensitivity is similar to CEST agents (few mM).

Consequently, ^{19}F agents are almost solely represented by nanosystems, where perfluorocarbon nanoparticles (PFCs) are by far the most commonly used.[9] The important advantage of fluorinated agents over the other types of contrast media systems from the possibility to correlate straightly the MR signal to the agent concentration, thus enabling the quantification of selected biomarkers and/or drugs transported at the site of interest.[10]

Hyperpolarized probes:

This class of MRI agents is by far the most sensitive one. These agents have some similarity with PET tracer, not only for the distinguished sensitivity, but also for the setback of the signal they generate (caused by the return back to the thermal polarization) that occurs on the timescale of the T_1 of the polarized spin. Hence, one restriction in the use of hyperpolarized probes is the loss of the signal over time that requires fast injection and rapid accumulation at the target site.[11]

Design of new contrast agents:

A contrast agent for MR must have the ability to change efficiently the T_1 and/or T_2 in tissues at low (μM to mM) concentrations with acceptable tolerance. The following points summarize the most important features of paramagnetic MRI contrast agents.

High Relaxivity:

The efficiency of the contrast agents is described by the parameter relaxivity (r_{1p}), which is defined as the paramagnetic enhancement of the longitudinal relaxation rate ($1/T_1$) of the water protons in 1mM aqueous CA solution. The value of the relaxivity is the combination of the inner, -second and the outer sphere contributions. The inner sphere contribution represents the transfer of the paramagnetic relaxation effect to the bulk *via* the exchange of directly coordinated water molecule(s) to the paramagnetic ion. The second sphere contribution arises from water molecules hydrating the complex (via hydrogen-bonding interactions) with a relatively long residency time, whereas the long-range interaction involving solvent molecules diffusing next to the complex represents the outer sphere term.

Relaxivity is the most important property of contrast agents. Each agent's fundamental ability to reduce T_1 and/or T_2 is referred to as its ''relaxivity,'' r_{1p} and r_{2p}. An agent with a higher relaxivity will lower the T_1 and/or T_2 more at equivalent concentrations than an agent with a lower relaxivity. Higher relaxivities are associated with larger molecular weight ligands, and higher relaxivity means that lower dose is enough to reach good resolution.

High Stability:

Stability in this case means two different stabilities. One is thermodynamic stability and the other is kinetic inertia (commonly referred to as kinetic stability). Both of them are important to avoid toxicity problems. In general, thermodynamics describes the energy necessary to break the bonds between the metal ion and its chelating ligand and release the free metal ion (dissociation) independently from time. Kinetic stability refers to the rate at which dissociation occurs. Thermodynamic stability can be described quantitatively by the thermodynamic stability constant K_{therm} (value given on a logarithmic scale, with larger values representing exponentially tighter binding) and the conditional thermodynamic stability constant K_{cond}. K_{therm} is independent of pH, while K_{cond} is conditional, specifically reported in this context at physiologic pH. K_{cond} is therefore more useful than K_{therm} to describe thermodynamic stability also in *in vivo* or *ex vivo* conditions.[13] Kinetic stability is characterized by the dissociation rate constants of the Gd chelates, a measure of how rapidly equilibrium is reached or how fast the Gd ion is released from a Gd(III) chelate when thermodynamic conditions are such that release can occur.[14] In this case slower dissociation means higher kinetic inertness and more stable complex.

Specific Biodistribution:

Tissue specificity refers to the distribution of contrast agents to some organs or tissues with a higher concentration than to others, lowering the required contrast agent dose, and/or increasing the sensitivity of lesion detection. Currently, there are agents that use hepatobiliary, renal, or both routes of excretion.[15]

Rapid Clearance:

MRI contrast agents should clear out rapidly and completely from the body after injection and subsequent imaging. This is necessary to prevent chronic toxicity due to the slow deposit of dissociated free metal ions in specific tissues or organs.

Low Osmolality and Viscosity:

Osmolality reflects the concentration of dissolved particles in a contrast agent's formulation. Most Gadolinium Based CAs are formulated at 0.5 M because of the need for rapid administration and therefore necessarily have some hyperosmolality relative to plasma. When used at clinical, approved doses, Gadolinium based CAs have a small total body osmotic load

(0.5–2 mOsm/L compared to blood osmolality of 300 mOsm/L), i.e., much lower than that of iodinated contrast media. There are preclinical data showing the deleterious effect of high osmolality in the case of Gadolinium based CAs and cases of extravasated Gadolinium based CAs have been described.[16,17] Viscosity is a measure of the "thickness" and internal resistance to motion of a fluid. Formulations producing lower osmolality and viscosity may have improved dose tolerance and offer formulation flexibility, particularly for rapid bolus administration via a power injector.

Low Toxicity:

Contrast agents should have low acute toxicity, not producing side effects, such as allergic reactions and changes in normal serum parameters. Typically, ratios of >30 between rodent LD50 and human doses are sought. Problems in terms of chronic tolerance of agents should be nonexistent. Care regarding special patient populations such as those with renal impairment is of high importance.

Nephrogenic systemic fibrosis (NSF) is a serious late adverse reaction associated with exposure to Gadolinium based CAs in patients with renal insufficiency or on dialysis.[18,19] NSF is a rare, progressive, usually fatal disease characterized by skin thickening, painful joint contractures, and fibrosis of multiple organs including the lungs, liver, muscles, and heart. Basically all cases that has been documented have occurred in patients with chronic severe renal insufficiency who have received gadolinium contrast.[20] Therefore, researchers started to find an alternate solution for Gd. Complexes of Mn(II) can represent a possible solution.

Manganese(II) shares several advantageous properties with gadolinium(III): high spin (five unpaired electrons), fast water exchange kinetics and slow electronic relaxation. Although Gadolinium has seven unpaired electrons and a larger magnetic moment, the water exchange rates on Mn^{2+} complexes are sufficiently fast not to limit relaxivity. Another advantage is that manganese is an essential metal ion and then the organism has developed a mechanism to remove the Mn(II) from the living system; a serum concentration of 0.5–1.2 μg/L[21] is essential for normal development and body function. Despite the important biological role of Mn^{2+}, large doses of this metal ion are neurotoxic (LD50 = 0.22 mmol/kg for rat).[22,23] Humans overexposed to Mn^{2+} can suffer from neurological disorders, which results in a form of Parkinsonism termed manganism,[24] likely caused by the damage of basal ganglia.[25]

In comparison with Gd^{3+}, Mn^{2+} is less paramagnetic and has a lower charge and lower ionic radius. These differences lead to synthesize different ligands with a structure suitable for stable Mn^{2+}complexation. Depending on the denticity and rigidity of the ligand (open chain,

macrocycle, benzene ring included), Mn^{2+} has common coordination numbers of 6 or 7 in its complexes. In order to act as an efficient CA, a Mn^{2+} chelate has to allow direct coordination of water molecule(s) to the metal ion. The outer-sphere contribution to relaxivity is even lower than that for a Gd^{3+} complex with a higher spin. In fact, a problem with Mn-based contrast agents could be the lack of inner sphere water molecule, which is essential for use as MRI contrast agent. The relation between ligand geometry and coordination number is hardly predictable. Hexadentate ligands can form complexes with both coordination numbers {$[Mn(NOTA)]^-$ CN = 6, $[Mn(EDTA)(H_2O)]^-$ CN = 7} and rigid pentadentate aza-crown-ethers can form pentagonal-bipyramidal complexes with CN = 7.

The complex needs to have also high thermodynamic stability and kinetic inertness. In general, the thermodynamic stability of Mn^{2+} complexes is lower in comparison to that of Gd^{3+} analogues, because of the lower charge of the Mn^{2+} ion. Kinetic inertness is another important issue for safe *in vivo* application of CAs. In general most of the Mn(II) complexes of open-chain ligands were found to be kinetically too labile for *in vivo* use. Macrocyclic Mn(II) complexes have been reported to have reasonably high thermodynamic stability and kinetic inertness.

Paramagnetic enhanced relaxation rate:

In the presence of paramagnetic media, the theory of the solvent nuclear relaxation was developed by Solomon, Bloembergen, Morgan and others.[26-31] The paramagnetic complexes are able to reduce both the T_1 and T_2 relaxation times of solvent nuclei in the region where they are present. The observed relaxation rate ($1/T_{i,obs}$) is the sum of the diamagnetic ($1/T_{i,d}$) and the paramagnetic relaxation rates ($1/T_{i,p}$):

$$\frac{1}{T_{i,obs}} = \frac{1}{T_{i,d}} + \frac{1}{T_{i,p}} \qquad i=1, 2 \qquad (1)$$

The diamagnetic term ($1/T_{i,d}$) respects to the contribution of the diamagnetic environment (generally the water) to the observed relaxation rate in the absence of paramagnetic solute. The paramagnetic term ($1/T_{i,p}$) represents the "catalytic" effect of the paramagnetic substances on the relaxation rate of solvent nuclei. The $1/T_{i,p}$ values are directly proportional to the concentration of the paramagnetic complexes ([M]):

$$\frac{1}{T_{i,obs}} = \frac{1}{T_{i,d}} + r_{i,p}[M] \qquad i=1, 2 \qquad (2)$$

The relaxivity is usually given in terms of the increase in the longitudinal relaxation rates of water protons. The specific chemical interactions are generally realized by the coordination of the water molecule(s) in the empty coordination site(s) of the metal ion ($r_{i,p}^{is}$ inner-sphere) and by the translation diffusion of the water molecules in the surrounding of the paramagnetic complexes ($r_{i,p}^{os}$ outer-sphere). The third type of interaction is linked to the approximately long residence time of the water molecules in the proximity of the paramagnetic centers due to the hydrogen bond formation with the strongly polarized functional groups (e.g. carboxylate or phosphonate) of ligands used for the complexation of metal ions. The contribution of these processes to the overall relaxation enhancement is called second-sphere relaxivity ($r_{i,p}^{ss}$). The observed paramagnetic relaxation rate ($r_{i,p}$) of water protons may be considered as the sum of the inner- ($r_{i,p}^{is}$), outer- ($r_{i,p}^{os}$) and second-sphere ($r_{i,p}^{ss}$) contribution of the paramagnetic complexes:

$$r_{i,p} = r_{i,p}^{is} + r_{i,p}^{os} + r_{i,p}^{ss} \qquad i=1,2 \qquad (3)$$

The inner-sphere relaxation mechanism is governed by the chemical exchange between the coordinated water protons and the bulk water. The longitudinal and transversal inner-sphere relaxation time of water protons are given by:

$$\frac{1}{T_{1p}} = \frac{q[M]}{55.5(T_{1M} + \tau_M)} \qquad (4)$$

$$\frac{1}{T_{2p}} = \frac{q[M]}{55.5\tau_M}\left[\frac{T_{2M}^{-2} + \tau_M^{-1}T_{2M}^{-1} + \Delta\omega_M^2}{(\tau_M^{-1} + T_{2M}^{-1})^2 + \Delta\omega_M^2}\right] \qquad (5)$$

where q, τ_M (corresponding to the inverse of water exchange rate $1/k_{ex}$), $1/T_{1M}$, $1/T_{2M}$ and $\Delta\omega_M$ are the number of the inner-sphere water molecules, the lifetime of the water molecules in the inner coordination sphere of the paramagnetic metal ion, the longitudinal and transversal relaxation rate of the inner sphere water protons and the chemical shift difference between the inner-sphere and bulk water, respectively. According to the Solomon-Bloembergen theory developed for the simple paramagnetic aqua ions, the relaxation rate of the inner-sphere water

protons are originated from the sum of the dipole-dipole (DD) and scalar/contact (SC) terms. The dipole-dipole interaction is affected by the modulation of the proton spin – electron vector, whereas the scalar term is only influenced by the electron spin relaxation and the water exchange. The dipole-dipole and scalar relaxation rates of the inner-sphere water protons are given by the Eqn.(6) – (11):

$$\frac{1}{T_{i,M}} = \frac{1}{T_{i,M}^{DD}} + \frac{1}{T_{i,M}^{SC}} \qquad \text{i=1,2} \tag{6}$$

$$\frac{1}{T_1^{DD}} = \frac{2}{15}\left(\frac{\gamma_I^2 g^2 \mu_B^2}{r_{MnH}^6}\right) S(S+1)\left(\frac{\mu_0}{4\pi}\right)^2 \left(7\frac{\tau_{c2}}{1+\omega_S^2\tau_{c2}^2} + 3\frac{\tau_{c1}}{1+\omega_I^2\tau_{c1}^2}\right) \tag{7}$$

$$\frac{1}{T_1^{SC}} = \frac{2S(S+1)}{3}\left(\frac{A}{\hbar}\right)^2 \left(\frac{\tau_{e2}}{1+\omega_S^2\tau_{e2}^2}\right) \tag{8}$$

$$\frac{1}{T_2^{DD}} = \frac{1}{15}\left(\frac{\gamma_I^2 g^2 \mu_B^2}{r_{MnH}^6}\right) S(S+1)\left(\frac{\mu_0}{4\pi}\right)^2 \left(13\frac{\tau_{c2}}{1+\omega_S^2\tau_{c2}^2} + 3\frac{\tau_{c1}}{1+\omega_I^2\tau_{c1}^2} + 4\tau_{c1}\right) \tag{10}$$

$$\frac{1}{T_2^{SC}} = \frac{2S(S+1)}{3}\left(\frac{A}{\hbar}\right)^2 \left(\frac{\tau_{e2}}{1+\omega_S^2\tau_{e2}^2} + \tau_{e1}\right) \tag{11}$$

where γ_I, g, μ_B, r_{MnH}, S, $A/\hbar$, ω_I and ω_S are the nuclear gyromagnetic ratio of proton, the Landé-factor for the free electron (2.0023), the Bohr magneton, the distance between the proton and the metal ion, the electron spin quantum number (5/2 for Mn^{2+}), the hyperfine/scalar coupling constant between the unpaired electrons of the paramagnetic ion and the protons of the inner-sphere water molecule, the Larmor frequencies of the proton and electron (ω_S=658.21ω_I), respectively. The correlation times (τ_{ci} and τ_{ei}) which characterize the relaxation of the inner-sphere water protons are expressed as follows:

$$\frac{1}{\tau_{ci}} = \frac{1}{\tau_R} + \frac{1}{T_{ie}} + \frac{1}{\tau_M} \qquad \text{i=1, 2} \tag{12}$$

$$\frac{1}{\tau_{ei}} = \frac{1}{T_{ie}} + \frac{1}{\tau_M} \qquad \text{i=1, 2} \qquad (13)$$

where τ_R, T_{1e} and T_{2e} are the reorientation time of the metal – proton vector (rotational correlation time), the longitudinal and transversal electronic relaxation times of the metal ion. Since the interaction between the Mn^{2+} ion and the donor atoms is predominantly ionic in nature, the scalar coupling between the protons of the inner-sphere water molecule and the electrons of the Mn^{2+} ion is very weak (to the best of our knowledge the value of the A/ħ value is unknown). On the other hand, the contribution of the $\tau_{e2}/(1+\omega_S{}^2\tau_{e2}{}^2)$ term can be neglected at higher frequencies (>10 MHz). By taking into account these considerations, the scalar contribution to the overall relaxation rate of the inner sphere water protons is very small.

According to the Bloembergen-Morgan model,[26] the magnetic field dependence of the electronic relaxation times (T_{1e} and T_{2e}) of the paramagnetic ions is interpreted by the variation of the transient zero-field splitting (ZFS_T) of the electronic spin states resulted in by the interaction of the ligand fields of the solvent molecules and the donor atoms participating in the coordination of the metal ion. The magnetic field dependence of the electronic relaxation times are given by the following equations:

$$\frac{1}{T_{1e}} = \frac{1}{25}\Delta^2\tau_v\left[4S(S+1)-3\right]\left(\frac{1}{1+\omega_S^2\tau_v^2}+\frac{4}{1+4\omega_S^2\tau_v^2}\right) \qquad (14)$$

$$\frac{1}{T_{2e}} = \frac{1}{50}\Delta^2\tau_v\left[4S(S+1)-3\right]\left(3+\frac{5}{1+\omega_S^2\tau_v^2}+\frac{2}{1+4\omega_S^2\tau_v^2}\right) \qquad (15)$$

where Δ^2 and τ_v are the mean-square ZFS_T energy and the correlation time for the modulation of the zero-field splitting interaction. The complete paramagnetic enhanced inner-sphere relaxation theory can be obtained by the combination of Eq. 4 and 5 with the Solomon-Bloembergen (Eqs. 6 – 11) and Bloembergen-Morgan (Eqs. 14 and 15) models which are referred to as the Solomon-Bloembergen-Morgan (SBM) theory. According to the SBM theory, the various determinants of the inner-sphere proton relaxivity can be taken into account separately. Eqs. 4 – 15 clearly indicate that the relaxation enhancement of the inner-sphere water protons is limited by the residence time of the inner-sphere water molecule

under the slow exchange conditions ($\tau_M >> T_{1M}$) and by the relaxation rate of water protons directly coordinated to the paramagnetic center in the fast exchange condition ($\tau_M << T_{1M}$). Moreover the relaxation time of the water protons (T_{1M}) is also influenced by the rate of the exchange between the coordinated and the bulk water molecules, the rotational correlation time (τ_R) and the electronic relaxation time of the paramagnetic center (T_{1e}, Eq. 14). The variation of the Mn – H distances (r_{MnH} in Eqs. 7 and 10) and the hydration number (q in Eq. 4 and 5) strongly affects the inner-sphere relaxivity. In order to obtain an easy overview of the effects of these parameters, the inner-sphere relaxivity have been calculated as a function of water exchange ($1/\tau_M$) and the rotational correlation rates ($1/\tau_R$) by using fixed τ_v and Δ^2 values (Fig. 1A). These model calculations were also performed by the simulation of the inner-sphere relaxivities as a function of τ_v and Δ^2 at constant $1/\tau_M$ and $1/\tau_R$ values (Fig. 1B and C). The prediction of the inner-sphere relaxivity values were made at 0.47 and 1.41 T field strength. Figure 1 clearly shows that the exchange rate of the inner-sphere water molecule, the reorientation correlation time and the electron relaxation time strongly influence the value of the inner-sphere relaxivity, which decreases with the increase of the field strength. In order to obtain the maximum relaxivity value, the reorientation correlation time must be increased ($\tau_R \geq 10^9$ s^{-1}) whereas the exchange rate of the inner sphere water molecule ($1/\tau_M$) must be within the 3 - 30×10^7 s^{-1} range. The maximum of the inner-sphere relaxivity of the low molecular mass monohydrated Mn(II)-complexes is around 3.5 $mM^{-1}s^{-1}$ at 0.47 and 1.41 T field strength (Fig. 1A). With the use of the τ_M=10 ns and τ_R=100 ps values, the maximum of the inner-sphere relaxivity (r_{1p}^{in}=3.5 $mM^{-1}s^{-1}$) can be obtained at $\Delta^2 < 1\times10^{19}$ s^{-2} mean-square ZFS_T energy value (Fig. 1B). However, the elongation of the reorientation correlation time (τ_R = 33 ns) results in the large variation of the maximum inner-sphere relaxivity as a function of τ_v and Δ^2 values at different field strength (Fig. 1C). At 0.47 T, the plateau of the relaxivity (r_{1p}^{in}=125 $mM^{-1}s^{-1}$) can be achieved at $\Delta^2 < 4\times10^{18}$ s^{-2} mean-square ZFS_T energy. However, the inner-sphere relaxation enhancement of the monohydrated Mn(II)-complex endowed with the slow reorientational correlation time (τ_R = 33 ns) shows the maximum curve as a function of τ_v and Δ^2 values at 1.41 T field strength. The maximum of the r_{1p}^{in} is about 46 $mM^{-1}s^{-1}$ which can be attained at 1.41 T in the $\Delta^2 = 2 - 8\times10^{19}$ s^{-2} and τ_v=0.4 – 20 ps parameter range (Fig 1C).

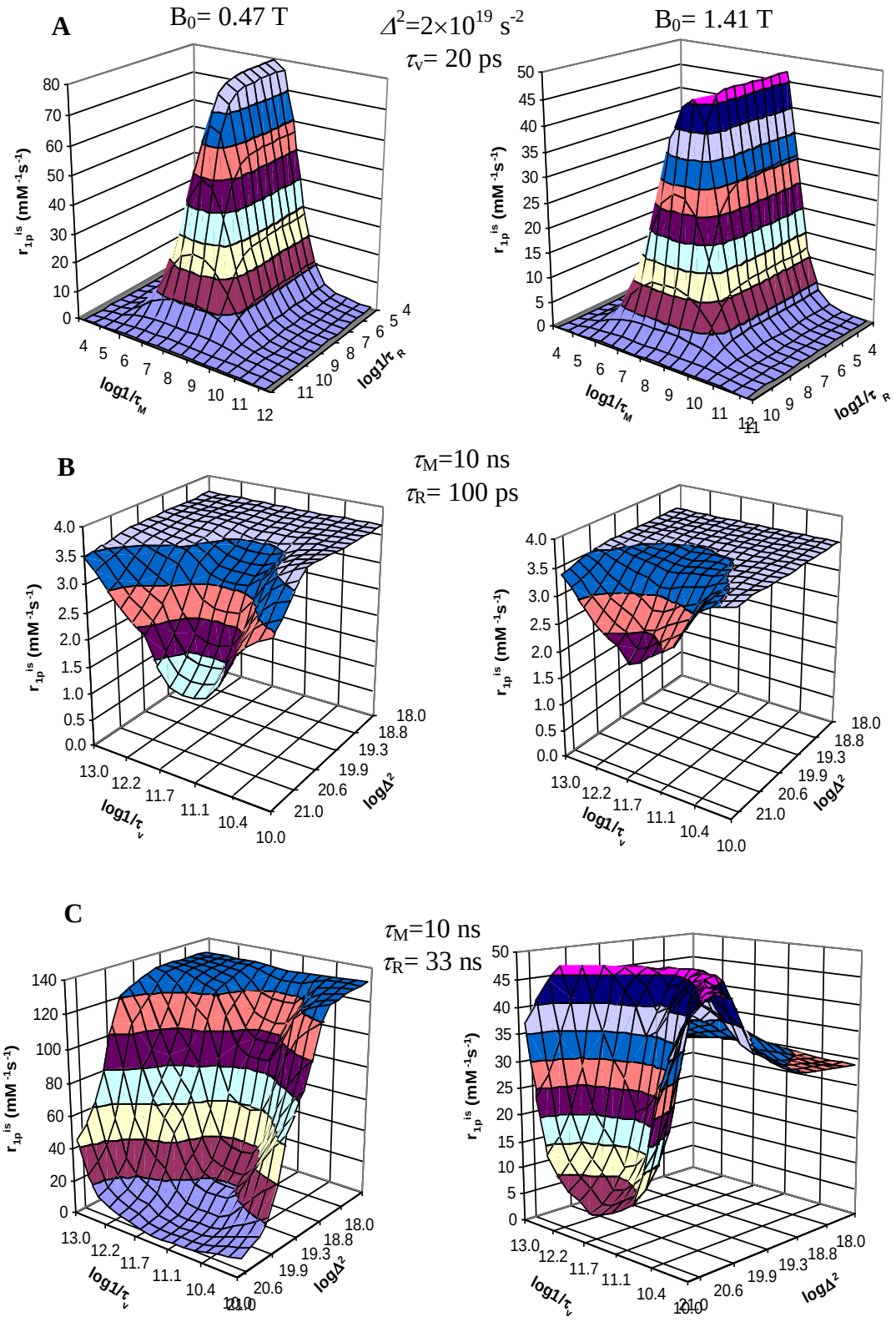

Figure 1. r_{1p}^{is} values as a function of $\log(1/\tau_M)$ and $\log(1/\tau_R)$ (**A**) and as a function of $\log(1/\tau_v)$ and $\log\Delta^2$ for τ_R=10 ps (**B**) and τ_R=33 ns (**C**) (q=1; r_{MnH}=2.75 Å)

Hydration number of Mn(II)-complexes:

The contribution of the paramagnetic metal ions to the inner-sphere relaxivity values is directly proportional to the number of the water molecules (*q*) directly coordinated to the metal ion (Eq. 4). The aqua complex of Mn^{2+} ion contains six inner-sphere water molecules, which results in a high enhancement of the relaxation rate due to the fast exchange between the inner-sphere and the bulk water molecules. By taking into account the known biochemistry[32] and chemical properties of Mn^{2+}-ion, the free Mn^{2+} can interact with enzymes[32,33] and the Ca^{2+} or Mg^{2+} binding sites of proteins[34,35] and nucleic acids[36] which limit the *in vivo* application of the Mn(II)-salts (e.g. $MnCl_2$ or $MnSO_4$) in the MRI investigations, and as we mentioned before the free Mn^{2+} ion is neurotoxic. Therefore, the highly stable and kinetically inert polyamino-polycarboxylate complexes of Mn(II), which prevent the release of Mn^{2+} ion, are proposed to use in biological systems.

Mn(II)-complexes are generally formed with the open-chain and macrocyclic polyamino-polycarboxylate ligands (Scheme 1). The coordination number, the *q* values, the relaxivity, the water exchange rate and the reorientational correlation time of the Mn(II)-complexes are presented in Table 1. The open-chain chelating agents are generally the derivatives of EDTA and DTPA ligands. The detailed ^{17}O-NMR, relaxometric and X-ray diffraction studies in solution and solid state indicate that the coordination number of the Mn^{2+}-ion is 7 with one inner-sphere water molecule in the Mn(EDTA) and in the EDTA derivative complexes.[2] However, the relaxivity of the Mn(DEBPN) complex is double of that of Mn(EDTA), which was explained by the coordination of two or three water molecules directly to the Mn^{2+}-ion.[37] The DTPA ligand is octadentate which hinders the direct coordination of the water molecule to the Mn^{2+}-ion.[38] The relaxation enhancement observed for the Mn(DTPA)-derivatives is derived from the outer- and second-sphere contributions.[38]

The coordination number of the Mn(II)-complexes formed with macrocyclic polyamino-polycarboxylate ligands is 6, 7 or 8, determined by the size of the macrocyclic ring and the nature of the donor atoms. The Mn(II)-ion is hexacoordinated with no inner-sphere water molecule in the complexes formed with the nine-membered NOTA and its derivative ligands.[39,40] The coordination number of the Mn(II)-ion is 6 in the Mn(II)-complexes of the dimeric ENOTA[41] and 9-aneN_2O-2P ligands[42] which contain one inner-sphere water molecule per Mn(II)-center. Interestingly, the relaxometric studies of the Mn(9-aneN_2O-2A) complex indicate the hydration equilibrium between the 6 and 7 coordinatated Mn(II) with one and two inner-sphere water molecules.

The 12-membered macrocyclic ligands used for the complexation of Mn^{2+}-ion are generally the DOTA and its derivative ligands furnished with the reduced number of donor atoms. The coordination number of the Mn(II)-ion is 6 with no inner-sphere water molecule in the Mn(DOTA),[38], Mn(DO3A)[43] and Mn(1,4-DO2A)[44] and Mn(1,7-DO2A) complexes (80% of Mn(1,4-DO2A) is presented in monohydrated form in solution, so CN=7).[45] The gradual replacement of the acetate pendant arms of DOTA with amide groups results in the formation of Mn(II)-complexes with seven (e.g. Mn(DO3AM), Mn(DO3AM-cyOH)) and eight coordinated (Mn(DOTAM) Mn(II)-ions with no water molecule directly coordinated to the metal center.[38] Similarly to the DOTA derivatives, the coordination number of the Mn(II)-ion is 6 in the Mn(12-pyN4A) and Mn(12pyN4P) complexes with one inner-sphere water molecule.[46]

The structure of the Mn(II)-complexes of aza- or aza-oxa crown ethers are generally pentagonal-bipyramidal (CN=7) with two inner-sphere water molecules in the axial positions.[47] However, the nature of the donor atoms, the size and rigidity of the macrocyclic ring may influence the coordination number of the Mn(II)-ion. In the Mn(II)-complexes of 15-aneN_5, 17-pydienN_5, 18-pydienN_5 and 15-pyaneN_5, the Mn(II) is six-coordinated with an inner-sphere water molecule, whereas the Mn(II)-ion is heptacoordinated with two inner-sphere water molecules in the complexes of 15-pydienN_5, 16-pydienN_5, 16-pyaneN_5 and $(NH_2Et)_2$-15-pydienN_5.[47] The Mn(II)-complexes of the 15-membered macrocyclic 15-pyN_3O_2 and 15-pyN_5 ligands are bis-hydrated with heptacoordinated Mn(II)-ion.[48] Similar structural phenomena were identified in the Mn(II)-complexes of porphyrins.[49,50]

The heptadentate AAZTA ligand can be regarded as a combination of open-chain and macrocyclic ligands, which represent the formation of the relatively flexible coordination cage wrapping around Mn^{2+}-ion.[51] Because of the seven donor atoms, the coordination sphere of the Mn(II) is fully occupied in the Mn(AAZTA). The replacement of the acetate pendant arm with hydrogen or methyl group in the exocyclic imino-diacetate fragment of AAZTA results in the hexadentate AAZ3A, AAZ3AMA and MeAAZ3A ligands which can form Mn(II)-complexes in different hydration states. The hydration number of the Mn(AAZ3A)-derivative complexes are varied from 0.64, 0.32 and to 0.24 for the Mn(AAZ3A), Mn(MeAAZ3A) and Mn(AAZ3MA), which indicate that the coordination number of the Mn(II) are changed from mainly 7 to mainly 6 due to the different structural rigidity of the Mn(II)-complexes.[51]

Table 1. The relaxivity (r_{1p}, 20 MHz), the coordination number (CN), the number of the inner-sphere water molecules (q), the water exchange rate (k_{ex}^{298}) and the reorientational correlation time (τ_R^{298}) for the Mn(II)-complexes.

	r_{1p} (25/37°C; $mM^{-1}s^{-1}$)	CN	q	k_{ex}^{298} (10^7 s^{-1})	τ_R^{298} (ps)
$[Mn(H_2O)_6]^{2+}$[44]	7.4/6.76	6	6	2.1	30 (308 K)
$Mn(NTA)^{-}$[45]	–	6	2	150	–
$Mn(EDTA)^{2-}$[45]	3.08	7	1	47.1	57
$Mn(CyDTA)^{2-}$[47]	3.47	7	1	14	–
$Mn(PhDTA)^{2-}$[46]	–	7	1	35	–
$Mn(TMDTA)^{2-}$[48]	2.2	7	1	13	–
$Mn(EDTA\text{-}BOM)^{2-}$[49]	3.6	7	1	9.3	83.7
$Mn(EDTA\text{-}(BOM)_2)^{2-}$[49]	4.3	7	1	13	110.8
$Mn(diPHEDTA)^{2-}$[50]	5.8	7	1	23	–
$Mn_2(ENOTA)$[51]	3.39/2.71	6	$1/Mn^{2+}$	5.5	85
Mn(1,4-DO2A)[45]	2.1	7/6	0.87	113.4	46
Mn(DO1A)[45]	2.4	6	1	595.7	22
$Mn(9\text{-}aneN_2O\text{-}2A)$[35]	2.83/2.30	6/7	1/2	119	22
$Mn(9\text{-}aneN_2O\text{-}2P)$[52]	5.08/4.29	6	1	1.20	103
$Mn(12\text{-}pyN_4A)$[53]	2.39/1.94	6	1	303	23
$Mn(12\text{-}pyN_4P)$[53]	2.84/2.32	6	1	177	39
$Mn(15\text{-}pyN_3O_2)^{2+}$[54]	4.48/3.61	7	2	0.38	40.3
$Mn(15\text{-}pyN_5)^{2+}$[54]	3.56/3.13	7	2	6.9	28.3
$Mn(AAZ3A)^{-}$[55]	2.49	6/7	0.64	4.7	50
$Mn(MeAAZ3A)^{-}$[55]	2.01	6/7	0.32	12.6	50
$Mn(AAZ3MA)^{-}$[55]	1.90	6/7	0.24	13.3	51

***Mn^{2+} - H distance*:**

The effect of the Mn^{2+} - H distance (r_{MnH}) on the relaxation rate of inner-sphere water protons governed by dipole-dipole interaction between the electron and nuclear spins are clearly indicated in Eqs. 7 and 10. In order to visualize the effects of the Mn^{2+} - H distance, the inner-sphere relaxivity have been calculated as a function of r_{Mn-H} by using the fixed values of Δ^2, τ_M, τ_R and τ_v (Figure 2).

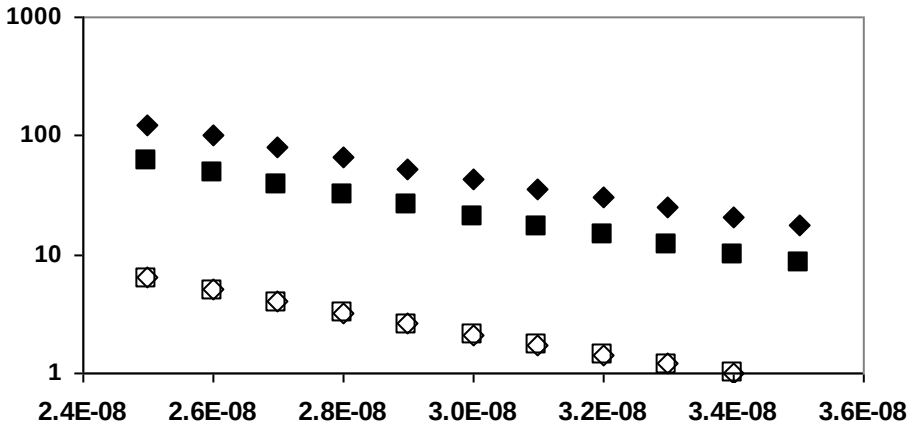

Figure 2. The logarithmic inner-sphere relaxivity values (log r_{1p}^{is}) as a function of r_{Mn-H} at 20 MHz (♦, ◊) and 60 MHz (■, □). ($\Delta^2=1\times10^{19}$ s^2; τ_M=10 ns, τ_R=100 ps (open symbols), τ_R=33 ns (filled symbols) and τ_v=20 ps)

As shown in Figure 2, the inner-sphere relaxivity increases by about 50% with the 0.2 Å decrease of the r_{Mn-H} distance due to the dependence of the $1/T_i^{DD}$ on the sixth power of the r_{Mn-H}. The reduction of the r_{Mn-H} distance can be promoted by two ways: i) the increase of the tilt angle of the Mn^{2+} – O-H bond; ii) the increase of the electron delocalisation towards of the ligand or the residual charge of the Mn(II)-ion. The first possibility could be achieved by the H-bond formation between the coordinated water molecule and the strongly polarised donor groups attached to the appropriate side of the ligand, which distorts the angle of Mn^{2+} – O-H bond. The second variation might be controlled by the engage of the unsaturated C – C into the ligand backbone or the substitution of the charged donor groups with neutral donor atoms. In this order, there is an intense scrutiny to optimize the structural feature of the polyamino-polycarboxylate ligands for the complexation of Mn^{2+}.

In spite of the important role of the Mn^{2+} - H distance, it is difficult to obtain the r_{Mn-H} values experimentally because the tilt angle of the Mn^{2+} – O-H bond is not well defined in

solution. The r_{Mn-H} values are generally deduced from the Mn^{2+} – **O**H_2 distance that can be determined more easily. The Mn^{2+} – **O**H_2 distances obtained from the solid-state X-ray structure are used to estimate the r_{Mn-H} value in solution. The average Mn^{2+} – **O**H_2 and Mn^{2+} – O**H**$_2$ distances of the $[Mn(H_2O)_6]^{2+}$ and Mn(II)-complexes determined by X-ray diffraction studies in solid-state are presented in Table 2.

Table 2. The r_{Mn-O} and r_{Mn-H} distances of the Mn(II)-complexes determined by X-ray diffraction studies in solid state.

	r_{Mn-O} (Å)	r_{Mn-H} (Å)	Ref.
$[Mn(H_2O)_6]^{2+}$	2.17	2.68	53
Mn(EDTA)	2.24	2.84	56
Mn(CyDTA)	2.27	2.79	56
Mn(PhDTA)	2.24	2.80	57
Mn(DEBPN)	2.16	2.76	37
Mn_2(ENOTA)	2.14	2.75	41
Mn(15-pyN_3O_2)	2.23; 2.29	2.76; 2.77; 2.79; 2.80	48
Mn(15-pyN_5)	2.30; 2.27	2.77; 2.86; 2.74; 2.98	
Mn(15-pydieneN_5)	2.22	2.75	58
Mn(15-pyaneN_5)	2.28; 2.24	2.78, 2.70	

The solid-state structure of the Mn(EDTA), Mn(CyDTA), Mn(PhDTA), Mn(15-pyN_3O_2), Mn(15-pyN_5), Mn(15-pydieneN_5) and Mn(15-pyaneN_5) complexes of heptacoordinated Mn(II) reveals that the r_{Mn-O} and r_{Mn-H} distances of the coordinated water molecules are 2.23 - 2.30 and 2.74 – 2.98 Å, respectively (Table 2). The X-ray analysis of the hexacoordinated Mn(II)-complexes ($[Mn(H_2O)_6]^{2+}$ and Mn_2(ENOTA)) indicate that the Mn^{2+} – **O**H_2 and Mn^{2+} – O**H**$_2$ distances are 2.14 – 2.17 and 2.68 - 2.75 Å, respectively (Table 2). The comparison of the r_{Mn-O} and r_{Mn-H} values of heptacoordinated Mn(DEBPN) and Mn(EDTA) complexes (Mn(EDTA): r_{Mn-O}=2.24 Å, r_{Mn-H}=2.84 Å; Mn(DEBPN): r_{Mn-O}=2.16 Å, r_{Mn-H}=2.76 Å) shows that the replacement of the charged carboxylates with non-charged ester and pyridine groups results in the decrease of the Mn^{2+} – **O**H_2 and Mn^{2+} – O**H**$_2$ distances due to the higher residual charge on the Mn(II)-ion.

References:

1. P. Caravan *Chem. Soc. Rev*., **2006**, 35, 512.
2. B. Drahoš, I. Lukeš, É. Tóth, *Eur. J. Inorg. Chem.,* **2012**, 1975.
3. E. R. Andrew, *Brit Med Bull.,* **1984**, 40, 115.
4. D. M. Grant, R. K. Harris, *Encyclopedia of Nuclear Magnetic Resonance*, **1996**. 3456.
5. P. Caravan, C. T. Farrar, L. Frullano, R. Uppal, *Contrast Media Mol Imaging*, **2009**, 4: 89.
6. C. F. G. C Geraldes, S. Laurent, *Contrast Media Mol Imaging*, **2009**, 4: 1.
7. S. Aime, D. Delli Castelli, S. Geninatti Crich, E. Gianolio, E. Terreno, *Acc. Chem. Res.*, **2009**, 42 (7) 822.
8. A. K. Srivastava, D. K. Kadayakkara, A. Bar-Shir, A. A. Gilad, M. T. McMahon, J. W. Bulte, *Dis. Model Mech.,* **2015**, 8, 323.
9. C. Jacoby, S. Temme, F. Mayenfels, N. Benoit, M. P. Krafft, R. Schubert, et al. *NMR Biomed*., **2013**, 27, 261.
10. G. M. Lanza, X. Yu, P. M. Winter, D. R. Abendschein, K. K. Karukstis, M. J. Scott, L. K. Chinen, et al. *Circulation*, **2002** 106, 2842.
11. E. Terreno, S. Aime *Front. Pharmacol*., **2015,** 6, 290.
12. W. A. Gibby, K. A. Gibby, *Invest Radiol.,* **2004,** 39, 138.
13. W. P. Cacheris, S. C. Quay, S. M. Rocklage, *Magn. Reson. Imaging,* **1990,** 8, 467.
14. T. Frenzel, P. Lengsfeld, H. Schirmer, J. Hutter, H. J. Weinmann, *Invest Radiol.,* **2008**, 43, 817.
15. J. L. Major, T. J. Meade, *Acc. Chem. Res.,* **2009**, 42, 893.
16. D. A. Carrier, J. J. Ford, L. A. Hayman, *Am J Neuroradiol.,* **1993**, 14, 363.
17. V. M. Runge, K. M. Dickey, N. M. Williams, X. Peng, *Invest Radiol*., **2002**, 37, 393.
18. H. S. Thomsen, *Eur Radiol*., **2006**, 16, 2619.
19. T. R. Elmholdt, M. Pedersen, B. Jorgensen, et al. *Br J Dermatol.,* **2011**, 165, 828.
20. S. P. Lin, J. J. Brown, *J Magn Reson Imaging*, **2007**, 25, 884.
21. J. Crossgrove, W. Zheng, *NMR Biomed.*, **2004**, 17, 544.
22. M. Aschner, K. M. Erikson, D. C. Dorman, *Crit. Rev. Toxicol.*, **2005**, 35, 1.
23. A. C. Silva, J. H. Lee, I. Aoki, A. P. Koretsky, *NMR Biomed.,* **2004**, 17, 532.
24. M. G. Cersosimo, W. C. Koller, *NeuroToxicology,* **2006**, 27, 340.
25. N. A. Bock, A. C. Silva, *Future Neurol.*, **2007**, 2, 297.
26. N. Bloembergen, E. M. Purcell, R. V. Pound, *Phys. Rev.,* **1948** 73, 679.
27. I. Solomon, *Phys. Rev.,* **1955**, 99, 559.
28. I. Solomon, N. Bloembergen, *J. Chem. Phys.,* **1956**, 25, 261.
29. N. Bloembergen, *J. Chem. Phys.,* **1957**, 27, 572.
30. N. Bloembergen, L. O. Morgan, *J. Chem. Phys.,* **1961**, 34, 842.
31. R. E. Connick, D. Fiat, *J. Chem. Phys.,* **1966**, 44, 4103.
32. D. W. Christianson, *Prog. Biophys. Mol. Biol.*, **1997**, 67, 217.
33. F. C. Wedler, R. B. Denman, *Curr. Top. Cell Regul.,* **1984**, 24, 153.
34. A. S. Mildvan, M. Cohn, *Biochemistry*, **1963**, 2, 910.
35. S. Aime, S. Canton, S. G. Crich, E. Terreno, *Magn. Reson. Chem.*, **2002**, 40, 41.
36. J. Eisinger, F. Fawaz-Estrup, R. G. Shulman, *J. Chem. Phys*., **1965**, 42, 43.
37. Q. Zhang, J. D. Gorden, R. J. Beyers, C. R. Goldsmith, *Inorg. Chem.,* **2011**, 50, 9365.

38. J. S. Troughton, M. T. Greenfield, J. M. Greenwood, S. Dumas, A. J. Wiethoff, J. Wang, M. Spiller, T. J. McMurry, P. Caravan, *Inorg. Chem.*, **2004**, 43, 6313.
39. C. F. G. C. Geraldes, A. D. Sherry, R. D. Brown III, S. H. Koenig, *Magn. Reson. Med.,* **1986**, 3, 242.
40. M. Tan, Z. Ye, E.-K. Jeong, X. Wu, D. L. Parker, D.-R. Lu, *Bioconjugate Chem.*, **2011**, 22, 931.
41. E. Balogh, Z. He, W. Hsieh, S. Liu, É. Tóth, *Inorg. Chem*., **2007**, 46, 238.
42. B. Drahos, M. Pniok, J. Havlícková, J. Kotek, I. Císarová, P. Hermann, I. Lukes, É. Tóth, *Dalton Trans.*, **2011**, 40, 10131.
43. S. Aime, P. L. Anelli, M. Botta, M. Brocchetta, S. Canton, F. Fedeli, E. Gianolio, E. Terreno, *J. Biol. Inorg. Chem.*, **2002**, 7, 58.
44. A. Bianchi, L. Calabi, C. Giorgi, P. Losi, P. Mariani, D. Palano, P. Paoli, P. Rossi, B. Valtancoli, *J. Chem. Soc., Dalton Trans.,* **2001**, 917.
45. G. A. Rolla, C. Platas-Iglesias, M. Botta, L. Tei, L. Helm, *Inorg. Chem*., **2013**, 52, 3268.
46. B. Drahos, J. Kotek, I. Císarová, P. Hermann, L. Helm, I. Lukes, É. Tóth, *Inorg. Chem.*, **2011**, 50, 12785.
47. S. C. Jackels, M. M. Durham, J. E. Newton, T. C. Henninger, *Inorg. Chem.*, **1992**, 31, 234.
48. B. Drahos, J. Kotek, P. Hermann, I. Lukes, É. Tóth, *Inorg. Chem.,* **2010**, 49, 3224.
49. D. Lieb, A. Zahl, T. E. Shubina, I. Ivanovic-Burmazovic, *J. Am. Chem. Soc.*, **2010**, 132, 7282.
50. A. Budimir, J. Kalmár, I. Fábián, G. Lente, I. Bányai, I. Batinic- Haberle, M. Birus, *Dalton Trans.*, **2010**, 39, 4405.
51. L. Tei, G. Gugliotta, M. Fekete, F. K. Kálmán, M. Botta, *Dalton Trans*., **2011**, 40, 2025.
52. P. M. T. Piggot, L. A. Hall, A. J. P. White, D. J. Williams, L. K. Thompson, *Inorg. Chem.*, **2004**, 43, 1167.
53. G. E. Kostakis, K. C. Mondal, C. E. Anson, A. K. Powell, *Polyhedron*, **2010**, 29, 24.
54. P. Wang, J. P. Ma, Y. B. Dong, R. Q. Huang, *J. Am. Chem. Soc.,* **2007**, 129, 10620.
55. B. Wu, J. Liang, J. Yang, C. Jia, X. J. Yang, H. Zhang, N. Tang, C. Janiak, *Chem. Commun*., **2008**, 1762.
56. X. F. Wang, J. Gao, J. Wang, Zh. H. Zhang, Y. F. Wang, L. J. Chen, W. Sun, X. D. Zhang *Zh. Strukt. Khim. (Russ.) (J. Struct. Chem.)* **2008**, 49, 753.
57. N. Nakasuka, S. Azuma, C. Katayama, M. Honda, J. Tanaka, M. Tanaka, *Acta Crystallogr. Sect. C: Cryst. Struct. Commun*., **1985**, 41, 1176.
58. O. Jiménez-Sandoval, D. Ramírez-Rosales, M. del Jesús Rosales-Hoz, M. E. Sosa-Torres, R. Zamorano-Ulloa, *J. Chem. Soc., Dalton Trans.*, **1998**, 1551.

Chapter 2

Outline of the thesis

The main goal of this thesis is the characterization in aqueous solutions of new Mn(II) complexes as MRI probes. Our investigation included thermodynamic, kinetic and detailed ^{1}H and ^{17}O NMR relaxometric measurements. We have taken into account Mn-complexes belonging to two different main types of structural units.

One encompasses the Mn(II) complexes containing the pentadentate coordinating units 6,6-((methylazanediyl)bis(methylene))dipicolinic acid. We considered several derivatives of the monomeric DPAMA ligand, including mono-, bi- and trinuclear bis-hydrated complexes (Chapter 4). In addition, we investigated a number of derivatives featuring different side arms and a couple of lipophilic derivatives (Chapter 5). All these complexes represent a fairly homogeneous series that has allowed us to obtain useful information on the relationship between the molecular structure, the thermodynamic stability and the relaxation parameters.

The other class of complexes are those containing the macrocyclic unit cyclen and two coordinating pendant arms. These macrocyclic derivatives have been studied in detail, considering the chemical nature of the pendant arms, their relative position (*cis*/*trans*), the possible presence of isomers with different states of hydration, the kinetic and thermodynamic stability of the complexes and their relaxometric properties (Chapter 6). The synthesis of two novel derivatives bearing hydrophobic pendant groups enabled the investigation of the binding association with human serum albumin (Chapter 7).

The global set of experimental results has allowed us to deepen our understanding of the chemistry of Mn(II) complexes as potential MRI probes. We are confident that the new information gained will help in the future design and development of more effective and safer MRI contrast enhancing agents.

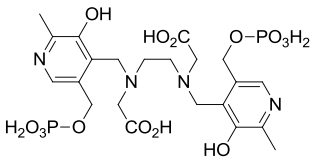

H_8DPDP *(Chapter 4)*

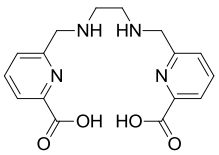

H_2BCPE *(Chapter 4)*

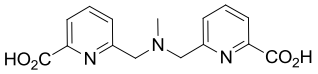

H_2DPAMA *(Chapter 4)*

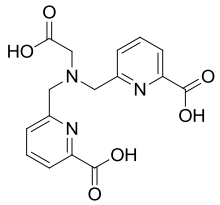

H_3DPAA *(Chapter 5)*

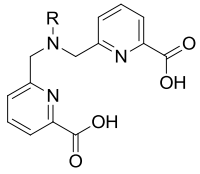

H_2DPADA: R = $C_{12}H_{25}$
(Chapter 5)

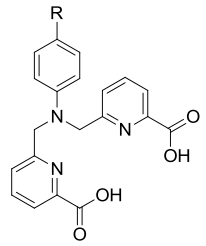

H_2DPAPhA: R = H*(Chapter 5)*
H_2DPAHPhA: R = C_6H_{13}*(Chapter 5)*

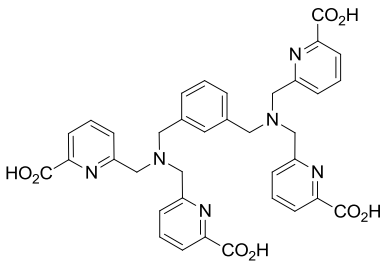

m*X(H_2DPAMA)$_2$(Chapter 4)*

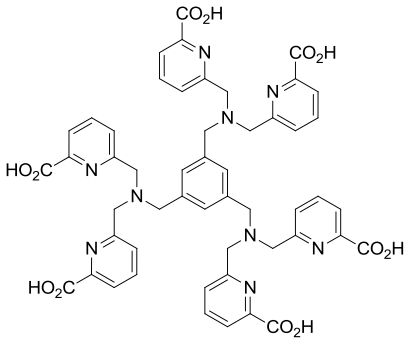

m*X(H_2DPAMA)$_3$(Chapter 4)*

Scheme 1. Ligands investigated in Chapters 4 and 5.

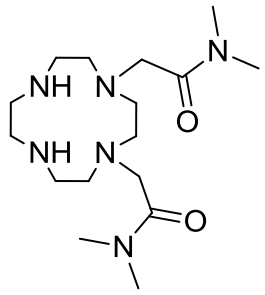

1,4-DO2AM (*Chapter 6)*

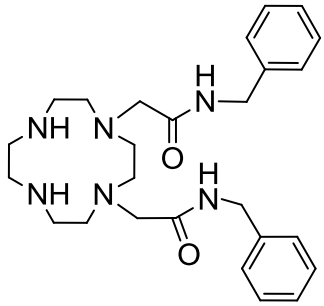

1,4-DO2AMBz
(Chapter 7)

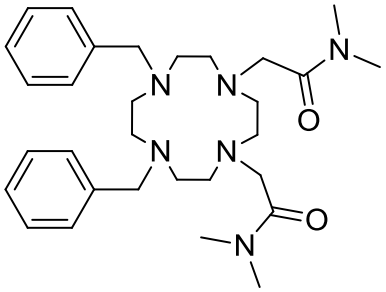

1,4-BzDO2AM
(Chapter 7)

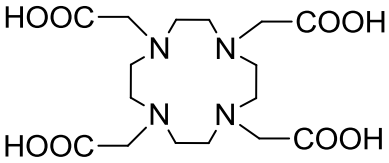

DOTA *(Chapters 6,7)*

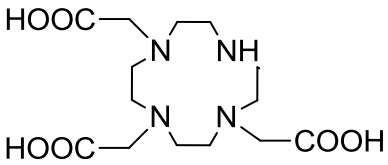

DO3A *(Chapters 6,7)*

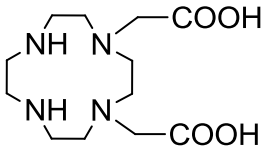

1,4-DO2A *(Chapters 6,7)*

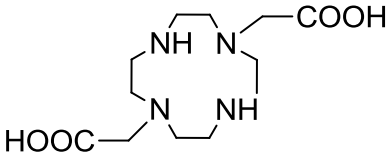

1,7-DO2A *(Chapters 6,7)*

Scheme 1. Ligands investigated in Chapters 6 and 7.

Chapter 3

Experimental techniques

Fast Field Cycling (FFC) NMR Relaxometry:

Field-cycling NMR relaxometry is the preferred technique for obtaining the frequency (or magnetic field) dependence of relaxation times (or equivalently of relaxation rates). For this reason it is also known as nuclear magnetic relaxation dispersion (NMRD).The relaxation of a nuclear magnetic spin in general is a function of experimental parameters such as temperature, pressure, sample composition and magnetic field, B_0. Changing thermodynamic parameters, like the temperature, influences the physical or chemical state of the sample under investigation. Change of the magnetic field, however, has typically no influence on the chemistry of the sample. It is therefore a useful tool for separation of different interaction mechanisms and dynamic processes influencing the relaxation behavior. Fast Field Cycling (FFC) NMR relaxometry is an important analytical tool for NMR research and material characterization in both industrial and academic environments and has been successfully used in a wide range of fields. For example in: pharmaceutical, food, oil, gas and petroleum industry. FFC NMR relaxometry is a non-destructive low-field magnetic resonance method, which is performed in the range of a few kHz up to around 100 MHz, depending on the instrument. The information obtained is connected to the molecular dynamics of a material or complex substance through the characterization of the nuclear spin-lattice constant $1/T_1$ over a large range of magnetic field strengths, which is carried out on the same instrument (relaxometer). The technique is excellent in revealing information on slow molecular dynamics, which can only be done at very low magnetic field strengths. Examples of important molecular dynamics information that can be obtained through FFC NMR relaxometry:

- Characterization of rotational dynamics
- Identification of the presence of paramagnetic substances
- Evaluation of MRI CAs (coordination number, kinetics of exchange, electronic relaxation, correlation times in the spectrum of re-orientation and diffusional dynamics of molecules)
- Determination of aggregation states of complex biomolecules such as proteins

The magnetic field dependence of $1/T_1$ of a substance or material is shown in the graphical form as a Nuclear Magnetic Resonance Dispersion (NMRD) profile (Figure 1).

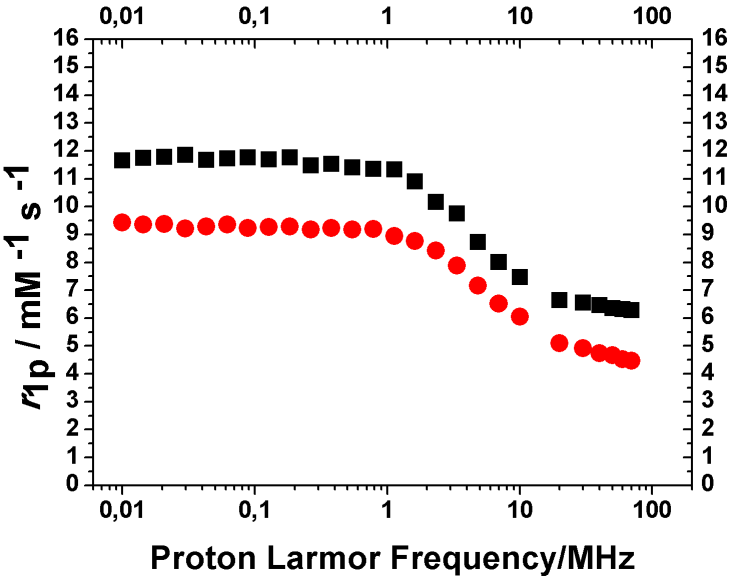

Figure 1. NMRD profile of a Mn(II) complex at 25 (black) and 37 °C (red)

The relaxation rate $1/T_1$ of a substance or material will tend to change when there is a variation in molecular dynamics, which may be caused by:

- change of state (e.g. solid to liquid; complex systems phase change, such as liquid crystals)
- concentration changes (e.g. effect on aggregation states of biomolecules)
- temperature changes
- viscosity changes
- paramagnetic impurities

FFC NMR relaxometry is a non-destructive method requiring a small amount of a solid or liquid sample (enough to fill a standard 10mm NMR tube to a volume of around $1cm^3$) with no other form of preparation required.

The basic FFC NMR experiment consists of cycling the Zeeman field, B_0, which is applied to the sample, through three different values. In the first instance, a high magnetic field, B_{pol} (polarization field), is applied to pre-polarize the sample in order to boost signal intensity. The sample is then allowed to relax in a second field, B_{relax} (relaxation field), which can be set to any desired value, including zero. Finally, the field is set to the detection field, B_{acq} (acquisition field), for signal acquisition.[1]

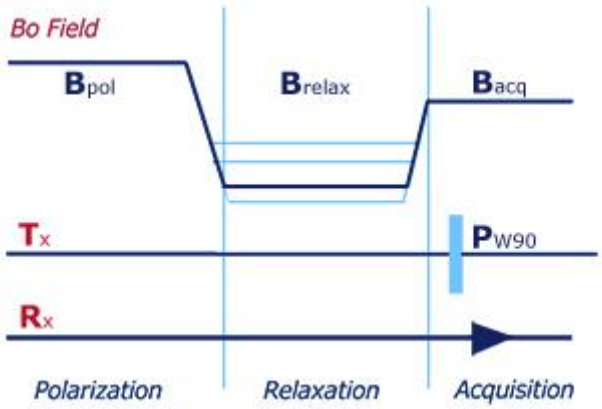

Figure 2. Working of FFC NMR[1]

Changes in the relaxation rate, $1/T_1$, of a substance or material, are sometimes not evident at single magnetic field strengths, but when studied over a wide range of magnetic field strengths, as with FFC NMR relaxometry, changes are easier to identify as they are often more visible with the NMRD profile, especially at the lower magnetic field strengths.

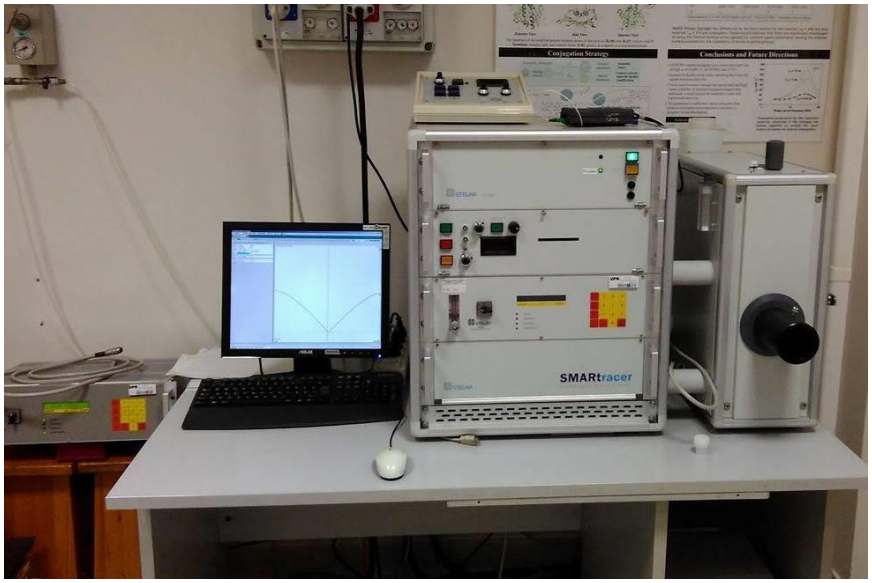

Figure 3. The SmarTracer FFC-NMR relaxometer.

^{17}O NMR measurements:

In the ^{17}O NMR measurements we measure the temperature dependence of the ^{17}O NMR longitudinal and transverse relaxation rates as well as the chemical shifts of aqueous solutions of the Mn(II) complexes. The observed acceleration of the relaxation rates and the observed shift of the resonance frequencies can be described by the formulas developed by Swift and

Connick [2] for $1/T_2$ and Δ_ω, the chemical shift difference, and by Zimmermann and Brittin[3] for $1/T_1$.

The detailed equations are in Chapter 4.

Figure 4. The superconductive magnet of the 500 MHz NMR spectrometer

pH-potentiometric titrations:

There are several ways to determine stability and protonation constants. In this work, we used direct pH-potentiometric titrations. The pH-potentiometry with a suitable ion-selective electrode can be a possibility to determine components (metal ion, ligand) equilibrium activity. A pH-potentiometric titration is one of the most common way to determine stability constants. The ligands are usually weak bases, so in the lack of metal ion the ligand is in a protonated form in a quite range pH-region. During the forming of the metal complexes a proton is removed from the coordinated group. Thanks to that with an indirect pH effect, we can use pH-potentiometry. The system is showing the difference in the pH during the measurement. In a pH-potentiometric titration, a generally used glass-electrode can be used between pH 1.7 and 11.8. The complexes stability constants can be calculated from the fit of the titration curves. For the calculation, it is necessary to know the ligand protonation

constants, and every other type of side effect that can have an influence of the complex's formation. For example, we can calculate the stability constant with a general equation (Eq 1).

$$pM + qL + rH \Leftrightarrow M_pL_qH_r; \qquad \beta_{pqr} = \frac{[M_pL_qH_r]}{[M]^p[L]^q[H]^r}$$

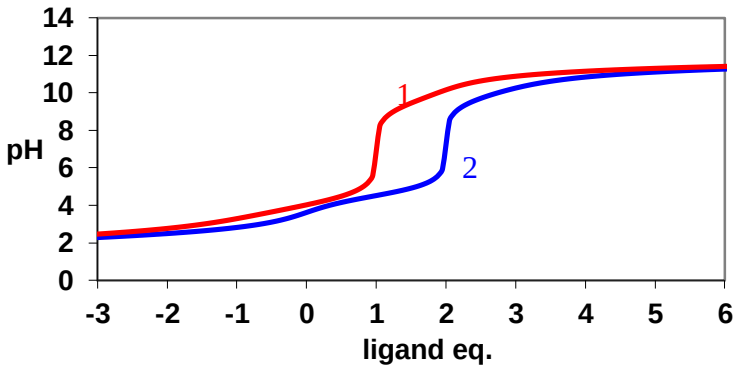

Figure 5. Titration curves of the well-known H_3DO3A (1), and H_4DOTA (2) ligands.

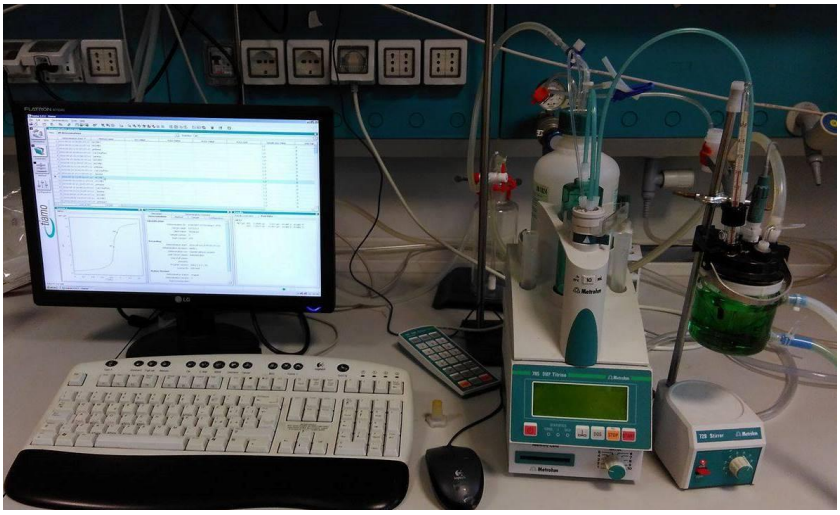

Figure 6. The automatic pH-potentiometric titrator.

References:

1. http://stelar.it/ffc_nmr.htm
2. T. J. Swift, R. Connick, *E. J. Chem. Phys.,* **1962**, 37, 307.
3. J. R. Zimmermann, W. Brittin, *E. J. Phys. Chem.*, **1957**, 61, 1328.

Chapter 4

Bis-Hydrated Mn^{2+} Complexes with the picolinate binding unit

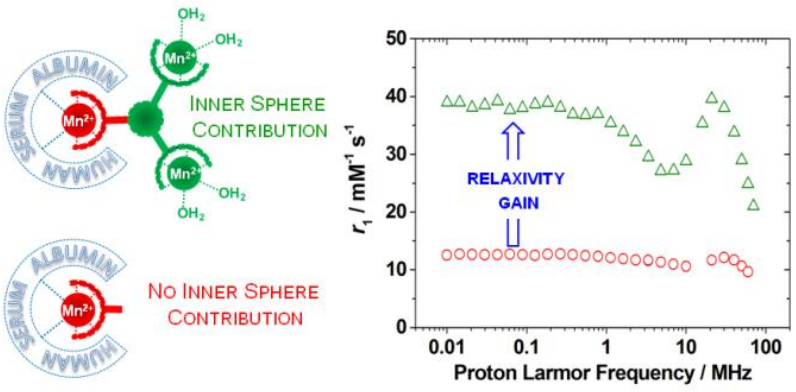

Introduction:

Earlier we already mentioned that the application of Mn^{2+} complexes as MRI CAs was envisaged in the early times of MRI, in the late 1970s.[1,2] As a result of these pioneering studies a Mn^{2+}-based CA, mangafodipir trisodium (Mndpdp, TESLASCAN, Scheme 1) was approved for clinical use. More recently, a mixture of $MnCl_2$, alanine and vitamin D3, denoted as CMC-001, has been proposed as a CA for visualization of liver and bile, and it is currently undergoing phase III clinical trials.[3] Furthermore, preclinical safety assessment of Mndpdp serendipitously revealed superoxide dismutase activity, a useful property that can be potentially exploited for the treatment of several pathological conditions characterized by oxidative stress (i. e. cancer treatment, acute myocardial infarction…).[4] An important advantage of Mn^{2+} CAs over the traditional Gd^{3+} counterparts is the lower toxicity of free Mn^{2+}, which is highlighted by the formulation of CMC-001. On the other hand, the lower effective magnetic moment of Mn^{2+} complexes with respect to Gd^{3+} analogues generally results in lower relaxivities of the Mn^{2+} complexes.[5] An obvious strategy to increase relaxivity is to increase the number of water molecules coordinated to the paramagnetic ion (q), as the inner-sphere contribution to relaxivity is directly proportional to q. This approach has been successfully used to increase the relaxivities of Gd^{3+} complexes, although generally reducing the denticity of the ligand to increase the hydration number results in lower thermodynamic stabilities of the complexes.[6] Some attempts have also been made to obtain bis-hydrated Mn^{2+} complexes as potential MRI contrast agents, but the expected relaxivity gain was not observed due to a low exchange rate of the coordinated water molecule with the bulk water.[7] A second advantage of Mn-based contrast agents is that, in principle, they can be used as redox-sensitive MRI probes, providing that a suitable ligand stabilizes both Mn^{2+} and Mn^{3+}.[8,9]

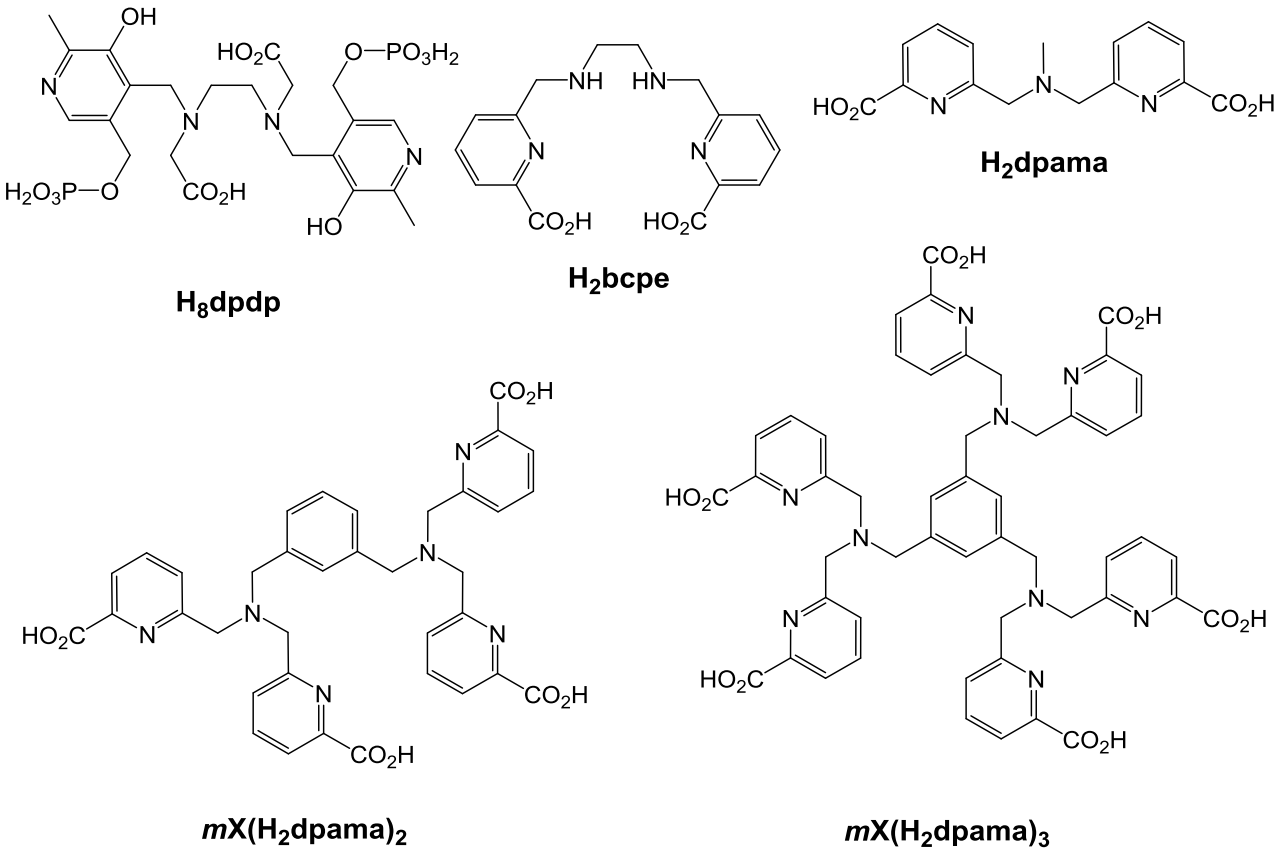

Scheme 1. Ligands mentioned in the chapter.

We decided to explore these issues and thus we have undertaken a study of the complexes based on a well-defined structural unit, the potentially pentadentate ligand dpama. So, we investigated the potential of the Mn^{2+} complex of H_2dpama, *m*X(H_2dpama)$_2$ and *m*X(H_2dpama)$_3$. These ligand form, mono- bi- and trinuclear Mn^{2+} complexes potentially containing two water molecules coordinated to each metal center. These complexes are expected to display enhanced relaxivities, as well as relatively high affinities towards human serum albumin (HSA). In this chapter, we describe a detailed characterization of the Mn^{2+} complexes with these three ligands using ^{1}H relaxometry and ^{17}O NMR measurements. Furthermore, the ligand protonation constants and stability constants of the metal complexes were determined using potentiometric measurements. Cyclic voltammetry experiments were also carried out to investigate the relative stability of the Mn^{2+} and Mn^{3+} complexes. The hexadentate ligand H_2bcpe was reported earlier.[10] It forms rather stable complexes with different divalent and trivalent metal ions.[11,12] Given the ability of Mn^{2+} complexes to form both six- and seven-coordinate complexes in aqueous solution, we have also checked whether

the [Mn(bcpe)] complex contains a coordinated water molecule or not by using ^{1}H relaxometric measurements and X-ray diffraction studies.

Synthesis:

Prof. Carlos-Platas Iglesias, at the Departamento de Química Fundamental, Universidade da Coruña, performed the syntheses of the ligands. The H_2dpama was synthesized in two steps. First step was a reaction of 6-chloromethylpyridine-2-carboxylic acid ethyl ester (1) with methylamine chlorohydrate in the presence of K_2CO_3,[13] followed by hydrolysis of the ethyl ester groups in 6 M HCl (Scheme 2). The desired ligand was isolated as the chlorohydrate salt with a yield of 66% over the two steps. This represents a 2.6-fold increase with respect to the yield reported previously for the analogous ligand derived from ethylamine.[14] Ligand mX(H_2dpama)$_2$ was prepared in 76% yield following a similar procedure by reaction of 1 with 1,3 phenylenedimethanamine (3) followed by acid hydrolysis of the ester groups. Reaction of H_2dpama and mX(H_2dpama)$_2$ with $Mn(ClO_4)_2 \cdot 6H_2O$ in the presence of triethylamine resulted in the formation of the charge neutral complexes $[Mn(dpama)(H_2O)_2] \cdot 2H_2O$ and $[mX(Mn(dpama)(H_2O)_2)_2] \cdot 6H_2O$, respectively, which were isolated in 65% yield. The synthesis of *m*X(H_2dpama)$_3$ (Scheme 3) was achieved in two steps by reaction of benzene-1,3,5-triyltrimethanamine (1b) and 6-chloromethylpyridine-2-carboxylic acid ethyl esther (2b) in the presence of K_2CO_3, and subsequent hydrolysis of the ethyl ester groups in 6M HCl. Reaction of the ligand with $MnCl_2 \cdot 4H_2O$ in the presence of trimethylamine produced the desired charge neutral complex. The synthesis of H_2bcpe was achieved by following the previously reported procedure.[10] Reaction of H_2bcpe with $Mn(ClO_4)_2 \cdot 6H_2O$ in the presence of trimethylamine provided the charge neutral [Mn(bcpe)] complex, which was isolated in 60% yield The high-resolution mass spectra (ESI^+) and analytical data confirm the formation of the desired neutral complexes (Figure 1-4).

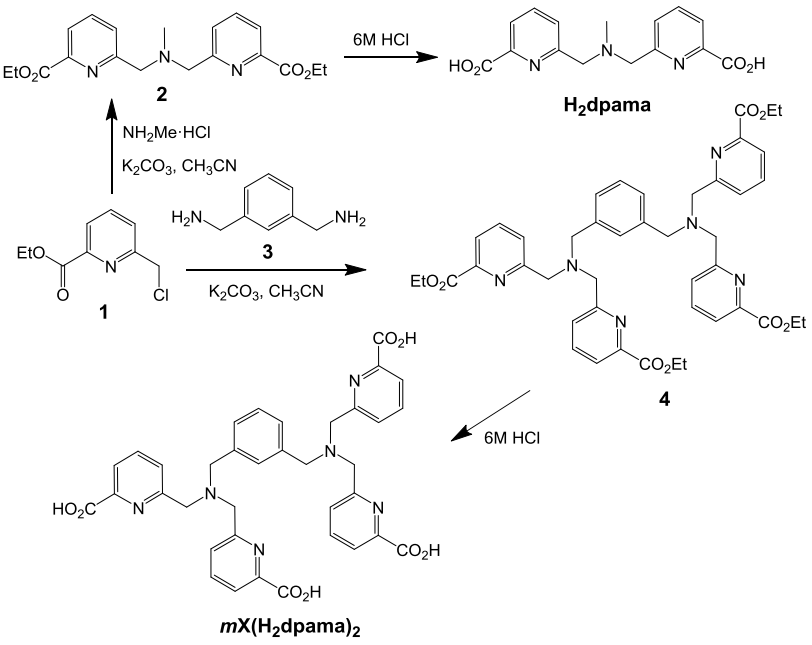

Scheme 2. Synthesis of H_2dpama and mX(H_2dpama)$_2$

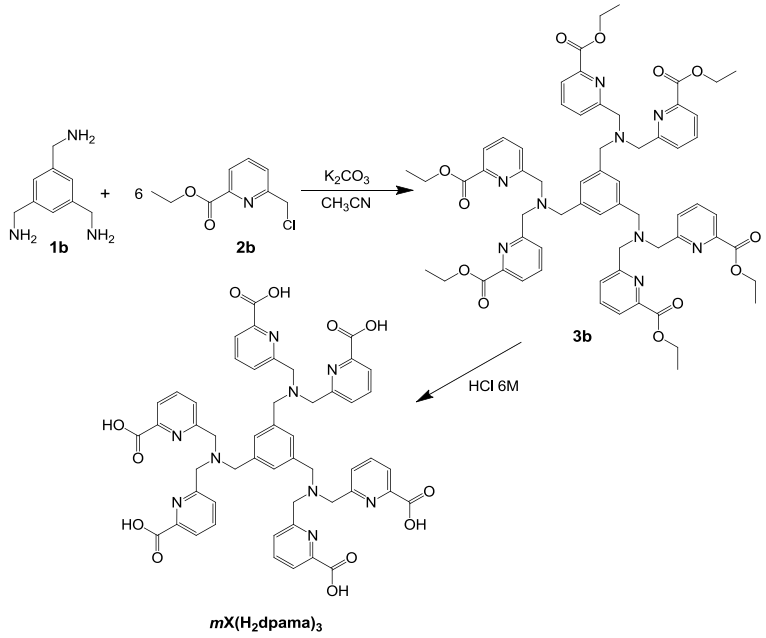

Scheme 3. Synthesis of *m*X(H_2dpama)$_3$.

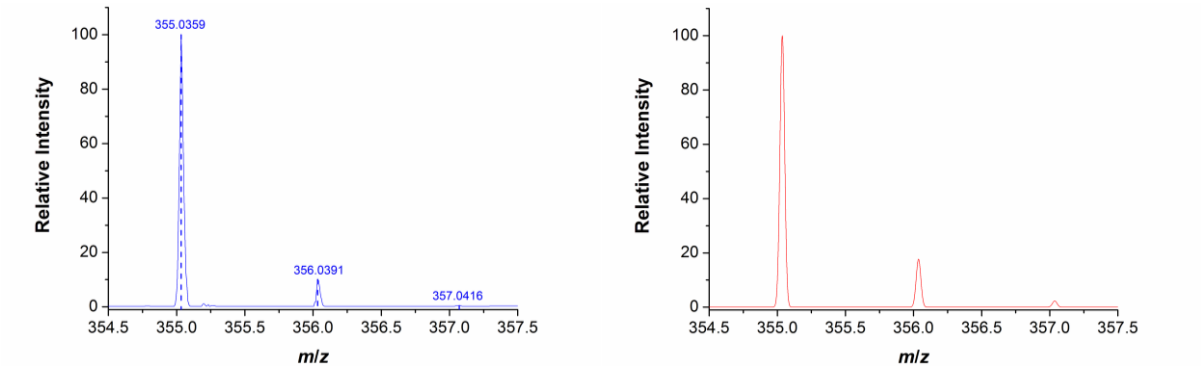

Figure 1. Observed (left) and calculated (right) mass spectral isotopic distribution for the fragment **[Mn(dpama)+H]**$^{+}$ obtained from a solution of the complex in a H_2O:CH_3CN:MeOH mixture.

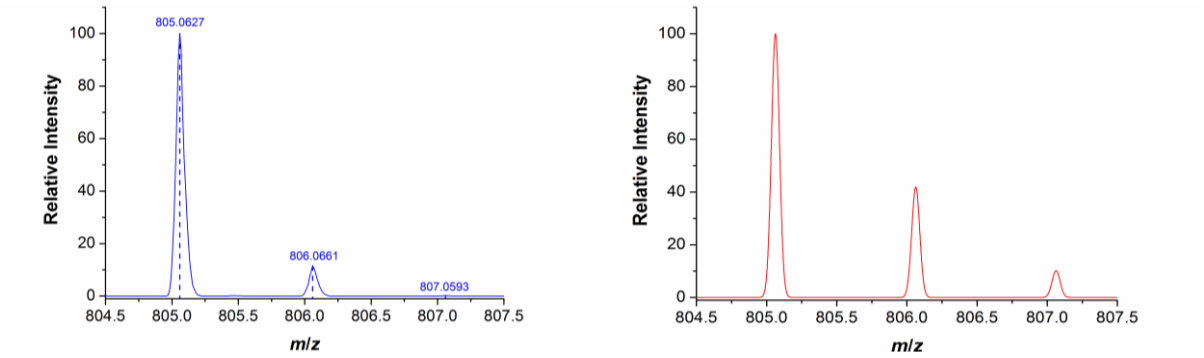

Figure 2. Observed (left) and calculated (right) mass spectral isotopic distribution for the fragment **[(*m*X(Mndpama)$_2$+Na]**$^{+}$ obtained from a solution of the complex in a H_2O:CH_3CN:MeOH mixture.

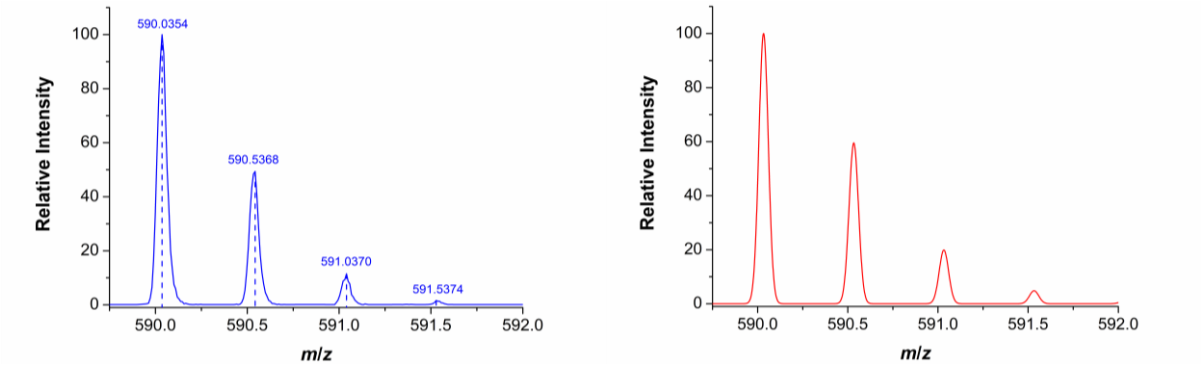

Figure 3. Observed (left) and calculated (right) mass spectral isotopic distribution for the fragment $[Na_2mX(Mndpama)_3]^{2+}$ obtained from a solution of the complex in a H_2O:MeOH 1:1 mixture.

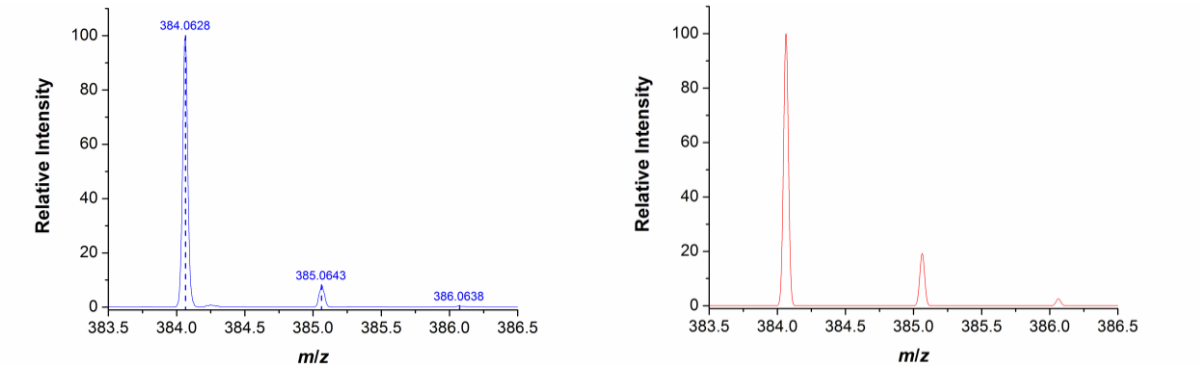

Figure 4. Observed (left) and calculated (right) mass spectral isotopic distribution for the fragment $[Mn(Hbcpe)]^{+}$ obtained from a solution of the complex in a H_2O:MeOH 1:1 mixture.

Aiming to obtain information on the solution structure of the $[Mn(dpama)(H_2O)_2]$ complex we turned our attention to theory. Prof. Carlos-Platas Iglesias carried out the DFT calculations and X-ray diffraction analyses. I report a representative figure of the optimized geometry and X-ray diffraction analyses of the Mn(II) complexes.

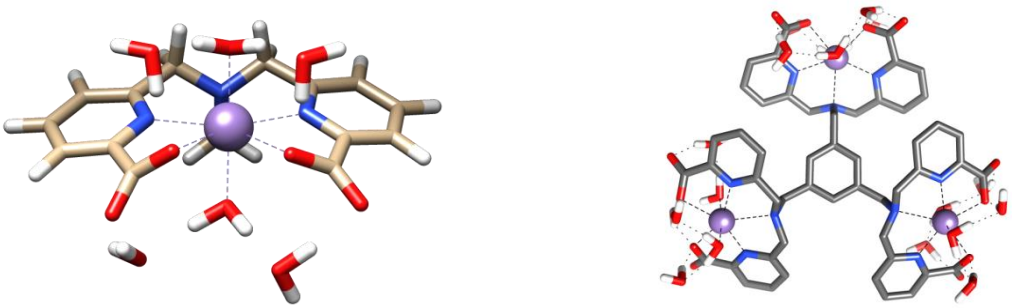

Figure 5. Optimized geometry of the $[Mn(dpama)(H_2O)_2]\cdot 4H_2O$ complex obtained with DFT calculations performed in aqueous solution at the TPSSh/SVP level. (left) Average bond distances (Å) of the Mn^{II} coordination environment: $Mn\text{-}O_{water}$ 2.205(1); $Mn\text{-}O_{COO}$ 2.335(64); $Mn\text{-}N_{amine}$ 2.569; $Mn\text{-}N_{PY}$ 2.287(9). Optimized geometry of the $[mX(Mn(dpama)(H_2O)_2)_3]\cdot 12H_2O$ complex obtained with DFT calculations performed in aqueous solution at the TPSSh/SVP level.(right) Average bond distances (Å) of the Mn^{2+} coordination environment: $Mn\text{-}O_{water}$ 2.213(19); $Mn\text{-}O_{COO}$ 2.315(58); $Mn\text{-}N_{amine}$ 2.620(6); $Mn\text{-}N_{PY}$ 2.280(14). Hydrogen atoms, except those of water molecules, have been omitted for simplicity.

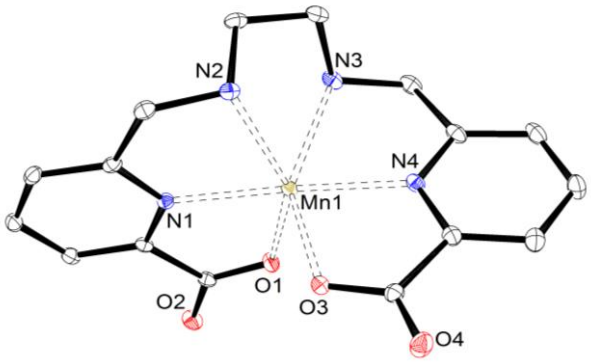

Figure 6. View of the X-ray structure of the [Mn(bcpe)] complex. Water molecules and hydrogen atoms are omitted for simplicity. The ORTEP plot is at the 30% probability level. Bond distances: Mn(1)-O(1), 2.1771(12); Mn(1)-O(3), 2.1783(12); Mn(1)-N(1), 2.1919(15); Mn(1)-N(4), 2.1948(15); Mn(1)-N(2), 2.3046(14); Mn(1)-N(3), 2.3217(14) Å.

Ligand protonation constants and stability constants of the metal complexes:

The protonation constants ($\log K_i^H$) of the previously mentioned ligands investigated in this chapter have been determined by pH-potentiometry in 0.15 M NaCl. The values of the constants and standard deviations are listed in Table 1. The protonation constants are defined by eq 1:

$$H_{i-1}L + H^+ \rightleftharpoons H_iL$$

$$K_i^H = \frac{[H_iL]}{[H_{i-1}L][H^+]} \qquad i=1, 2,\ldots, 8. \qquad (1)$$

Table 1. Protonation constants of ligands $bcpe^{2-}$, $dpama^{2-}$, $mX(dpama)_2^{4-}$, $mX(dpama)_3^{6-}$ and picolinate (0.15 M NaCl, 298 K)

	$dpama^{2-}$	$mX(dpama)_2^{4-}$	$mX(dpama)_3^{6-}$	$bcpe^{2-}$	Picolinate[a]
$\log K_1^H$	7.82(1)	7.77(1)	7.73(1)	8.83(2)	5.25
$\log K_2^H$	3.71(2)	6.49(1)	6.82(1)	6.22(3)	0.92
$\log K_3^H$	2.61(2)	4.24(2)	6.06(1)	3.27(3)	-
$\log K_4^H$	-	3.45(2)	4.31(1)	2.03(3)	-
$\log K_5^H$	-	2.93(2)	3.70(1)		-
$\log K_6^H$	-	2.24(2)	3.30(1)		-
$\log K_7^H$	-	-	2.79(1)		-
$\log K_8^H$	-	-	2.36(1)		-
			1.01(3)		
$\sum \log K_i^H$	14.14	27.13	38.09	20.36	6.17

[a] Taken from ref. 15.

By taking into account the protonation constants and protonation scheme of picolinic acid,[15] we can presume that the first and second protonation constants of $dpama^{2-}$ correspond to the amine nitrogen and the carboxyl groups of the picolinate fragments, respectively. The first and second protonation constants of $mX(dpama)_2^{4-}$ are related to the protonation of the amine nitrogen atoms, whereas subsequent protonations of the ligand take place at the carboxylate groups. Also in the case of $mX(dpama)_3^{6-}$, the $\log K_1^H$, $\log K_2^H$ and $\log K_3^H$ values are also attributed to the protonation of the amine nitrogen atoms, while subsequent protonation processes take place at the carboxylate groups of the picolinate residues.

The difference between successive protonation constants of identical and independent coordination sites are expected to follow the statistical factor,[16] which predicts a difference between two successive identical protonation sites of $\Delta\log K^H = \log K_1^H - \log K_2^H = 0.6$. In the case of three independent protonation sites this factor reduces to $\Delta\log K^H = 0.5$. The second protonation constant of $mX(dpama)_2^{4-}$ is ca. 1.3 log*K* units lower than $\log K_1^H$. This difference is larger than that expected for the statistical factor, which is explained by the repulsive electrostatic interaction between the protonated amine nitrogen atoms in the bis-protonated species. Similarly to the $mX(dpama)_2^{4-}$ ligand, the differences between $\log K_1^H$, $\log K_2^H$ and $\log K_3^H$ of $mX(dpama)_3^{6-}$ are larger than expected according to the statistical factor. However, the protonation of the carboxylate groups of $mX(dpama)_2^{4-}$ characterized by $\Delta\log K^H = \log K_3^H - \log K_4^H = 0.8$, as well as those of $mX(dpama)_3^{6-}$ given by $\Delta\log K^H = \log K_4^H - \log K_5^H = 0.6$, approach the behavior expected according to the statistical factor. This is likely related to the longer distances between the involved protonation sites in comparison to the amine nitrogen atoms. Comparison of the $\sum\log K_i^H$ of $dpama^{2-}$ (14.14), $\sum\log K_i^H/2$ of dimeric $mX(dpama)_2^{4-}$ (13.56) and $\sum\log K_i^H/3$ of trimeric $mX(dpama)_3^{6-}$ (12.36) indicates that the total basicity of $dpama^{2-}$ is higher than that of the average basicity of the $dpama^{2-}$ units in $mX(dpama)_2^{4-}$ and $mX(dpama)_3^{6-}$.

The protonation constants determined for $bcpe^{2-}$ in 0.15 M NaCl are almost identical to those determined previously using a 0.1 M $(Me_4N)(NO_3)$ ionic strength.[10]

The first and second protonation processes occur at the amine nitrogen atoms of the ligand, while the third and fourth protonation constants are assigned to the protonation of the carboxylate groups of the picolinate part.

The stability and protonation constants of Mn^{2+} complexes formed with $bcpe^{2-}$, $dpama^{2-}$, $mX(dpama)_2^{4-}$ and $mX(dpama)_3^{6-}$ were determined by pH-potentiometric titration. Moreover, we have also determined the stability and protonation constants of the Zn^{2+} and Cu^{2+}

complexes with $dpama^{2-}$. The metal-to-ligand concentration ratios were 1:1, as well as 2:1 and 3:1 in the case of $mX(dpama)_2^{4-}$ and $mX(dpama)_3^{6-}$. The stability and protonation constants of the metal complexes are defined by eq 2:

$$pM^{2+} + qH^{+} + rL^{n-} \rightleftharpoons [M_pH_qL_r]^{n-(q+2p)-}$$

$$\beta_{pqr} = \frac{[M_pH_qL_r]}{[M^{2+}]^p[H^+]^q[L]^r} \qquad (2)$$

Table 2. Stability and protonation constants of Mn^{2+} complexes formed with $bcpe^{2-}$, $dpama^{2-}$, $mX(dpama)_2^{4-}$ and $mX(dpama)_3^{6-}$ ligands (0.15 M NaCl and 298 K).

	$bcpe^{2-}$	$dpama^{2-}$	$mX(dpama)_2^{4-}$	$mX(dpama)_3^{6-}$
$\log K_{101}$ (MnL)	10.63(2)	10.13(2)	11.60(6)	10.99(9)
$\log K_{111}$ (MnHL)	3.42(7)	2.57(4)	6.50(4)	7.23(9)
$\log K_{121}$ (MnH_2L)			3.61(2)	6.11(7)
$\log K_{131}$ (MnH_3L)			2.56(1)	4.07(6)
$\log K_{141}$ (MnH_4L)				3.29(3)
$\log K_{151}$ (MnH_5L)				2.73(4)
$\log K_{201}$ (Mn_2L)			8.43(2)	9.17(9)
$\log K_{211}$ (Mn_2HL)				6.00(9)
$\log K_{301}$(Mn_3L)				8.51(4)
$\log K_{311}$(Mn_3HL)				2.54(3)
$\log K_{1-11}$($MnH_{-1}L$)		11.09(4)	10.41(8)	

Table 3. Stability and protonation constants of Zn^{2+} and Cu^{2+} complexes formed with the $bcpe^{2-}$ and $dpama^{2-}$ ligands (0.15 M NaCl, 298 K).

	Zn^{2+}:$dpama^{2-}$	Cu^{2+}:$dpama^{2-}$	Zn^{2+}:$bcpe^{2-}$	Cu^{2+}:$bcpe^{2-}$
$\log\beta_{101}$ (ML)	11.75(1)	13.32(4)[a]	17.53(2)	19.846(9)[a]
$\log K_{111}$ (MHL)	1.51(2)	3.60(4)	2.07(2)	1.45(3)
$\log K_{121}$ (MH_2L)		1.40(4)		
$\log K_{1-11}$($MH_{-1}L$)	9.18(6)	9.53(4)		
$\log K_{1-21}$($MH_{-2}L$)	11.16(7)	11.60(6)		

[a] Determined by spectrophotometry.

The stability constants and protonation constants of the metal complexes are reported in Tables 2 and 3. The $\log K_{101}$ values determined for the four Mn^{2+} complexes are really similar. Which shows that the pentadentate $dpama^{2-}$ ligand and the di- and tri-nucleating $mX(dpama)_2^{4-}$ and $mX(dpama)_3^{6-}$ ligands provide metal complexes with stabilities that are very similar to that of the complex with the hexadentate ligand $bcpe^{2-}$, with $\log\beta_{101}$ values in the range 10.1 – 11.6.

The stability of the Mn^{2+} complex of the pentadentate ligand $dpama^{2-}$ is very similar to that of the complex with the hexadentate ligand $bcpe^{2-}$. The stability constants of the mononuclear Mn(dpama), $mX(Mndpama)_2$ and $mX(Mndpama)_3$ complexes are analogous, indicating that in all cases the Mn^{2+} ion is coordinated by a $dpama^{2-}$ unit characterized by similar metal ion affinity. Since the mononuclear $mXMn(dpama)_2$ and $(mX(dpama)_3Mn)$ complexes have one and two non-coordinated $dpama^{2-}$ units, the free donor atoms can be protonated with the formation of several protonated MnH_iL species ($mX(dpama)_2$: i=1 – 3; $mX(dpama)_3$: i=1 – 5). The protonation constants of mononuclear $mXMn(dpama)_2$ and mXMn $(dpama)_3$ complexes (Table 2) are comparable to the corresponding $\log K_i^H$ values of the free ligands (Table 1).

The stability constants of the dinuclear ($mX(Mndpama)_2$), ($mXMn_2(dpama)_3$) and trinuclear $mX(Mndpama)_3$ complexes are very similar and somewhat lower than the $\log K_{101}$ values of the mononuclear $mXMn(dpama)_2$ and $mXMn(dpama)_3$ entities (Table 2). A recent study has reported virtually identical stability constants for the mono- and bi-nuclear Mn^{2+} complexes of ditopic do3a-based ligands containing a long spacer separating the two metal binding units.[17] Thus, the slightly lower stability constants of the dinuclear and trinuclear Mn^{2+} complexes of $mX(dpama)_2$ and $mX(dpama)_3$ might be explained by the electron withdrawing effect caused by the coordination of Mn^{2+} to a $dpama^{2-}$ unit on the non-coordinated amine nitrogen atom of the neighbor $dpama^{2-}$ moiety. If we study the $\log K_{101}$ value of Mn(dpama) (10.13) with the $\log\beta_{201}/2$ value of dinuclear $Mn_2(mX(dpama)_2)$ (10.01) and $\log\beta_{301}/3$ value of trinuclear $Mn_3(mX(dpama)_3)$ (9.56), we can assume that the average Mn^{2+} affinities of the $dpama^{2-}$ units in the mono-, bi- and trimeric ligands decrease in the following order: $dpama^{2-} > mX(dpama)_2^{4-} > mX(dpama)_3^{6-}$.

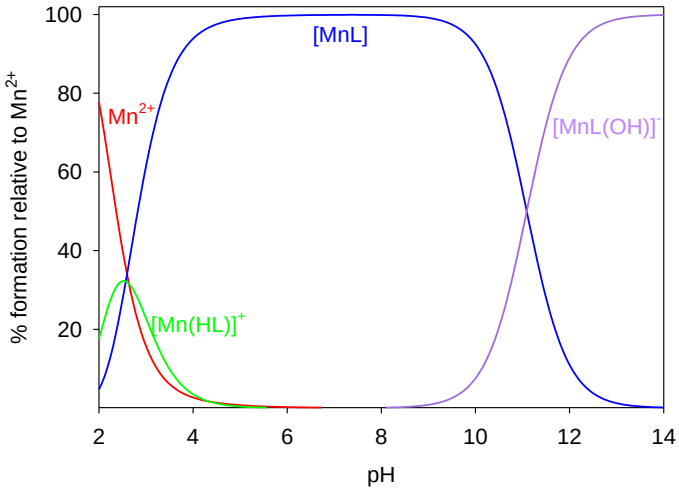

Figure 7. Species distribution diagrams of the Mn^{2+}- dpama ($[Mn^{2+}]$=[dpama]=1.0 mM) system (0.15 M NaCl, 298 K).

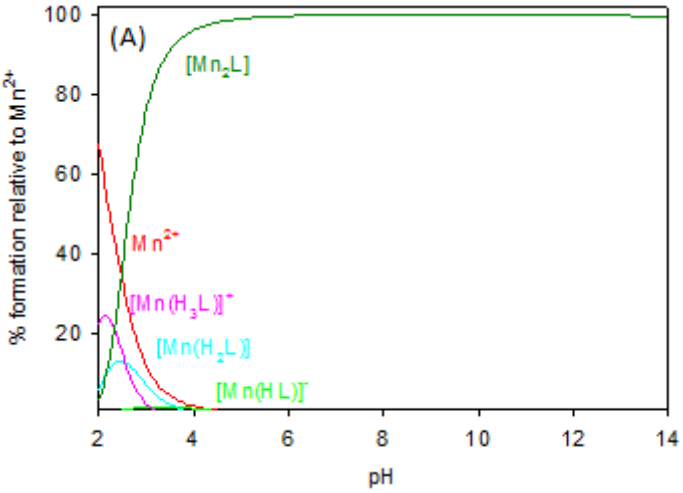

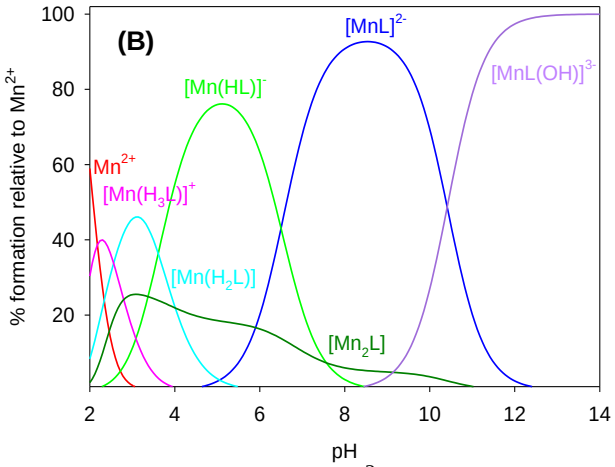

Figure 8. Species distribution diagram of the Mn^{2+}- $mX(dpama)_2$ system at metal-to-ligand ratio of 1:1 ($[mX(dpama_2)]$=1.0 mM, 0.15 M NaCl, 298 K) (A), and Mn^{2+}-$mX(dpama)_2$ ($[Mn^{2+}]$= 2 mM, $[mX(dpama)_2]$=1.0 mM) (B).

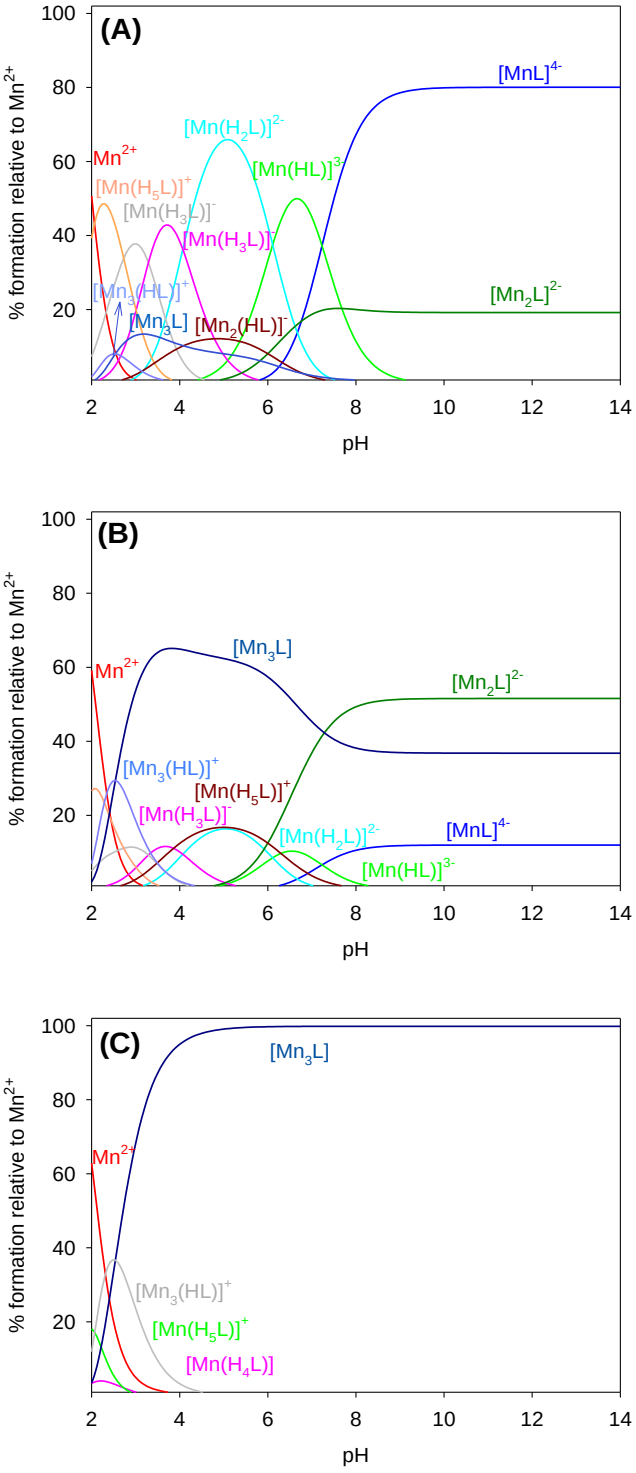

Figure 9. Species distribution diagrams of the Mn^{2+}-mX(dpama)$_3$ systems at metal-to-ligand ratio of 1:1 (A), 2:1 (B) and 3:1 (C) ([mX(dpama$_3$)]=1.0 mM, 0.15 M NaCl, 298 K).

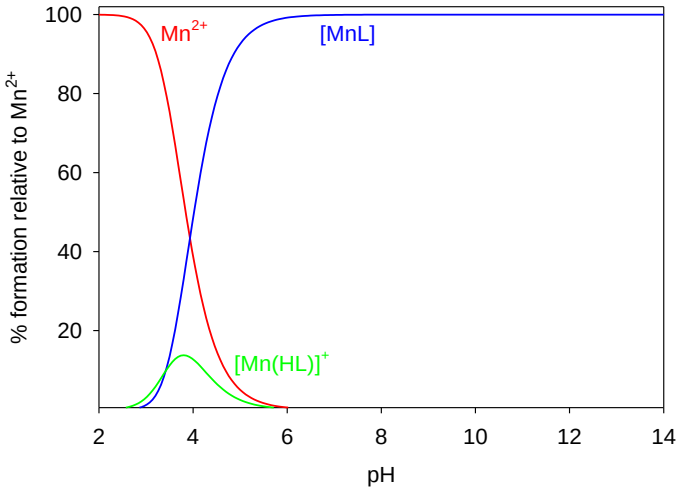

Figure 10. Species distribution diagram of the Mn^{2+} - bcpe system at metal-to-ligand ratio 1:1 ([bcpe]=1.0 mM, 0.15 M NaCl, 298 K)

The stabilities of the Mn^{2+}, Cu^{2+} and Zn^{2+} complexes are following the Irving-Williams order (Mn^{2+} < Cu^{2+} > Zn^{2+}).[18] However, the stability of the [Cu(bcpe)] complex is 9 orders of magnitude higher than that of [Mn(bcpe)], while the Zn^{2+} complex is about 7 orders of magnitude more stable than the Mn^{2+} one. In the case of the $dpama^{2-}$ complexes the stabilities of the Zn^{2+} and Cu^{2+} complexes are only 1.6 and 3.2 log*K* units higher than that of the Mn^{2+} analogue. These results show that the pentadentate $dpama^{2-}$ ligand is suprisingly well preorganized to provide a seven-coordinate Mn^{2+} complex with pentagonal bipyramidal coordination. Pentagonal bipyramidal coordination is much more less favorable for Cu^{2+} and Zn^{2+} complexes,[19] which likely results in a modest increase of complex stability of the latter complexes with respect to Mn^{2+}.

The species distribution of the Mn^{2+} - dpama, Mn^{2+} - $mX(dpama)_2$ and Mn^{2+} - $mX(dpama)_3$ systems have been calculated by taking into account the equilibrium constants of Tables 1 and 2 (Figure 7-10). The dissociation of [Mn(dpama)] occurs below pH ~ 5, while it represents the major species in solution up to pH ~ 11. However, at pH>8.5 deprotonation of the complex takes place with the formation of a $MnH_{-1}L$ species, likely as a result of the coordination of a OH^- anion to the Mn^{2+}-ion. The $[mX(Mndpama)_2]$ and $[mX(Mndpama)_3]$ complexes dissociate below pH ~ 4, which results in the formation of complex species with reduced nuclearity. No evidence for the formation of hydroxo complexes was found in any of these cases.

Relaxometric studies:

The efficiency of a paramagnetic complex as a CA in vitro is often and conveniently evaluated by its proton relaxivity, r_{1p}, which is defined as the relaxation enhancement of water protons normalized to a 1 mM concentration of the paramagnetic metal ion. The r_{1p} values determined for [Mn(bcpe)] and [Mn(dpama)] in the pH range ~10.0-5.0 (20 MHz, 25 ºC) are fairly constant (Figure 11). Below pH 5.0 relaxivity progressively increases due to the dissociation of the complex and formation of $[Mn(H_2O)_6]^{2+}$,[20] in agreement with the speciation diagrams obtained from equilibrium data. The relaxivity measured for [Mn(bcpe)] is rather low (1.4 mM^{-1} s^{-1} at 25 ºC, 20 MHz, pH 7.47), and compares well to those measured for $[Mn(do3a)]^-$, $[Mn(dtpa)]^{3-}$ and [Mn(1,7-do2a)], which lack inner-sphere water molecules (1.3 – 1.5 mM^{-1} s^{-1} at 25 ºC and 20 MHz).[21] Thus, the relaxivity observed for [Mn(bcpe)] can be attributed to the outer-sphere mechanism, in full agreement with the X-ray structure of the complex described above. The relaxivity (r_{1p}) measured for [Mn(dpama)] at 20 MHz and 298 K (pH = 7.3) amounts to 5.32 mM^{-1} s^{-1}. This value is *ca.* 60% higher than those measured under the same conditions for small Mn^{2+} complexes containing one coordinated water molecule (i. e. r_{1p} = 3.3 mM^{-1} s^{-1} for $[Mn(edta)]^{2-}$, Figure 12, Table 4).[21] Interestingly, the relaxivity measured for [Mn(dpama)] is also higher than those determined for bis(aquated) seven-coordinate Mn^{2+} complexes with neutral pentadentate macrocyclic ligands (r_{1p} = 3.5-4.5 mM^{-1} s^{-1}, 20 MHz, 25 ºC),[22] or most commercially available Gd^{3+}-based contrast agents (r_{1p} = 4-5 mM^{-1} s^{-1}, 20 MHz, 25 ºC).[23] A further improvement of the relaxivity is observed for [(*m*X(Mndpama)$_2$], which presents a r_{1p} value (8.63 mM^{-1} s^{-1}, 20 MHz, 25 ºC) higher than those usually observed for small Gd^{3+} bisaqua complexes for example Gd(do3a) and $Gd(aazta)^-$.[6d] The high relaxivity values determined for [Mn(dpama)] and [(*m*X(Mndpama)$_2$] can only be explained by the presence of two water molecules in the inner coordination sphere of the metal ion.

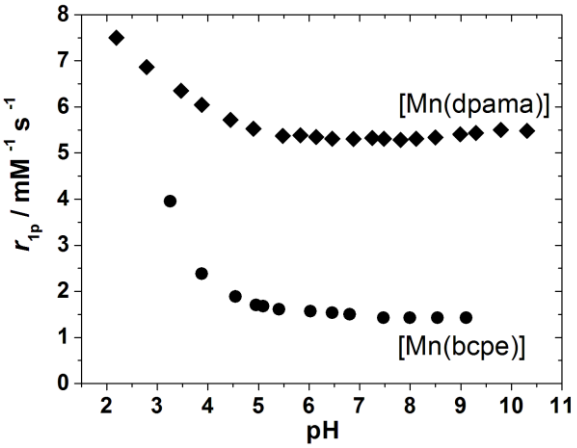

Figure 11. Plot of the relaxivity (20 MHz; 25 ºC) of the [Mn(bcpe)] and [Mn(dpama)] complexes as a function of pH.

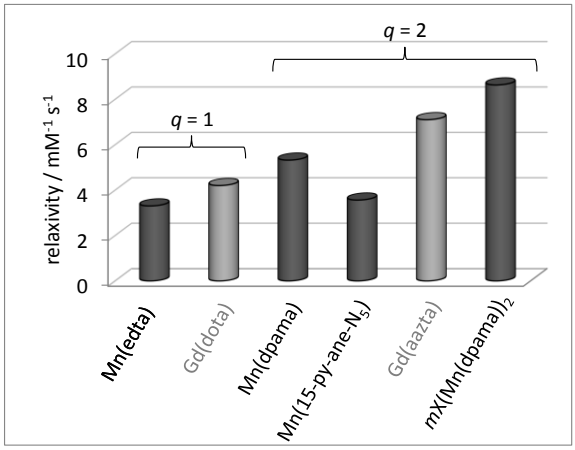

Figure 12. Plot of the relaxivity, r_{1p}, for selected Gd^{3+} and Mn^{2+} complexes at 20 MHz and 298 K.

To gain more insight into the physicochemical parameters that govern the relaxivities observed for [Mn(bcpe)] and [Mn(dpama)] we recorded ^{1}H nuclear magnetic relaxation dispersion (^{1}H NMRD) profiles of aqueous solutions of these complexes in the proton Larmor frequency range 0.01−70 MHz, corresponding to magnetic field strengths varying between 2.343×10^{-4} and 1.645 T (Figure 13). The relaxivity of [Mn(dpama)] decreases with increasing temperature, this behavior is typical for small chelates in which fast rotation of the complex in solution limits proton relaxivity. Furthermore, the ^{1}H NMRD profiles of [Mn(dpama)] show a single dispersion between 1 and 10 MHz, which rules out any scalar contribution to ^{1}H

relaxivity.[20,24] Since the inner-sphere contribution to relaxivity depends upon a relatively large number of parameters, we have also measured reduced transverse ^{17}O NMR relaxation rates and chemical shifts of an aqueous solution of [Mn(dpama)] (3.89 mM, pH = 7.2). These data provide independent information about some important parameters that control ^{1}H relaxivity, especially the exchange rate of the coordinated water molecule(s) (k_{ex}^{298}). The $1/T_{2r}$ values increase with decreasing temperature, which is typical of systems in the fast-exchange regime. Despite, the changeover between the fast and slow exchange regimes can be observed in the temperature dependence of the chemical shifts (Figure 14), as also observed for the $[Mn(edta)]^{2-}$ complex.[21]

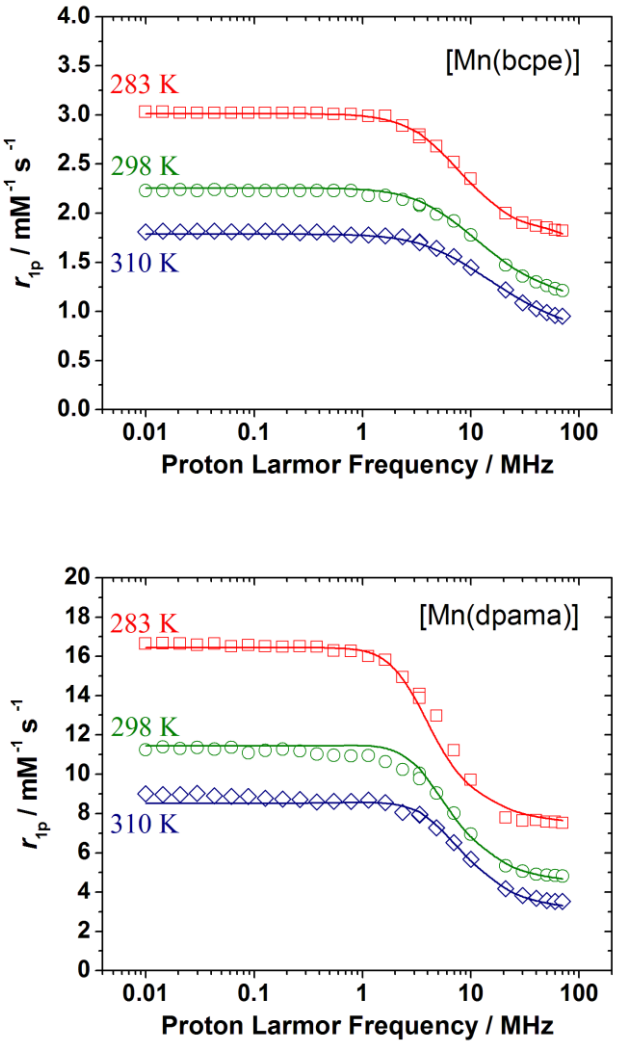

Figure 13. ^{1}H NMRD profiles recorded at different temperatures for [Mn(bcpe)] and [Mn(dpama)]. The lines represent the fit of the data as explained in the text.

Table 4. Parameters obtained from the simultaneous analysis of ^{17}O NMR and ^{1}H NMRD data.

	bcpe^{2-}	**dpama^{2-}**	**mX(dpama)$_2^{4-}$**	**mX(dpama)$_3^{6-}$**	**edta^{4-}** [b]
r_{1p} at 25/37 °C / mM^{-1} s^{-1} [b]	1.4/1.2	5.3/4.2	8.6/6.1	11.4/8.3	3.3/2.8
$k_{ex}^{298}/10^6$ s^{-1}		306 ± 16	306[a]	306[a]	471
$\Delta H^{\ddagger}$ kJ mol^{-1}		28.1 ± 2.2	28.1[a]	28.1[a]	33.5
τ_R^{298}/ps		47.8 ± 0.9	95.8 ± 1.8	136 ± 3.0	57
E_r/kJ mol^{-1}		25.3 ± 0.6	27.3 ± 0.7	31.6 ± 1.0	21.8
τ_v^{298}/ps	19.9 ± 0.9	39.2 ± 5.6	57.6 ± 7.0	27.7 ± 3.4	27.9
E_v/kJ mol^{-1}	3.7 ± 0.7	1.0[a]	1.0[a]	1.0[a]	1.0[a]
$D_{MnH}^{298}/10^{-10}$ m^2 s^{-1}	21.8 ± 0.2	22.4[a]	22.4[a]	22.4[a]	23.1
E_{DMnH} /kJ mol^{-1}	21.6 ± 0.2	17.3[a]	17.3[a]	17.3[a]	18.9
$\Delta^2/10^{19}$ s^{-2}	9.0 ± 0.5	2.38 ± 0.39	1.48 ± 0.25	3.26 ± 0.50	6.9
$A_O/\hbar/10^6$ rad s^{-1}		-45.8 ± 0.8			-40.5
r_{MnH}/Å		2.74[a]	2.74[a]	2.74[a]	2.83[a]
a_{MnH}/Å	3.6[a]	3.6[a]	3.6[a]	3.6[a]	3.6[a]
q^{298}	0	2[a]	2[a]	2[a]	1[a]

[a] Parameters fixed during the fitting procedure. [b] Ref. 21.

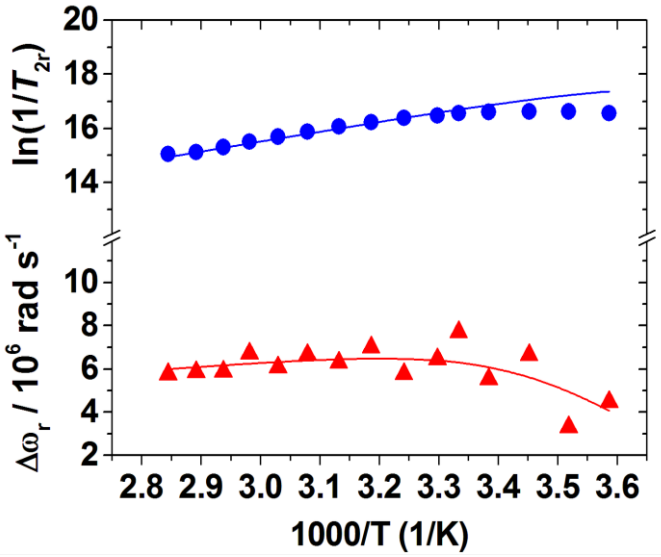

Figure 14. Reduced transverse (blue •) ^{17}O NMR relaxation rates and ^{17}O NMR chemical shifts (red ▲) measured for [Mn(dpama)] at 11.74 T. The lines represent the fit of the data as explained in the text.

The ^{1}H NMRD profiles of [Mn(bcpe)] were analyzed by using the Freed model,[25] which accounts for the outer-sphere contribution to relaxivity. The distance of closest approach for

the outer-sphere contribution a_{MnH} was fixed at 3.6 Å, while the remaining parameters were allowed to refine freely during the fitting procedure. The parameters characterizing the electron spin relaxation, the electronic correlation time for the modulation of the zero-field-splitting interaction (τ_V), its activation energy (E_V) and the mean square zero-field-splitting energy (Δ^2), take values that are similar to those reported for $[Mn(edta)]^{2-}$ and other Mn^{2+} complexes.[7,21,26,27] Furthermore, the values obtained for the diffusion coefficient, D_{MnH}^{298}, and its activation energy, E_{DMnH}, are close to those reported for the self-diffusion of water molecules in pure water ($2.3 \cdot 10^{-9}$ $m^2 \cdot s^{-1}$ and 17.3 kJ mol^{-1}).[74] Thus, we conclude that the value of 3.6 Å assumed for a_{MnH} is reasonable.

A simultaneous fitting of the ^1H NMRD and ^{17}O NMR data of [Mn(dpama)] was carried out by taking into account both the outer- and inner-sphere contributions to relaxivity.

From the measured ^{17}O NMR transversal relaxation rates and angular frequencies of the paramagnetic solutions, $1/T_1$, $1/T_2$ and ω, and of the acidified water reference, $1/T_{1A}$, $1/T_{2A}$ and ω_A, one can calculate the reduced relaxation rates, $1/T_{1r}$, $1/T_{2r}$ and reduced chemical shifts (Eq. (3) – (4)), where $1/T_{2m}$ is the relaxation rate of the bound water and $\Delta\omega_m$ is the chemical shift difference between bound and bulk water, τ_m is the mean residence time or the inverse of the water exchange rate k_{ex} and P_m is the mole fraction of the bound water.[28,29]

$$\frac{1}{T_{2r}} = \frac{1}{P_m}\left[\frac{1}{T_2} - \frac{1}{T_{2A}}\right] = \frac{1}{\tau_m}\frac{T_{2m}^{-2} + \tau_m^{-1}T_{2m}^{-1} + \Delta\omega_m^2}{\left(\tau_m^{-1} + T_{2m}^{-1}\right)^2 + \Delta\omega_m^2} + \frac{1}{T_{2OS}} \qquad (3)$$

$$\Delta\omega_r = \frac{1}{P_m}(\omega - \omega_A) = \frac{\Delta\omega_m}{(1 + \tau_m T_{2m}^{-1})^2 + \tau_m^2\Delta\omega_m^2} + \Delta\omega_{os} \qquad (4)$$

The outer sphere contributions to the ^{17}O relaxation rates and chemical shifts have been considered to be negligible in the present study. $\Delta\omega_m$ is determined by the hyperfine or scalar coupling constant, $A/\hbar$, according to Equation (5), where B represents the magnetic field, S is the electron spin (S = 5/2 for high-spin Mn(II) complexes) and g_L is the isotropic Landé g factor.[75]

$$\Delta\omega_m = \frac{g_L\mu_B S(S+1)B}{3k_B T}\frac{A}{\hbar} \qquad (5)$$

The exchange rate is supposed to assume the Eyring equation. In Eq. (6) $\Delta S^{\ddagger}$ and $\Delta H^{\ddagger}$ are the entropy and enthalpy of activation for the water exchange process, and k_{ex}^{298} is the exchange rate at 298.15 K.

$$\frac{1}{\tau_m} = k_{ex} = \frac{k_B T}{h} \exp\left\{\frac{\Delta S^{\ddagger}}{\mathrm{R}} - \frac{\Delta H^{\ddagger}}{RT}\right\} = \frac{k_{ex}^{298} T}{298.15} \exp\left\{\frac{\Delta H^{\ddagger}}{R}\left(\frac{1}{298.15} - \frac{1}{T}\right)\right\} \qquad (6)$$

In the transverse relaxation the scalar contribution, $1/T_{2sc}$, is the most important, Eq. (7). $1/\tau_{s1}$ is the sum of the exchange rate constant and the electron spin relaxation rate.

$$\frac{1}{T_{2m}} \cong \frac{1}{T_{2SC}} = \frac{S(S+1)}{3}\left(\frac{A}{\hbar}\right)^2 \tau_{S1} \qquad (7)$$

$$\frac{1}{\tau_{S1}} = \frac{1}{\tau_m} + \frac{1}{T_{1e}} \qquad (8)$$

The measured longitudinal proton relaxation rate, R_1^{obs} is the sum of a paramagnetic and a diamagnetic contribution as expressed in Eq. (9), where r_{1p} is the proton relaxivity:

$$R_1^{obs} = R_1^d + R_1^p = R_1^d + r_{1p}[Mn(II)] \qquad (9)$$

The relaxivity can be divided into an inner and an outer sphere term as follows:

$$r_1 = r_{1is} + r_{1os} \qquad (10)$$

The inner sphere term is given in Eq. (11), where q is the number of inner sphere water molecules.[30]

$$r_{1is} = \frac{1}{1000} \times \frac{q}{55.55} \times \frac{1}{T_{1m}^H + \tau_m} \qquad (11)$$

The longitudinal relaxation rate of inner sphere protons, $1/T_{1m}{}^{H}$ is expressed by Eq. (12):

$$\frac{1}{T_{1m}^{H}} = \frac{2}{15}\left(\frac{\mu_0}{4\pi}\right)^2 \frac{\gamma_I^2 g^2 \mu_B^2}{r_{MnH}^6} S(S+1)\left[\frac{3\tau_{d1}}{1+\omega_I^2\tau_{d1}^2} + \frac{7\tau_{d2}}{1+\omega_S^2\tau_{d2}^2}\right] \qquad (12)$$

where r_{MnH} is the effective distance between the electron charge and the ^{1}H nucleus, ω_I is the proton resonance frequency and ω_S is the Larmor frequency of the Mn(II) electron spin.

$$\frac{1}{\tau_{di}} = \frac{1}{\tau_m} + \frac{1}{\tau_R} + \frac{1}{T_{ie}} \qquad i = 1, 2 \qquad (13)$$

The longitudinal and transverse electronic relaxation rates, $1/T_{1e}$ and $1/T_{2e}$ are expressed by Eqs. (14)-(16), where τ_V is the electronic correlation time for the modulation of the zero-field-splitting interaction, E_V the corresponding activation energy and Δ^2 is the mean square zero-field-splitting energy. We assumed a simple exponential dependence of τ_V versus $1/T$ as written in Eq. (16).

$$\frac{1}{T_{1e}} = \frac{1}{25}\Delta^2\tau_V\{4S(S+1)-3\}\left(\frac{1}{1+\omega_s^2\tau_v^2} + \frac{4}{1+4\omega_s^2\tau_v^2}\right) \qquad (14)$$

$$\frac{1}{T_{2e}} = \left(\left(0.02\times\left(4S^2+4S-3\right)\times\tau_V\times\Delta^2\times\left(\left(\frac{5}{1+\omega_s{}^2\tau_V{}^2}\right)\right)\right) + \left(\frac{2}{1+4\omega_s{}^2\tau_V{}^2}\right) + 3\right) \qquad (15)$$

$$\tau_v = \tau_v^{298}\exp\left\{\frac{E_v}{R}\left(\frac{1}{T} - \frac{1}{298.15}\right)\right\} \qquad (16)$$

The outer-sphere contribution can be described by Eq. (17) where N_A is the Avogadro constant, and J_{os} is its associated spectral density function.[25,31]

$$r_{1os} = \frac{32N_A\pi}{405}\left(\frac{\mu_0}{4\pi}\right)^2 \frac{\hbar^2\gamma_S^2\gamma_I^2}{a_{MnH}D_{MnH}} S(S+1)[3J_{os}(\omega_I;T_{1e}) + 7J_{os}(\omega_I;T_{2e})] \qquad (17)$$

$$J^{OS}(\omega,T_{je}) = \mathrm{Re}\left[\frac{1+\frac{1}{4}\left(i\omega\tau_{MnH}+\frac{\tau_{MnH}}{T_{je}}\right)^{1/2}}{1+\left(i\omega\tau_{MnH}+\frac{\tau_{MnH}}{T_{je}}\right)^{1/2}+\frac{4}{9}\left(i\omega\tau_{MnH}+\frac{\tau_{MnH}}{T_{je}}\right)+\frac{1}{9}\left(i\omega\tau_{MnH}+\frac{\tau_{MnH}}{T_{je}}\right)^{3/2}}\right] \quad (18)$$

$$\text{where } j=1,2,\ \tau_{MnH}=\frac{{a_{MnH}}^2}{D_{MnH}}.$$

The diffusion coefficient for the diffusion of a water proton away from a Gd(III) complex, D_{GdH}, is assumed to obey an exponential law versus the inverse of the temperature, with an activation energy E_{GdH}, as given in Eq. (19). ${D_{GdH}}^{298}$ is the diffusion coefficient at 298.15 K.

$$D_{MnH} = D_{MnH}^{298}\exp\left\{\frac{E_{MnH}}{R}\left(\frac{1}{298.15}-\frac{1}{T}\right)\right\} \quad (19)$$

In line with the results obtained for [Mn(bcpe)], the distance of closest approach for the outer-sphere contribution a_{MnH} was fixed at 3.6 Å during the fitting procedure, while D_{MnH}^{298} and E_{DMnH} were set to the values obtained for the self-diffusion of water molecules in pure water. Furthermore, the distance between the proton nuclei of the coordinated water molecules and the Mn^{2+} ion (r_{MnH}) was fixed at 2.74 Å, which corresponds to the average Mn···H distance obtained from our DFT calculations. Number of water molecules in the inner coordination sphere of Mn^{2+} was fixed to q=2. The parameters obtained from the fittings are listed in Table 4, while the curve fits are shown in Figures 13 and 14.

The measured water exchange rate for [Mn(dpama)] (${k_{ex}}^{298}$=3.1 10^8 s^{-1}) is close to that reported for $[Mn(edta)(H_2O)]^{2-}$ (${k_{ex}}^{298}$=4.7 10^8 s^{-1}),[21] and one order of magnitude faster than that determined for the aquated ion $[Mn(H_2O)_6]^{2+}$ (${k_{ex}}^{298}$=2.8 10^7 s^{-1}).[20] The value obtained for the ^{17}O hyperfine coupling constant ($A_O/\hbar$=-45.8×10^6 $rads^{-1}$) is similar to those typically observed for Mn^{2+} complexes (-31×10^6 to -43×10^6 $rad\cdot s^{-1}$).[32] Theoretical DFT calculations carried out following previously reported methodology[33,20] provide A_{iso} values of -48.1×10^6 $rad\cdot s^{-1}$ and -52.5×10^6 $rad\cdot s^{-1}$ for the two coordinated water molecules, which present nearly identical Mn-O distances (2.206 and 2.205 Å). The excellent agreement between the

experimental and calculated $A_O/\hbar$ values clearly confirms that the [Mn(dpama)] presents two coordinated water molecules.

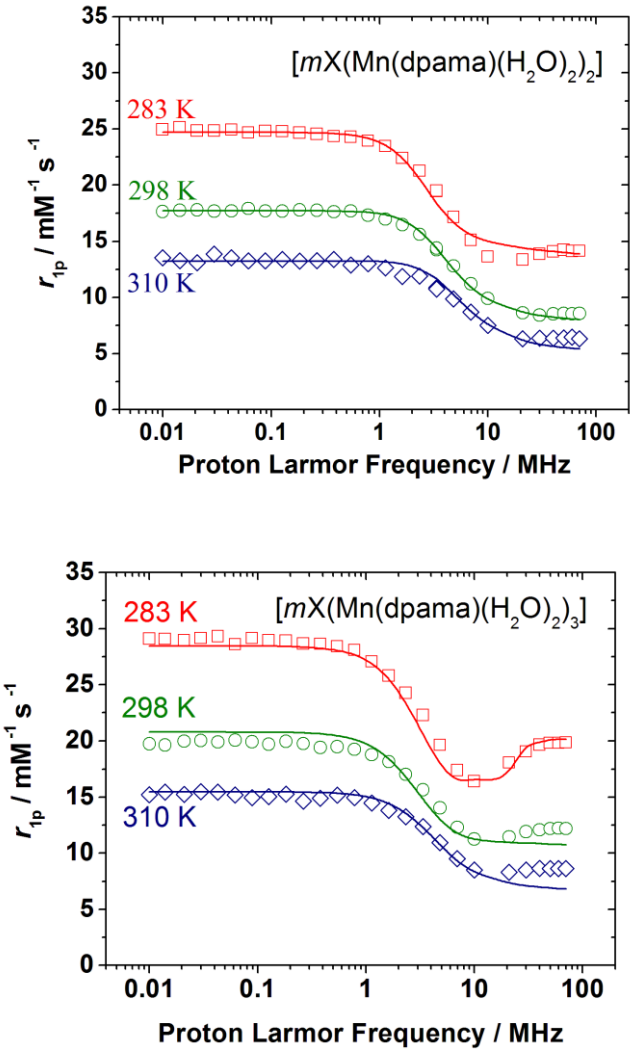

Figure 15. ^{1}H NMRD profiles recorded at different temperatures for [mX(Mn(dpama)$(H_2O)_2)_2$] and [mX(Mn(dpama)$(H_2O)_2)_3$]. The lines represent the fit of the data as explained in the text.

The ^{1}H NMRD profiles of the [mX(Mn(dpama)$(H_2O)_2)_2$] and [mX(Mn(dpama)$(H_2O)_2)_3$] complexes were also recorded at different temperatures (Figure 15). The relaxivities measured at high fields (>20 MHz) for the mono-, bi- and tri-nuclear complexes follow a linear correlation (R^2 > 0.9999) with their molecular weight (Figure 16.). At high fields the rotational dynamics (τ_R) plays a major role in determining the relaxivity because both the exchange lifetime (τ_M) and the electronic relaxation times are much longer than τ_R. The ^{1}H NMRD profiles recorded at three different temperatures could be fitted by fixing the structural parameters and those related to diffusion and water exchange to the values obtained for

[Mn(dpama)] (Table 4). Thus, only four parameters were allowed to vary during the fitting procedure: τ_R, τ_v, E_r, and Δ^2. Reasonably good fits of the relaxivity data were obtained using this procedure, which suggests that the water exchange of coordinated water molecules does not vary significantly in this series of complexes. The results of the fits are clearly showing that increasingly long τ_R values are the main responsible for the increase of relaxivity with molecular weight.

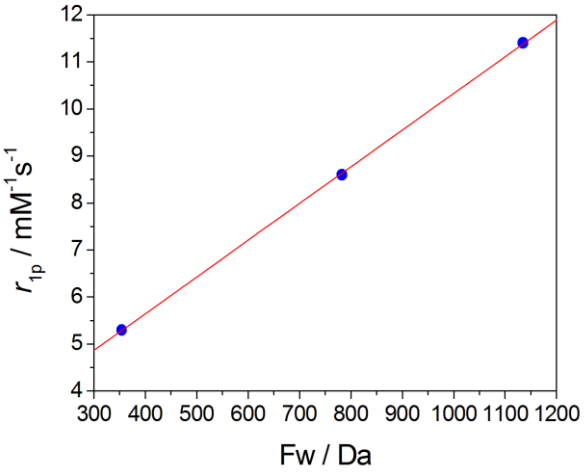

Figure 16. Plot of the relaxivity (20 MHz; 25 ºC) of the [Mn(dpama)], [mX(Mndpama)$_2$] and [mX(Mndpama)$_3$] complexes as a function of the molecular mass. The line represents the linear fit of the data.

Human Serum Albumin (HSA) binding studies:

The stability of the [Mn(dpama)] complex was first assessed by measuring its proton relaxivity (25 ºC, 20 MHz) as a function of pH. The relaxivity remains constant within a rather wide pH range from 10.3 to 5.5, while below pH~5.5 r_{1p} increases due to the stepwise dissociation of the complex and gradual Mn^{2+} release (Figure 17.). The stability with time of [Mn(dpama)] was assessed by relaxometric measurement (0.47 T, 37 ºC) of a 0.98 mM solution of the complex in a lyophilized serum of human origin (Seronorm^{TM}), which is normal human serum without added preservatives and therefore contains endogenous levels of the different serum components. The complex proved to be stable for more than 120 h (Figure 18.), as only very small and negligible fluctuations in the relaxation rate data were detected, well within the experimental error (±3-4%).

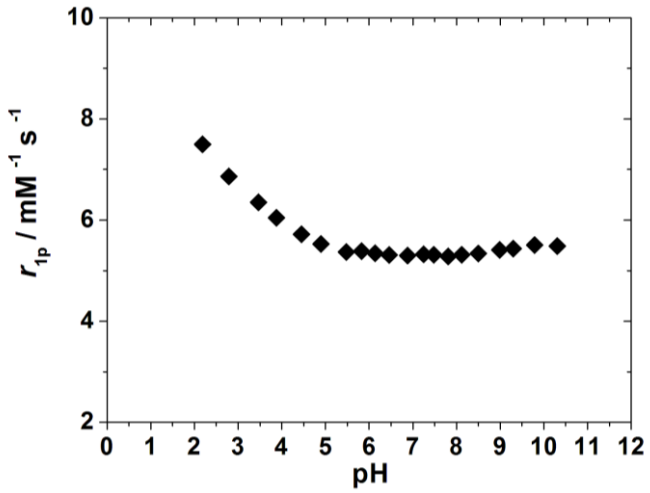

Figure 17. Proton relaxivity of [Mn(dpama)] (20 MHz, 25 ºC) recorded as a function of pH.

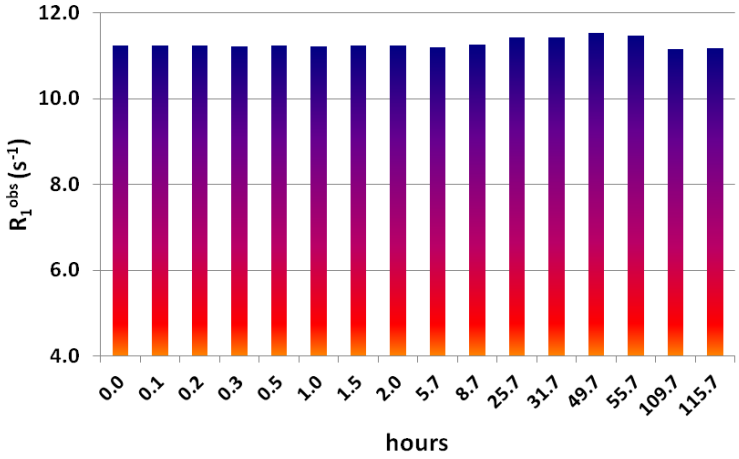

Figure 18. Proton relaxation rate at 0.47 T and 310 K of a 0.98 mM solution of [Mn(dpama)] in Seronorm™ as a function of time.

The proton relaxivity measured in Seronorm™ at 0.47 T and 37 ºC (11.14 mM^{-1} s^{-1}) was found to be significantly higher than that observed in pure water (4.17 mM^{-1} s^{-1}). This prompted us investigate the interaction of the complex with HSA, which is the most common protein present in human blood plasma, through the well-established proton relaxation enhancement technique.[34] Addition of HSA to an aqueous solution of [Mn(dpama)] (0.285 mM, pH 7.2, 310 K) induces a significant increase of the observed longitudinal relaxation rate of water proton nuclei of the solution (Figure 19). The least-squares fit of the relaxometric titration data provide an association constant of 3372 $\pm$ 138 M^{-1}, with a calculated relaxivity for the fully bound form of 12.2 $\pm$ 0.8 mM^{-1} s^{-1}. The ^{1}H nuclear magnetic relaxation dispersion (NMRD) obtained for the fully bound form presents a peak in the region 8-60

MHz, which is characteristic of slowly tumbling systems with long rotational correlation times (Figure 20). This confirms that [Mn(dpama)] binds to HSA, which slows down the rotation of the complex in solution. However, the overall relaxivity determined for the fully bound form is relatively low when compared to other Mn^{2+} complexes that bind HSA,[35] with a rather small relaxivity gain with respect to that of the complex in pure water. Moreover, the peak in the NMRD profile is rather broad and significantly lower than that typical of paramagnetic adducts with HSA.

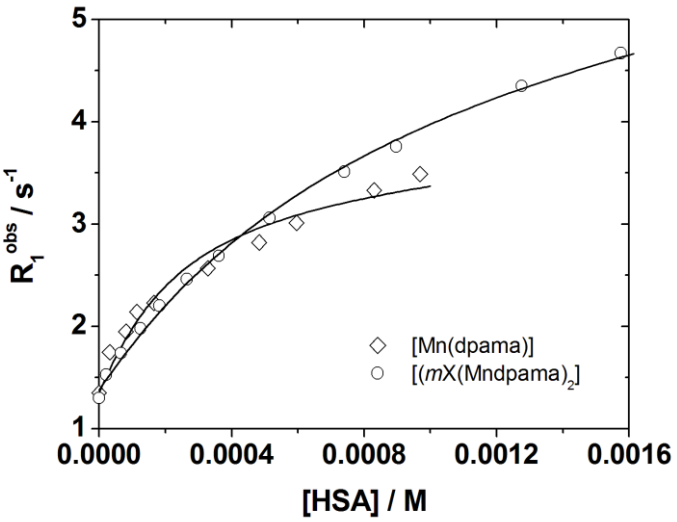

Figure 19. Changes in the observed longitudinal relaxation rates of water protons observed upon addition of HSA to solutions [Mn(dpama)] (0.285 mM) and [(*m*X(Mndpama)$_2$] (0.151 mM) complexes. The solid lines represent the least-squares fits of the data according to a 1:1 binding isotherm.

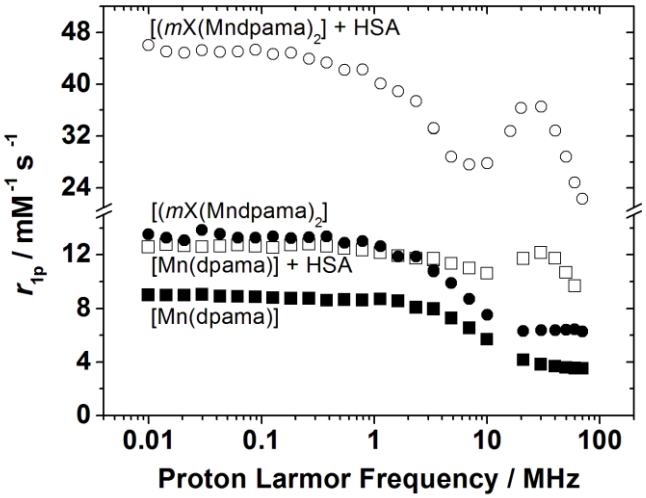

Figure 20. NMRD profiles recorded at 37 ºC for the [Mn(dpama)] and [(*m*X(Mndpama)$_2$] complexes and their fully bound forms to HSA. Note the break in the ordinate axis introduced for better visualization.

Rather, the shape of the profile and the value of r_{1p} corresponding to the maximum of the peak are more similar to those of q=0 Gd^{3+}- and Mn^{2+} chelates bound to HSA.[1,36] This suggests that protein binding results in the replacement of the two water molecules coordinated to Mn^{2+} by donor groups contained in residues of the protein.[37] In light of the results obtained for [Mn(dpama)], we hypothesized that a dimeric analogue of this complex could bind HSA while leaving a complex unit exposed to the solvent, which should result in a sizeable inner-sphere contribution to ^{1}H relaxivity.

The ^{1}H NMRD profile of [(*m*X(Mndpama)$_2$] is characteristic of a Mn^{2+} complex with a low molecular weight, with a single dispersion at 1-10 MHz. Titration of 0.151 mM solution of [(*m*X(Mndpama)$_2$] with HSA (pH = 7.2, 37 ºC) indeed confirmed the binding of the complex to the protein with an association constant of 1125 ± 35 M^{-1} (Figure 19). This association constant is somewhat lower than that obtained for [Mn(dpama)], which indicates that the association with the protein is hindered by the presence of the *m*X(Mndpama) unit. However, the relaxivity of the fully bound form at 20 MHz and 37 ºC (39.0 ± 1.3 mM^{-1} s^{-1}) is very high, confirming that one of the (Mndpama) moieties is exposed to the solvent providing a significant response in terms of relaxivity. Furthermore, the NMRD profile obtained for the fully bound form (Figure 20) is characteristic of a slowly tumbling species with sizeable inner-sphere contribution to relaxivity. It should be noted that this value of r_{1p} represents an average between that of a Mn^{2+} ion with q=0, which contributes to the relaxivity with only the

outer- and second-sphere mechanisms, and that of a q=2 Mn^{2+} ion whose contribution (inner-sphere) is largely dominant. Assuming in first approximation that the contribution of the q=0 Mn^{2+} is similar to that of [Mn(dpama)]-HSA (12.2 mM^{-1} s^{-1}), then we can estimate a relaxivity for the second Mn^{2+} of ca. 66 mM^{-1} s^{-1}.

The binding interaction of [mX(Mn(dpama)$(H_2O)_2)_3$] has been also investigated through the same proton relaxation enhancement (PRE) technique. Similarly, to several previous cases, the data were fitted to a 1:1 binding isotherm even though the presence of multiple affinity sites on HSA cannot be excluded. Titration of a 0.055 mM solution of [mX(Mn(dpama)$(H_2O)_2)_3$] with HSA (pH = 7.2, 20 MHz and 310 K) confirmed the binding of the complex to the protein with an association constant of 1286 ± 55 M^{-1} (Figure 21; Table 5), a value very similar to that assessed for the dimeric derivative. As for [mX(Mn(dpama)$(H_2O)_2)_2$], also the relaxivity of the adduct (45.2 ± 0.6 mM^{-1} s^{-1}) is remarkably high, in line with the reasonable assumption that also in this case a single chelating unit is involved in the binding, while the other two are freely accessible to solvent and responsible for the relaxivity increase. The value of r_1^b is the average relaxivity per Mn^{2+} ion, while the molecular relaxivity (per complex) is 135.6 mM^{-1} s^{-1}. If we assume for the unit with q = 0 (that embedded in the hydrophobic pocket of HSA) the same value of r_1^b found per [Mn(dpama)], then each q = 2 unit is characterized by a relaxivity of about 62 mM^{-1} s^{-1}. This value is quite comparable to that calculated previously for [mX(Mn(dpama)$(H_2O)_2)_2$].

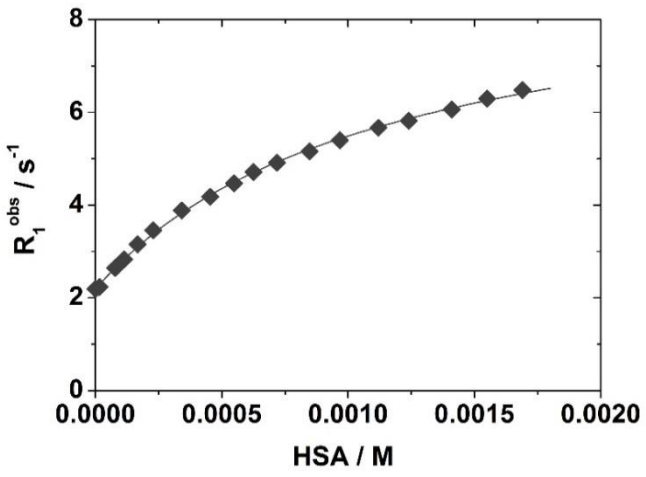

Figure 21. Plot of the water proton longitudinal relaxation rate of a solution of [mX(Mn(dpama)$(H_2O)_2)_3$] (0.055 mM) as a function of HSA concentration at 20 MHz, 310 K and pH = 7.2. The line through the data has been calculated with the parameters of Table 5.

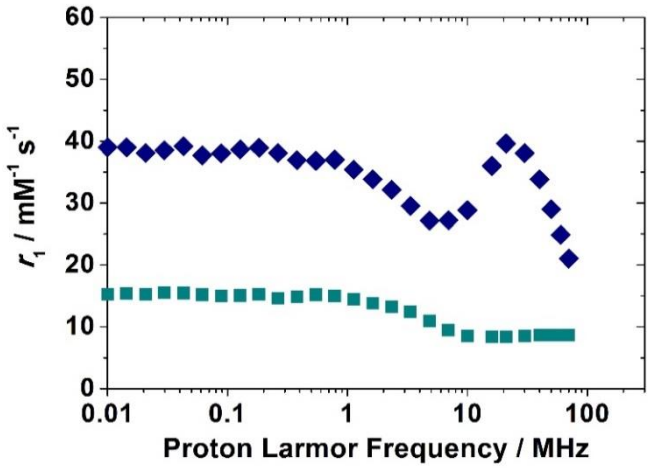

Figure 22. ^{1}H NMRD profiles for [mX(Mn(dpama)(H_2O)$_2$)$_3$] free (bottom) and fully bound to HSA (top) at 310 K and pH = 7.2.

The NMRD profile of the trinuclear complex has been measured for 0.055 mM complex solution in the presence of 1.7 mM HSA at 310 K. Under these conditions, ca. 68% of the complex is bound to the protein. The calculated profile corresponding to the fully bound form is reported in Figure 22 (the r_1^b values are expressed per Mn). The profile is characteristic of a slowly tumbling system with a pronounced peak around 30 MHz and a large relaxivity enhancement over the free complex due to the slow rotation and fast exchange conditions (long τ_R and short τ_M values).

Table 5. Best-fit parameters obtained from the analysis of the ^{1}H relaxometric titrations (20 MHz; 310 K) of the Mn^{2+} complexes with HSA.

	dpama^{2-}	**mX(dpama)$_2^{4-}$**	**mX(dpama)$_3^{6-}$**
$n{\cdot}K_A$ (M^{-1})	3372 ± 138	1125 ± 35	1286 ± 85
r_{1p}^b (mM^{-1} s^{-1})	12.2 ± 0.8	39.0 ± 1.3	45.2 ± 0.6
r_{1p}^f (mM^{-1} s^{-1})[a]	4.2	6.1	8.3

[a] r_{1p}^f is the relaxivity of the free complex

Conclusions:

We have investigated a series of ligands containing pentadentate-coordinating units designed for pentagonal bipyramidal coordination around Mn^{2+}, thanks to the presence of two coordinated water molecules. This imparts remarkably high relaxivities to the solutions of the

corresponding Mn^{2+} complexes. Furthermore, these relaxivities are further improved by interaction with HSA, particularly in the case of the trinuclear Mn^{2+} complex. This property is very interesting for MRI visualization of blood vessels, as well as to improve the residence time of the agent in the blood pool. The Mn^{2+} complexes formed with this family of ligands present moderate thermodynamic stabilities. Although this may not be a very serious limitation due to the far better safety profile of Mn^{2+} compared to Gd^{3+}, it is important to design and develop Mn^{2+} complexes that, while maintaining these favorable relaxometric properties, exhibit improved characteristics of kinetic inertia.

Experimental:

General. Chemicals were purchased from commercial sources and used without further purification. SiO_2 (Fluka, pore size 60 Å, 70-230 mesh) was used for preparative column chromatography. ^1H and ^{13}C NMR spectra were recorded at 25 ºC on a Bruker Avance 500 MHz spectrometer. High resolution ESI-TOF mass spectra were recorded using a **LC-Q-q-TOF Applied Biosystems QSTAR Elite** spectrometer in the positive mode. Elemental analyses were carried out on a ThermoQuest Flash EA 1112 elemental analyzer. IR spectra were recorded using a Bruker Vector 22 spectrophotometer equipped with a Golden Gate Attenuated Total Reflectance (ATR) accessory (Specac).

Equilibrium measurements. All the equilibrium measurements were conducted at a constant ionic strength maintained by 0.15 M NaCl at 298 K. For determining the protonation constants of the $bcpe^{2-}$, $dpama^{2-}$, $mX(dpama)_2^{4-}$ and $mX(dpama)_3^{6-}$ ligands pH-potentiometric titrations were performed with 0.2 M NaOH using 0.002 M ligand solutions. The stability and protonation constants of Mn^{2+} and Zn^{2+} complexes were determined by pH-potentiometric titrations. The metal to ligand concentration ratios were 1:1 for $bcpe^{2-}$ and $dpama^{2-}$, 1:1 and 2:1 for $mX(dpama)_2^{4-}$ and 1:1, 2:1 and 3:1 for $mX(dpama)_3^{6-}$ (the concentration of the ligand was generally 0.002 M). For the calculation of the equilibrium constants the mL base – pH data were used, obtained in the pH range 1.7–12.0. The pH-potentiometric titrations were carried out using a 785 DMP Titrino titration workstation with the use of a *Metrohm-6.0233.100* combined electrode. The titrated solution (8 mL) was thermostated at 25 °C. The samples were stirred and to avoid the effect of CO_2, N_2 gas was bubbled through the solutions. The titrations were performed in the pH range 1.7–12.0. For the calibration of the pH meter, KH-phthalate (pH = 4.002) and borax (pH = 8.970) buffers were used. For the calculation of the H^+ concentration from the measured pH values, the method proposed by

Irving et al. was used.[38] A 0.01 M HCl (0.15 M NaCl) solution was titrated with the 0.2 M NaOH and the difference between the measured and calculated pH values was used to calculate [H^+] from the pH values determined in the titration experiments.

The stability constants of the [Cu(bcpe)] and [Cu(dpama)] complexes have been determined by spectrophotometry, with the use of the competition reactions taking place between the concerned ligand ($bcpe^{2-}$ or $dpama^{2-}$) and $egta^{4-}$ for Cu^{2+} complexation in the pH range 6.8 – 7.2. The concentration of Cu^{2+} and $bcpe^{2-}$ (or $dpama^{2-}$) in the 8 samples was 3 mM, while the concentration of egta was varied between 0 mM and 8 mM. The molar absorptivity of $CuCl_2$ and the complexes [Cu(dpama)], [Cu(bcpe)] and $[Cu(EGTA)]^{2-}$ were determined in 1.5 mM, 3.0 mM and 4.5 mM solutions. The absorbance and pH values were determined in the samples after the equilibrium was reached (the time needed to reach the equilibria was determined by spectrophotometry). Spectrophotometric measurements were made between 700 and 800 nm at 11 wavelength values. The spectrophotometric measurements were recorded with the use of 1.0 cm cells using a Cary 1E spectrophotometer at 298 K. For the calculation of the equilibrium constants, the PSEQUAD program was used.[84]

^{1}H NMRD and ^{17}O NMR measurements. The water proton longitudinal relaxation rates as a function of pH (20 MHz) were measured with a Stelar Spinmaster Spectrometer FFC–2000 (Mede, PV, Italy) on about 0.6-2.0 mM aqueous solutions. The exact concentrations of Mn^{2+} ions were determined by measurement of bulk magnetic susceptibility shifts of a *t*BuOH signal on a Bruker Avance III spectrometer (11.7 T). The ^{1}H T_1 relaxation times were acquired by the standard inversion recovery method with typical 90° pulse width of 3.5 μs, 16 experiments of 4 scans. The temperature was controlled with a Stelar VTC-91 airflow heater equipped with a calibrated copper–constantan thermocouple (uncertainty of ±0.1 °C). The proton $1/T_1$ NMRD profiles were measured on a fast field-cycling Stelar SmartTracer relaxometer over a continuum of magnetic field strengths from 0.00024–0.25 T (corresponding to 0.01–10 MHz proton Larmor frequencies). Additional data points in the range 15–70 MHz were obtained on a Stelar Relaxometer equipped with a Bruker WP80 NMR electromagnet adapted to variable-field measurements (15–80 MHz proton Larmor frequency). Variable-temperature ^{17}O NMR measurements were recorded on a Bruker Avance III spectrometer (11.7 T) equipped with a 5 mm probe and standard temperature control unit. An aqueous solution of the complex (4 mM) containing 2.0% of the ^{17}O isotope (Cambridge Isotope) was used. The observed transverse relaxation rates were calculated from the signal width at half-height.

References:

1. C. F. G. C. Geraldes, A. D. Sherry, R. D. Brown III, S. H. Koenig, *Magn. Reson. Med.*, **1986**, 3, 242.
2. S. M. Rocklage; W. P. Cacheris, S. C. Quay, F. E. Hahn, K. N. Raymond, *Inorg. Chem.*, **1989**, 28, 477.
3. (a) M. Rief; P. Asbach, T. Franiel, M. Taupitz, B. Hamm, M. Wagner, *Contrast Media Mol. Imaging*, **2009**, 4, 267. (b) N. Albiin, N. Kartalis, A. Bergquist, B. Sadigh, T. B. Brismar, *Magn. Reson. Mater. Phy.,* **2012**, 25, 361.
4. J. O. G. Karlsson, L. J. Ignarro, I. Lundström, P. Jynge, T. Almén, *Drug Discov Today,* **2015**, 20, 411.
5. P. Caravan, C. T. Farrar, L. Frullano, R. Uppal, *Contrast Media Mol. Imaging*, **2009**, 4, 89.
6. (a) Z. Baranyai, M. Botta, M. Fekete, G. B. Giovenzana, R. Negri, L. Tei, C. Platas-Iglesias, *Chem. Eur. J.,* **2012**, 18, 7680. (b) R. Negri, Z. Baranyai, L. Tei, G. B. Giovenzana, C. Platas-Iglesias, A. Bényei, J. Bodnár, A. Vágner, M. Botta, *Inorg. Chem.*, **2014**, 53, 12499. (c) S. Aime, E. Gianolio, D. Corpillo, C. Cavallotti, G. Palmisano, M. Sisti, G. B. Giovenzana, R. Pagliarin, *Helv. Chim. Acta*, **2003**, 86, 615. (d) S. Aime, L. Calabi, C. Cavallotti, E. Gianolio, G. B. Giovenzana, P. Losi, A. Maiocchi, G. Palmisano, M. Sisti, *Inorg. Chem.*, **2004**, 43, 7588. (e) J. Costa, É. Tóth, L. Helm, A. E. Merbach, *Inorg. Chem.*, **2005**, 44, 4747. (f) L. Moriggi, C. Cannizzo, C. Prestinari, F. Berrière, L. Helm, *Inorg. Chem.,* **2008**, 47, 8357. (g) E. M. Gale, N. Kenton, P. Caravan, *Chem. Commun.,* **2013**, 49, 8060.
7. B. Drahos, J. Kotek, I. Císarová, P. Hermann, L. Helm, I. Lukes, É. Tóth, *Inorg. Chem.*, **2011**, 50, 12785.
8. (a) G. S. Loving, S. Mukherjee, P. Caravan, *J. Am. Chem. Soc.*, **2013**, 135, 4620. (b) E. M. Gale, S. Mukherjee, C. Liu, G. S. Loving, P. Caravan, *Inorg. Chem.* **2014**, 53, 10748.
9. P. B. Tsitovich, P. J. Burns, A. M. McKay, J. R. Morrow, *J. Inorg. Biochem.* **2014**, 133, 143.
10. R. Ferreirós-Martínez, D. Esteban-Gómez, C. Platas-Iglesias, A. de Blas, T. Rodríguez-Blas, *Dalton Trans*., **2008**, 5754.
11. E. Boros, C. L. Ferreira, J. F. Cawthray, E. W. Price, B. O. Patrick, D. W. Wester, M. J. Adam, C. Orvig, *J. Am. Chem. Soc.*, **2010**, 132, 15726.
12. E. Boros, J. F. Cawthray, C. L. Ferreira, B. O. Patrick, M. J. Adam, C. Orvig, *Inorg. Chem.,* **2012**, 51, 6279.
13. R. Fornasier, D. Milani, P. Scrimin, U. Tonellato, *J. Chem. Soc., Perkin Trans.,* **1986**, 233.
14. A. Pellissier, Y. Bretonniere, N. Chatterton, J. Pecaut, P. Delangle, M. Mazzanti, *Inorg. Chem.,* **2007**, 46, 3714.
15. O. Jons, E. S. Johansen, *Inorg. Chim. Acta,* **1988**, 151, 129.
16. S. W. Benson, *J. Am. Chem. Soc.,* **1958**, 80, 5151.
17. R. Artali, Z. Baranyai, M. Botta, G. B. Giovenzana, A. Maspero, R. Negri, G. Palmisano, M. Sisti, S. Tollari, *New J. Chem.* **2015**, 39, 539.
18. H. Irving, R. J. P. Williams, *J. Chem. Soc.* **1953**, 3192.
19. M. Regueiro-Figueroa, L. M. P. Lima, V. Blanco, D. Esteban-Gómez, A. de Blas, T. Rodríguez-Blas, R. Delgado, C. Platas-Iglesias, *Inorg. Chem.*, **2014**, 53, 12859.
20. D. Esteban-Gómez, C. Cassino, M. Botta, C. Platas-Iglesias, *RSC Adv.,* **2014**, 4, 7094.
21. G. A. Rolla, C. Platas-Iglesias, M. Botta, L. Tei, L. Helm, *Inorg. Chem.*, **2013**, 52, 3268.
22. B. Drahos, J. Kotek, P. Hermann, I. Lukes, É. Tóth, *Inorg. Chem.*, **2010**, 49, 3224
23. The Chemistry of Contrast Agents in Medical Magnetic Resonance Imaging (Eds: A. E. Merbach, L. Helm, É. Tóth), *Second Edition, Wiley*, New York, **2013**.
24. E. Balogh, Z. He, W. Hsieh, S. Liu, É. Tóth, *Inorg. Chem*., **2007**, 46, 238.

25. J. H. Freed, *J. Chem. Phys.*, **1978**, 68, 4034.
26. B. Drahos, M. Pniok, J. Havlícková, J. Kotek, I. Císarová, P. Hermann, I. Lukes, É. Tóth, *Dalton Trans.,* **2011**, 40, 10131.
27. L. Tei, G. Gugliotta, M. Fekete, F. K. Kálmán, M. Botta, *Dalton Trans*., **2011**, 40, 2025.
28. T. J. Swift, R. E. Connick, *J. Chem. Phys.,* **1962**, 37, 307.
29. J. R. Zimmermann, W. E. Brittin, *J. Phys. Chem.*, **1957**, 61, 1328.
30. Z. Luz, S. Meiboom, *J. Chem. Phys.,* **1964**, 40, 2686.
31. S. H. Koenig, R. D. Brown III, *Prog. Nucl. Magn. Reson. Spectrosc.*, **1991**, 22, 487.
32. (a) E. M. Gale, J. Zhu, P. Caravan, *J. Am. Chem. Soc.,* **2013**, 135, 18600. (b) J. Zhu, E. M. Gale, I. Atanasova, T. A. Rietz, P. Caravan, *Chem. Eur. J.,* **2014**, 20, 14507.
33. E. Molnar, N. Camus, V. Patinec, G. A. Rolla, M. Botta, G. Tircso, F. K. Kalman, T. Fodor, R. Tripier, C. Platas-Iglesias, *Inorg. Chem.,* **2014**, 53, 5136
34. S. Aime, M. Botta, M. Fasano, S. Geninatti Crich, E. Terreno, *J. Biol. Inorg. Chem.*, **1996**, 1, 312.
35. S. Aime, P. L. Anelli, M. Botta, M. Brocchetta, S. Canton, F. Fedeli, E. Gianolio, E. Terreno, *J. Biol. Inorg. Chem.,* **2002**, 7, 58.
36. P. Caravan, N. J. Cloutier, M. T. Greenfield, S. A. McDermid, S. U. Dunham, J. W. M. Bulte, J. C. Amedio, Jr., R. J. Looby, R. M. Supkowski, W. DeW. Horrocks, Jr., T. J. McMurry, R. B. Lauffer, *J. Am. Chem. Soc.* **2002**, 124, 3152
37. G. Fanali, Y. Cao, P. Ascenzi, M. Fasano, *J. Inorg. Biochem.* **2012**, 117, 198.
38. H. M. Irving, M. G. Miles, L. Pettit, *Anal. Chim. Acta,* **1967**, 38, 475.

Chapter 5

Developing the Family of Picolinate Ligands for Mn^{2+} Complexation

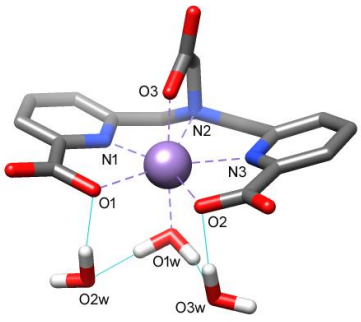

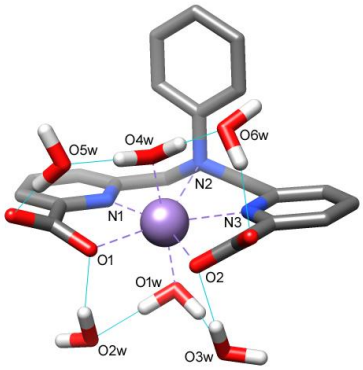

Introduction:

In general, the design of Mn^{2+}-based MRI contrast agents represents a challenge for coordination chemistry. Indeed, a Mn^{2+} complex should fulfil a number of requisites to become a potential candidate as a contrast agent:

i) a high thermodynamic and kinetic stability to avoid the release of the toxic Mn^{2+} ion. The lack of a crystal field stabilization energy associated with the high-spin d^5 configuration results in rather low thermodynamic stabilities of Mn^{2+} complexes, which are also generally rather labile with respect to complex dissociation;[1]

ii) the presence of at least one water molecule coordinated to the metal ion that exchanges rapidly with the bulk water, thereby imparting an efficient pathway to accelerate the relaxation rates of water proton nuclei. It is worth noting that Mn^{2+} chelates with high thermodynamic stability such as $[Mn(DOTA)]^{2-}$ and $[Mn(DO3A)]^{-}$ do not contain coordinated water molecules;[2]

iii) a good redox stability to avoid the oxidation of Mn^{2+} to Mn^{3+}, which generally provides lower relaxivities. However, redox Mn^{2+}/Mn^{3+} potentials accessible to biologically relevant reducing agents can be potentially exploited to design redox-activated MRI probes.[3,4]

Based on the previous results, we decided to expand the family of ligands containing picolinate groups by investigating the pentadentate ligand H_2DPAPhA and the hexadentate derivative H_3DPAA. The latter ligand was reported previously by M. Mazzanti and studied in the context of Gd^{3+} MRI CAs.[5] Furthermore, we also examined two lipophilic derivatives of H_2DPAMA and H_2PhDPAMA, which contain a dodecyl side chain attached to the amine nitrogen atom of H_2DPAMA or a hexyl chain at the aniline function of H_2DPAPhA, respectively. These lipophilic derivatives were designed to form micelles in solution and to bind HSA in a non-covalent fashion. Both effects are expected to increase the observed relaxivity by slowing down the rotation of the complex in solution. We report the synthesis and acid-base properties of the ligands, the stability constants of the Mn^{2+} complexes in solution, and a full physicochemical characterization of the chelates using ^{1}H and ^{17}O relaxometric techniques and theoretical (DFT) calculations.

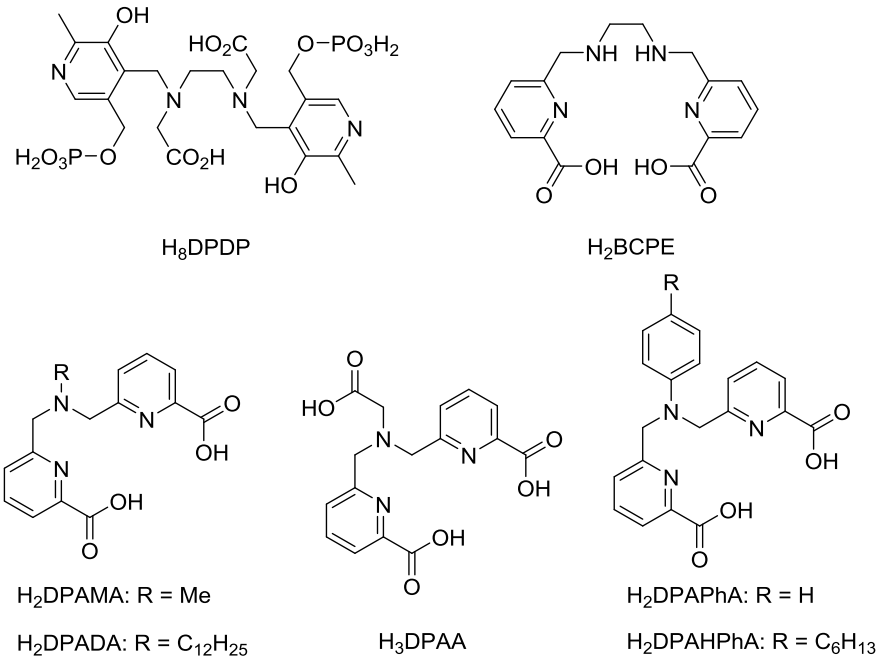

Scheme 1. Structures of the ligands presented in this chapter.

***Synthesis of the Ligands*:**

Prof. Carlos Platas Iglesias provided the ligands discussed in this chapter, which were synthesized following the two-step procedure shown in Scheme 2. The first step consisted in the reaction of 6-chloromethylpyridine-2-carboxylic acid ethyl ester with the appropriate amine in the presence of K_2CO_3 as a base. It is worth mentioning that the reactions with anilines required rather harsh conditions involving heating for prolonged periods and addition of catalytic KI. The ester intermediates were isolated in rather good yields (65-72%) after purification with column chromatography. Hydrolysis of the methyl ester groups (and the amide group of the precursor of H_3DPAA) provided the target ligands as the hydrochloride salts with good overall yields (52-61%).

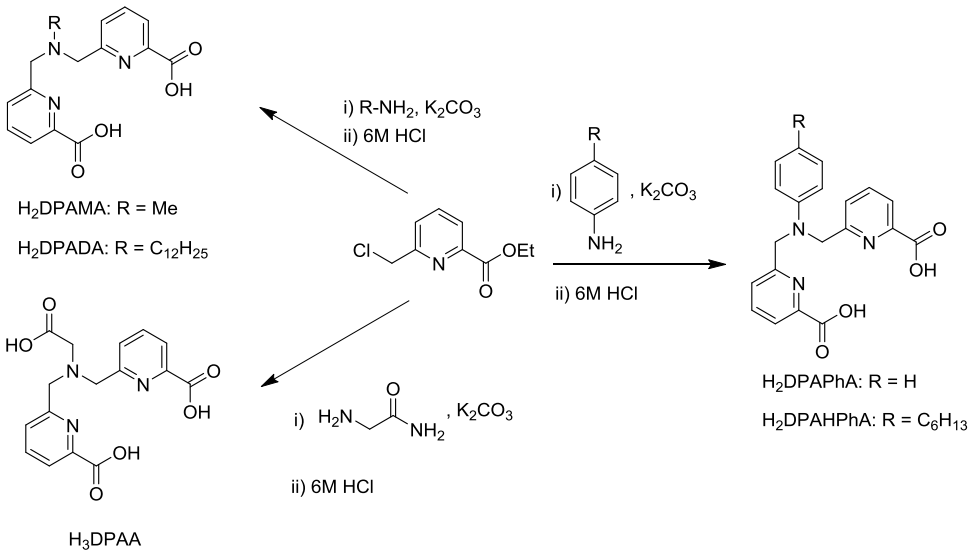

Scheme 2. Synthesis of the ligands.

Ligand protonation constants and stability constants of the Mn^{2+} complexes:

The protonation constants of the $DPAPhA^{2-}$ and $DPAA^{3-}$ were determined by potentiometry, in 0.15 NaCl. The ligand protonation constants are defined as in Eq 1.

$$H_{i-1}L + H^{+} \rightleftharpoons H_iL$$

$$K_i^H = \frac{[H_iL]}{[H_{i-1}L][H^{+}]} \qquad i=1, 2,\ldots, 8. \qquad (1)$$

The protonation constants, with their corresponding standard deviations are listed in Table 1. For the $DPAA^{3-}$ four protonation constants could be determined, indicating the stepwise protonation of the amine nitrogen atom and all the three carboxylate groups of the ligand. The first two protonation constants of $DPAA^{3-}$ are very similar to $DPAMA^{2-}$ ligand. These protonation processes are assigned to the protonation of the amine nitrogen atom (K_1^H) and one of the carboxylate groups of the picolinate arms (K_2^H). The first protonation constant of $DPAPhA^{2-}$ ($\log K_1^H = 5.48(4)$) is ca. two orders of magnitude lower than those determined for $DPAA^{3-}$ and $DPAMA^{2-}$, in line with the lower basicity of anilines compared to aliphatic amines.[7] In the case of $DPAPhA^{2-}$ four protonation constants could be determined, indicating the protonation of the aniline nitrogen atom, two carboxylate groups and likely a nitrogen atom of a pyridine moiety.

Table 1. Ligand protonation constants and stability and protonation constants of the corresponding Mn^{2+} complexes determined using potentiometric titrations (25 ºC, 0.15 M NaCl).[b]

	$DPAA^{3-}$	$DPAPhA^{2-}$	$DPAMA^{2-}$	$EDTA^{4-}$ [a]
$\log K_1^H$	7.26(2)	5.48(4)	7.82	10.17
$\log K_2^H$	3.90(3)	4.51(4)	3.71	6.11
$\log K_3^H$	3.29(2)	4.28(4)	2.61	2.68
$\log K_4^H$	1.77(2)	2.70(4)		
$\sum \log K_i^H$	16.22	16.97	14.14	
$\log K_{MnL}$	13.19(5)	9.55(1)	10.13	13.88
$\log K_{MnLH}$	2.90(6)	4.84(1)	2.57	
$\log K_{MnLH2}$		2.51(1)		
$\log K_{MLOH}$	11.97(6)		11.09	
pMn[c]	8.98	7.27	7.28	7.95

[a] Data from reference 6. [b] Defined as $-\log[Mn]_{free}$ with pH = 7.4, $[Mn^{2+}] = [L] = 10^{-5}$ M.

As a result, the $DPAA^{3-}$ and $DPAPhA^{2-}$ ligands present very similar overall basicities, as estimated by the $\sum \log K_i^H$ values (i = 1-4). The protonation constants determined for $DPAA^{3-}$ in 0.15 M NaCl are in general good agreement with those reported by Mazzanti in 0.1 M KCl ($\log K_1^H = 7.33$, $\log K_2^H = 3.8$ and $\log K_3^H = 2.9$).[5]

The stability and protonation constants of the Mn^{2+} complexes of $DPAA^{3-}$ and $DPAPhA^{2-}$ were determined by using direct potentiometric pH-titrations. The stability constants and protonation constants of the complexes are defined in Eqs 2 and 3:

$$K_{ML} = \frac{[ML]}{[M][L]} \qquad (2)$$

$$K_{H_iL} = \frac{[MH_iL]}{[MH_{i-1}L][H^+]} \qquad \text{with } i = 1, 2 \qquad (3)$$

The titration curve of the $Mn^{2+}/DPAA^{3-}$ system evidenced the formation of a hydroxo complex characterized by protonation constant K_{MLOH} defined as:

$$K_{MLOH} = \frac{[ML]}{[ML(OH)][H^+]} \qquad (4)$$

The stability constant of the [Mn(DPAMA)] complex is higher than [Mn(DPAPhA)] which is likely related to the weaker coordination of the aniline nitrogen atom of $DPAPhA^{2-}$ compared to the amine nitrogen atom of $DPAMA^{2-}$. The presence of an additional carboxylate group in $DPAA^{3-}$ increases the stability of the Mn^{2+} complex by three orders of magnitude with respect to $DPAMA^{2-}$. As a result, the stability constant of the $[Mn(DPAA)]^-$ complex ($\log K_{ML}$ = 13.19(5)) is close to the EDTA analogue ($\log K_{ML}$ = 13.88).[8]

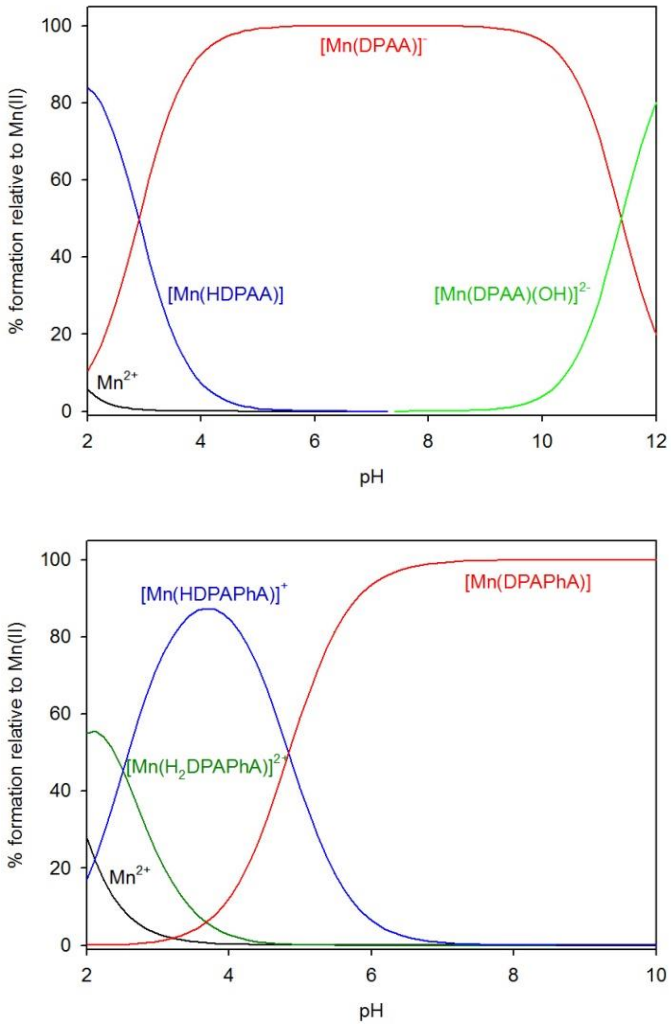

Figure 1. Species distribution diagrams calculated for the $H_3DPAA:Mn^{2+}$ (top) and $H_2DPAPhA:Mn^{2+}$ (bottom) systems. [L] = $[Mn^{2+}] = 10^{-3}$ M.

Figure 1 presents the species distribution diagrams calculated using the equilibrium constants reported in Table 1. The $[Mn(DPAA)]^-$ species is the most abundant in a wide range of pH from ca. 2.8 to 11.4. The formation of the hydroxo $[Mn(DPAA)(OH)]^{2-}$ species occurs above pH ~ 10, while below pH ~ 5.0 the protonation of the complex is observed. Dissociation of the complex takes place at a rather low pH, with only 5.6% of the manganese under the form of $[Mn(H_2O)_6]^{2+}$ at pH 2.0.

The dissociation of [Mn(DPAPhA)] starts at higher pH than for $[Mn(DPAA)]^-$, as 27.8% of the complex is dissociated at pH 2.0. However, the degree of dissociation of the complex at pH 2.0 is even higher in the case of [Mn(DPAMA)] (77.7%). [Mn(DPAPhA)] forms protonated species at higher pH (< 7.0).

A comparison of the thermodynamic stabilities of complexes with different ligands is more properly given by the pMn values ($pMn = -\log[Mn^{2+}]_{free}$) defined using the conditions suggested by Drahos[9] (pH = 7.4, $[Mn^{2+}] = [L] = 10^{-5}$ M). The pMn values calculated for [Mn(DPAMA)] and [Mn(DPAPhA)] are almost identical (7.3, Table 1) and somewhat lower than that of $[Mn(EDTA)]^{2-}$. The latter complex serves as a reference for potential MRI applications, as $[Mn(EDTA)]^{2-}$ derivatives have been successfully used for in vivo MRI studies.[10] Interestingly, the $[Mn(DPAA)]^-$ complex presents a pMn value one order of magnitude higher than $[Mn(EDTA)]^{2-}$ and very close to that reported for $[Mn(DOTA)]^{2-}$,[11] which highlights its remarkable thermodynamic stability at physiological pH.

^{1}H NMRD and ^{17}O NMR studies of the [Mn(DPAPhA)] and $[Mn(DPAA)]^-$ complexes:

The relaxivity determined for $[Mn(DPAA)]^-$ at pH 7.4 (25 ºC, 20 MHz) is 3.6 mM^{-1} s^{-1}, a value that is close to that reported to monohydrated complexes such as $[Mn(EDTA)]^{2-}$ (3.3 mM^{-1} s^{-1} at pH 7.4, 25 ºV and 20 MHz). The r_{1p} value for [Mn(DPAPhA)] under the same conditions (6.7 mM^{-1} s^{-1}) is remarkably higher, which indicates the presence of two coordinated water molecules (Fig 2).

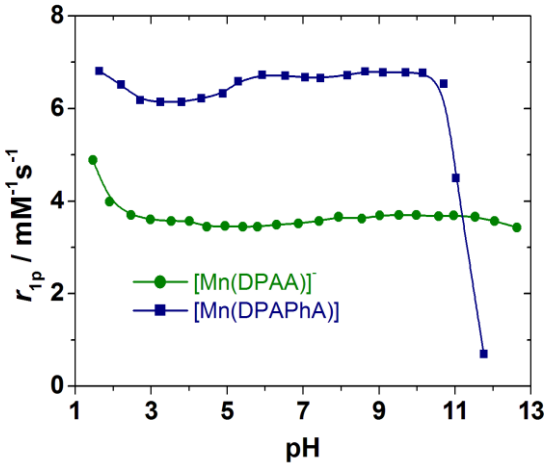

Figure 2. Plot of the ^{1}H relaxivities (20 MHz, 25 ºC) of [Mn(DPAPhA)] and [Mn(DPAA)]$^-$ as a function of pH.

The relaxivity of [Mn(DPAA)]$^-$ remains fairly constant (r_{1p} = 3.60 $\pm$ 0.15 at 25 ºC, 20 MHz)) in a broad pH range from 2.5 to 11.5. Below pH 2.5 relaxivity increases due to the dissociation of the complex and formation of $[Mn(H_2O)_6]^{2+}$, while the slight decrease in relaxivity observed at pH > 11.5 is attached to the formation of a hydroxo complex. Thus, the pH dependence of r_{1p} is in perfect agreement with the speciation in solution obtained from potentiometric measurements (Fig 1).

The relaxivity of [Mn(DPAPhA)] is constant in the pH range 5.9-10.2, dropping quickly at more basic pH due to the dissociation of the complex and precipitation of $Mn(OH)_2$.[12] ^{1}H relaxivity decreases from 6.7 at pH 5.9 to 6.1 at pH 3.3. This effect can be attributed to the formation of the protonated [Mn(HDPAPhA)]$^+$ species (logK_{MnLH} = 4.84(1), see above). Dissociation of the complex below pH ~ 2.7 is responsible for the slight increase in relaxivity under acidic conditions.

Proton nuclear magnetic relaxation dispersion (^{1}H NMRD) profiles were recorded in the proton Larmor frequency range 0.01−70 MHz (corresponding to magnetic field strengths varying between 2.343×10^{-4} and 1.645 T) of aqueous solutions [Mn(DPAPhA)] and [Mn(DPAA)]$^-$ (Fig 3). The relaxivities of both complexes decrease with increasing temperature, as expected for small chelates in which fast rotation in solution limits proton relaxivity. The NMRD profiles present a single dispersion in the range 1 - 10 MHz, which excludes rules out a sizeable scalar contribution to ^{1}H relaxivity.[13,14]

Reduced transverse ^{17}O NMR relaxation rates of aqueous solutions of the [Mn(DPAPhA)] and [Mn(DPAA)]$^-$ complexes were recorded to gain more insight into the physicochemical

parameters that govern the relaxivities of these systems (Fig 4). The $1/T_{2r}$ values increase with decreasing temperature, reach a maximum and then decrease at lower temperatures. This is typical of systems that present a changeover from a fast exchange regime at high temperatures to a slow exchange at low temperatures.[15] The lower temperature at which the maximum $1/T_{2r}$ value is observed for $[Mn(DPAA)]^-$ (ca. 15 ºC) compared with [Mn(DPAPhA)] (~23 ºC) is indicative of a somewhat faster water exchange rate in the former.

A simultaneous fitting of the ^1H NMRD and ^{17}O NMR data of the two complexes was carried out by using the method previously detailed in Chapter 4. Since the NMRD and ^{17}O NMR data depend upon a relatively large number of parameters some of them had to be fixed during the fitting procedure to achieve a reliable analysis. The distance of closest approach for the outer-sphere contribution a_{MnH} was fixed at 3.6 Å during the fitting procedure, while the distances between the proton nuclei of the coordinated water molecules and the Mn^{2+} ion (r_{MnH}) were fixed at values corresponding to the average Mn···H distances obtained from DFT calculations (2.756 and 2.782 Å for $[Mn(DPAA)]^-$ and [Mn(DPAPhA)], respectively). The number of water molecules in the inner coordination sphere of Mn^{2+} was fixed to q=2 for [Mn(DPAPhA)] and q=1 for $[Mn(DPAA)]^-$. The diffusion coefficient, D_{MnH}^{298}, and its activation energy, E_{DMnH}, were fixed to the values for the self-diffusion of water molecules in pure water.[16] The parameters obtained from the fittings are provided in Table 9, while the curve fits are shown in Figures 3 and 4.

The water exchange rate determined for $[Mn(DPAA)]^-$ ($k_{ex}^{298}=12.6\times10^7$ s^{-1}) is about twice that measured for [Mn(DPAPhA)] ($k_{ex}^{298}=5.6\times10^7$ s^{-1}). Both complexes present lower water exchange rates than $[Mn(EDTA)]^{2-}$,[17] approaching that determined for the aquated ion $[Mn(H_2O)_6]^{2+}$ ($k_{ex}^{298}=2.8\times10^7$ s^{-1}).[14] DFT calculations performed in aqueous solution at the TPSSh/TZVP level provide some insight into the different water exchange rates determined for [Mn(dpaPha)] and $[Mn(dpaa)]^-$ (Fig 5). In these calculations, we included two second-sphere water molecules involved in hydrogen bonding with each coordinated water molecule, while bulk solvent effects were considered using a polarized continuum model. This mixed cluster/continuum approach was shown to provide accurate Mn-O_{water} distances and ^1H and ^{17}O hyperfine coupling constants of the coordinated water molecules. The optimized geometries of the $[Mn(DPAPhA)(H_2O)_2]\cdot4H_2O$ and $[Mn(DPAA)(H_2O)]^-\cdot2H_2O$ systems indicate pentagonal bipyramidal coordination environments around the Mn^{2+} ion. The equatorial plane of the bipyramid is delineated by the amine nitrogen atom and the donor atoms of the picolinate units. In the case of $[Mn(DPAPhA)(H_2O)_2]\cdot4H_2O$ two coordinated

water molecules occupy the apical positions, while for $[Mn(DPAA)(H_2O)]^-\cdot 2H_2O$ the apical positions contain a coordinated water molecule and an oxygen atom of the acetate group of the ligand.

Table 2. Parameters obtained from the simultaneous analysis of ^{17}O NMR and ^{1}H NMRD data.[a]

	[Mn(DPAA)]$^-$	[Mn(DPAPhA)]	[Mn(DPAMA)]	[Mn(EDTA)]$^{2-}$[b]	$[Mn(H_2O)_6]^{2+}$
r_{1p} at 25/37 ºC / $mM^{-1}\ s^{-1}$ [b]	3.5/2.7	6.6/5.1	5.3/4.2	3.3/2.8	
k_{ex}^{298}/ $10^7\ s^{-1}$	12.6 ± 0.5	5.6 ± 0.6	30.6	47.1	2.82
$\Delta H^{\ddagger}$ / kJ mol^{-1}	42.7 ± 1.0	27.2 ± 2.3	28.1	33.5	45.6
τ_R^{298} / ps	47.6 ± 0.2	81.0 ± 0.5	47.8	57	30.0
E_r / kJ mol^{-1}	22.8 ± 0.4	27.0 ± 2.6	25.3	21.8	16.7
τ_V^{298}/ ps	19.4 ± 0.2	15.6 ± 0.1	39.2	27.9	10.0
E_v / kJ mol^{-1}	1.0[a]	1.0[a]	1.0[a]	1.0[a]	14.6
D_{MnH}^{298} / $10^{-10}\ m^2\ s^{-1}$	22.4[a]	22.4[a]	22.4[a]	23.1	23.0[a]
E_{DMnH} / kJ mol^{-1}	17.3[a]	17.3[a]	17.3[a]	18.9	29.7
Δ^2 / $10^{19}\ s^{-2}$	5.5 ± 0.2	11.5 ± 0.4	2.38	6.9	0.6
$A_O/\hbar$/ 10^6 rad s^{-1}	-31.5 ± 0.6	-25.0 ± 0.6	-45.8	-40.5	-34.6
r_{MnH}/Å	2.756[a]	2.782[a]	2.74[a]	2.83[a]	2.83
a_{MnH}/Å	3.6[a]	3.6[a]	3.6[a]	3.6[a]	3.6
q^{298}	1[a]	2[a]	2[a]	1[a]	6

[a] Parameters fixed during the fitting procedure. [b] Data from Ref 17

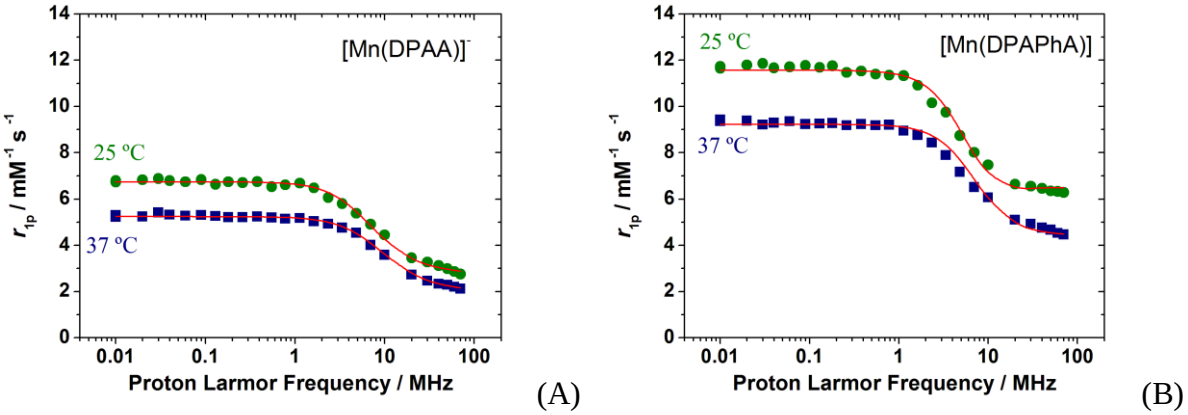

Figure 3. ^{1}H NMRD profiles recorded at different temperatures for $[Mn(DPAA)]^-$ and [Mn(DPAPhA)]. The lines represent the fit of the data as explained in the text.

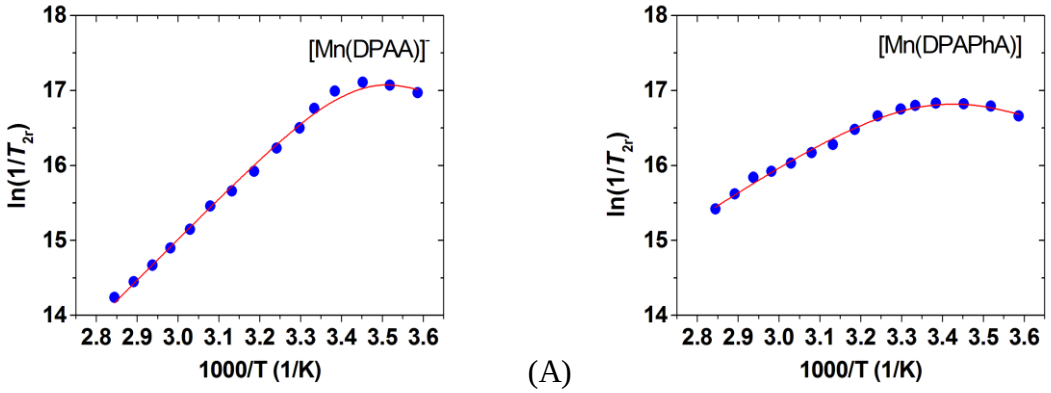

Figure 4. Reduced transverse ^{17}O NMR relaxation rates versus reciprocal temperature measured for $[Mn(DPAA)]^-$ and [Mn(DPAPhA)] at 11.74 T. The lines represent the fit of the data as explained in the text.

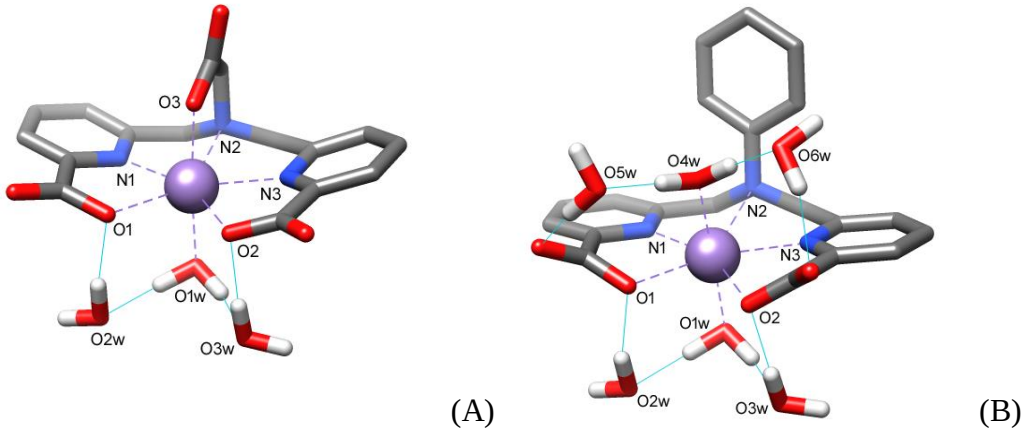

Figure 5. Structures of the $[Mn(DPAA)(H_2O)]^-\cdot 2H_2O$ and $[Mn(DPAPhA)(H_2O)_2]\cdot 4H_2O$ systems obtained with DFT calculations (TPSSh/TZVP). Calculated bond distances (Å): $[Mn(DPAA)(H_2O)]^-\cdot 2H_2O$, Mn-N(1), 2.314; Mn-N(2), 2.521; Mn-N(3), 2.316 ; Mn-O(1), 2.289; Mn-O(2), 2.291; Mn-O(1w), 2.288; Mn-O(3), 2.131; Mn-O(4w). $[Mn(DPAPhA)(H_2O)_2]\cdot 4H_2O$, Mn-N(1), 2.285; Mn-N(2), 2.885; Mn-N(3), 2.268; Mn-O(1), 2.225; Mn-O(2), 2.289; Mn-O(1w), 2.250; Mn-O(3); Mn-O(4w), 2.237.

Prof. Carlos-Platas Iglesias performed the DFT calculations briefly described here. The calculated Mn-O_{water} distances involving the coordinated water molecule(s) are 2.288 Å for $[Mn(DPAA)(H_2O)]^-\cdot 2H_2O$ and 2.237 and 2.250 Å for $[Mn(DPAPhA)(H_2O)_2]\cdot 4H_2O$. Thus, the Mn-$O_{water}$ distance in $[Mn(DPAA)(H_2O)]^-$ is significantly longer than those of the complex with $dpaPha^{2-}$, revealing a weaker binding of the coordinated water molecule in the

former. Water exchange in these seven-coordinated complexes is expected to follow a dissociatively activated mechanism, the rate determining step being the rupture of the $Mn\text{-}O_{water}$ bond to give a six-coordinated transition state. Thus, the strongest is the $Mn\text{-}O_{water}$ bond the slowest is expected to be the water exchange process. Similar trends correlation the strength of the $Gd\text{-}O_{water}$ bonds and the corresponding water exchange rates were observed for nine-coordinate Gd^{3+} complexes undergoing dissociatively activated water exchange processes.[18]

The values obtained for the ^{17}O hyperfine coupling constants are in the low part of the range typically observed for Mn^{2+} complexes ($A_O/\hbar = 25\times 10^6$ to 47×10^6 rad s^{-1}), being very similar to the value reported for $[Mn(H_2O)_6]^{2+}$ and other small complexes.[19] Concerning the parameters related to the electron spin relaxation of the metal ion (the electronic correlation time for the modulation of the zero-field-splitting interaction, τ_v, and the mean square zero-field-splitting energy, Δ^2), the parameters obtained from the analysis of NMRD and ^{17}O NMR data are similar to those obtained for other Mn^{2+} complexes (Table 2).

Characterization of the lipophilic derivatives [Mn(DPAHPhA)] and [Mn(DPADA)]:

The critical micelle concentration (cmc) of [Mn(DPAHPhA)] and [Mn(DPADA)] was investigated by using relaxometric measurements at 20 MHz and 25 ºC.[20] The paramagnetic relaxation enhancement of water proton nuclei (R_1^{obs}) increased linearly with the concentration of [Mn(DPAHPhA)] complex in the range 0.07-0.61 mM (Figure 6.). The slope of the linear plot provides a relaxivity of the non-aggregated form of 4.1 mM^{-1} s^{-1}. This value is consistent with that obtained from NMRD studies, which confirm the lack of self-aggregation of the complex under these conditions (Figure 7.). Precipitation of the complex was observed at higher concentrations, thus preventing cmc determination. Surprisingly, the relaxivity determined for [Mn(DPAHPhA)] is considerably lower than that of the bis-hydrated [Mn(DPAPhA)] complex (6.6 mM^{-1} s^{-1}), which suggests that the introduction of the hexyl chain in the ligand scaffold lowers the hydration number of the complex.

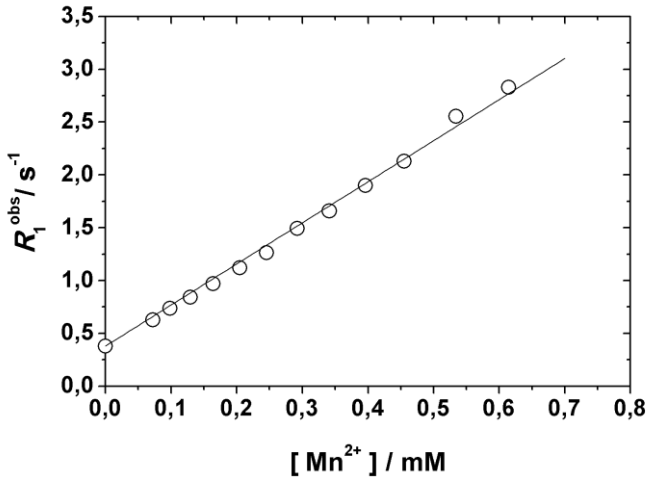

Figure 6. Determination of the CMC of the [Mn(DPAHPhA)] at 20 MHz and 298 K**.**

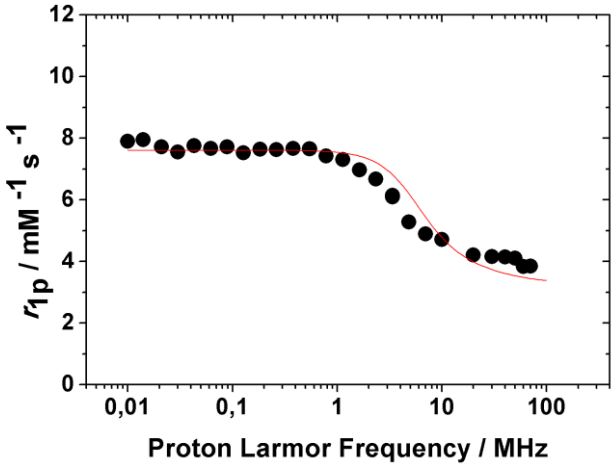

Figure 7. ^{1}H NMRD profile recorded at 298K for [Mn(DPAHPhA)] The line represent the fit of the data as explained in the text.

The R_1^{obs} values measured from solutions of [Mn(DPADA)] present two linear ranges with an inflection point at a complex concentration of ~0.1 mM (Figure 8.). The analysis of the data provides a cmc of 96(9) μM with relaxivity values of r_{1p} = 5.3 mM^{-1} s^{-1} and r_{1p} = 8.5 mM^{-1} s^{-1} for the non-aggregated and aggregated forms, respectively. The cmc determined for [Mn(DPADA)] is similar to that reported for a charge neutral Eu^{3+} complex having a C_{12} alkyl chain (67 μM),[21] but considerably lower than the one determined for a similar system having negatively charged hydrophilic head units (4.5 mM).[22] These results suggest that repulsive electrostatic interactions among the negatively charged head units are detrimental for the formation of micelles.

The relaxivity of [Mn(DPADA)] below the cmc (r_{1p} = 5.3 mM^{-1} s^{-1}) is lower than that of [Mn(DPAMA)], which suggests that the incorporation of the C_{12} alkyl chains to the ligand skeleton lowers the hydration number of the complex. As expected, the NMRD profile recorded below the cmc is typical of a small Mn^{2+} complex (Figure 9.). The best-fit analysis confirms these qualitative observations. The NMRD profile below cmc is well reproduced by fixing to one the number of inner sphere water molecules, at a distance of 2.782 Å and with a residence lifetime of 10 ns (298 K). The relaxivity is limited by the rotational dynamics even though the parameter τ_R assumes a value of 123 ps, more than twice that of $[Mn(EDTA)]^-$ and $[Mn(DPAA)]^-$. The longer τ_R reflects the presence of the pendant aliphatic chain and its effect is apparent from the nearly vanished field-dependence of relaxivity at high frequencies. The electronic relaxation parameters assume typical values: τ_V = 21.4 ps and $\Delta^2 = 8.1\times10^{19}$ s^{-2}. Conversely, above the cmc the NMRD profile presents a pronounced peak around 30 MHz that is characteristic of slowly tumbling systems. The NMRD at high field (> 3 MHz) was fitted using the Lipari-Szabo approach, which separates the global and local motions of the system.[23] The analysis was performed by using as adjustable parameters those describing electron spin relaxation (τ_v and Δ^2), the correlation times describing global (τ_{RG}) and local (τ_{RL}) motions and the generalized order parameter S^2, which takes a value of 0 if the internal motion is isotropic and a value of S^2 = 1 if the motion is completely restricted. The hydration number was fixed to q = 1, the Mn···H distance (2.74 Å), the distance of closest approach of a second-sphere water molecule (a_{MnH} = 3.6 Å) and diffusion coefficient (D_{MnH}^{298} = 2.24 10^{-10} m^2 s^{-1}) were fixed to reasonable values (Table 2). The results of the fit provided τ_{RG} = 5 ns and τ_{RL} = 95 ps, with S^2 = 0.27, indicating that relaxivity is limited by local rotational flexibility (Table 3).[24] Analysis of the NMRD profile recorded at 37 ºC provides very similar results (Figure 10.). ^{1}H relaxivity decreases upon increasing temperature, which indicates that the exchange rate of the coordinated water molecule is not limiting r_{1p}.

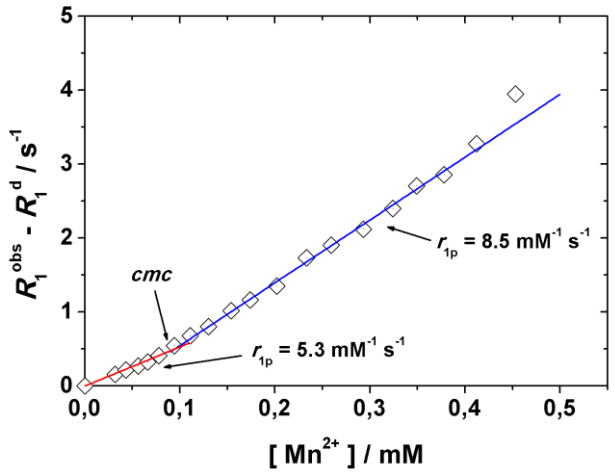

Figure 8. Determination of the CMC of the [Mn(DPADA)] at 20 MHz and 298 K**.**

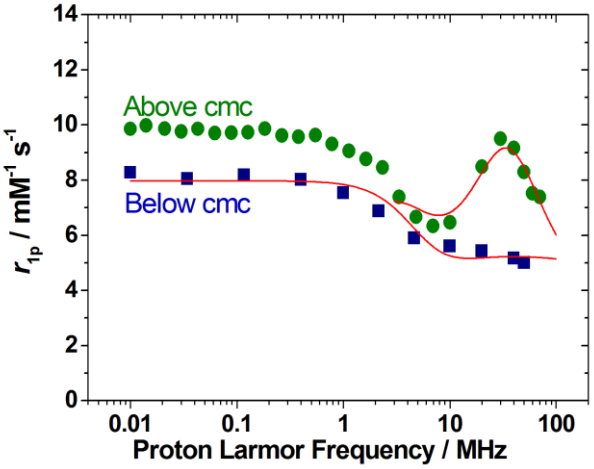

Figure 9. ^{1}H NMRD profiles recorded at 25 ºC for [Mn(dpada)] above and below the cmc. The red line represents the fit of the data above cmc using the Lipari-Szabo approach.

Table 3. Selected parameters obtained from the analysis of the NMRD profiles using the Lipari-Szabo approach (25 ºC).[a]

	Mn(DPADA)[a]	Mn(DPADA)+HSA[b]	Mn(DPAHPhA)+HSA[c]
r_{1p} (20 MHz)	8.5 ± 0.1	15.5 ± 0.3	45.5 ± 1.4
τ_{RG} (ns)	5.5 ± 0.7	50 (fixed)	50 (fixed)
τ_{RL} (ps)	91 ± 3	306 ± 10	1235 ± 52
S^2	0.27 ± 0.01	0.26 ± 0.01	0.43 ± 0.2
K_A / M^{-1}	-	1.3 ± 0.4 × 10^5	7.1 ± 0.1 × 10^3

[a] τ_v = 49 ± 8 ps; Δ^2 = 5.4 ± 0.6 s^{-2}. [b] τ_v = 22 ± 9 ps; Δ^2 = 1.0 ± 0.6 s^{-2}. [c] τ_v = 18 ± 8 ps; Δ^2 = 0.84 ± 0.04 s^{-2}

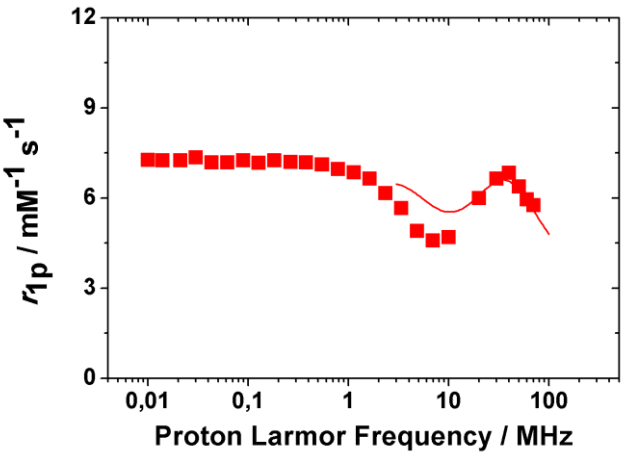

Figure 10. ^{1}H NMRD profiles recorded at 37 ºC for [Mn(dpada)]

Interaction of the lipophilic derivatives [Mn(DPAHPhA)] and [Mn(DPADA)] with HSA: We measured the interaction of [Mn(DPAHPhA)] and [Mn(DPADA)] with by measuring the R_1^{obs} values of a diluted solution of the complex as a function of protein concentration at a constant frequency and temperature. R_1^{obs} increases with the concentration of the protein, because of the increase in the fraction of bound complex that is characterized by a slower reorientational motion. The analysis of the titration data (fitted to a 1:1 binding isotherm) affords the association constant K_A, the number of equivalent and independent binding sites n (assumed to be 1) and the relaxivity of the bound form. The titration profile obtained for [Mn(DPAHPhA)] shows a rather sharp inflection point, which is indicative of a rather high stability constant (Figure 11). On the contrary [Mn(DPADA)] provides a smooth titration profile characteristic of a smaller association constant. Inspection of the titration profiles also shows that the relaxivity of the bound form is considerably higher in the case of [Mn(DPAHPhA)]. The fit of the data confirms these qualitative observations (Table 3). The association constant determined for [Mn(DPADA)] (7.1 x 10^5 M^{-1}) is 1-2 orders of magnitude higher than those determined for Mn^{2+} complexes containing benzyloxymethyl groups, and ca. 550 times higher than that obtained for [Mn(DPAHPhA)]. These results suggest that a lipophilic C_{12} alkyl chain provides a stronger interaction with the protein than benzyloxymethyl and 4-hexylphenyl moieties. This could be related to a better ability to penetrate inside the hydrophobic binding cavity of HSA.[25]

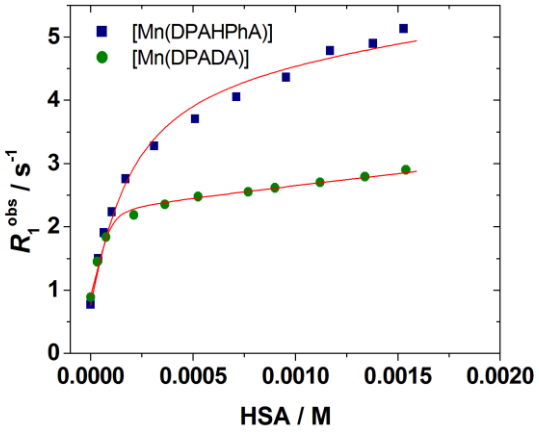

Figure 11. Changes in the observed longitudinal relaxation rates of water protons observed upon addition of HSA to solutions of the lipophilic [Mn(DPAHPhA)] (0.096 mM) and [Mn(DPADA)] (0.095 mM) complexes (25 ºC). The red lines represent the fit of the data to a 1:1 binding isotherm.

The analysis of the NMRD profiles recorded for the [Mn(DPAHPhA)] and [Mn(DPADA)] complexes fully bound to HSA (Figure 12) are characteristic of slowly tumbling species. The relaxivity of [Mn(DPADA)] at ca. 20 MHz and 25 ºC (45.5 mM^{-1} s^{-1}) is close to those observed for HSA adducts of Mn^{2+} complexes containing benzyloxymethyl groups, while the relaxivity of [Mn(DPADA)] under the same conditions is much lower (15.5 mM^{-1} s^{-1}). The analysis of the NMRD profiles using the Lipari-Szabo model (Table 3) clearly indicate that an increased local flexibility is responsible for the lower relaxivity of the adduct formed between [Mn(DPADA)] and HSA, as demonstrated by the lower values of τ_{RL} and S^2. Thus, the alkyl C_{12} chain provides strong interactions with the protein, but its flexibility prevents attaining high relaxivities.

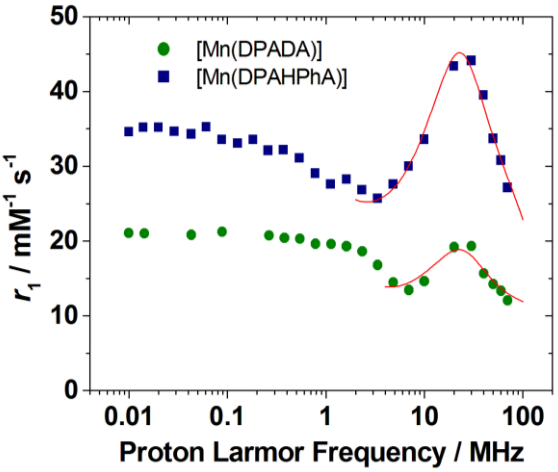

Figure 12. ^{1}H NMRD profiles obtained at 25 ºC for the adducts formed by [Mn(DPADA)] and [Mn(DPAHPhA)] with HSA. The red lines represent the fit of the data above cmc using the Lipari-Szabo approach.

Conclusions:

We have characterized a new series of pentadentate ligands that contain a pentadentate 6,6'-(azanediylbis(methylene))dipicolinic acid binding motif that can be easily functionalized with groups containing additional donor atoms or lipophilic chains. The hexadentate ligand $DPAA^{3-}$ forms a Mn^{2+} complex with stability comparable to that of $EDTA^{4-}$, although this decreases the hydration number of the complex from 2 to 1, which results in lower proton relaxivities. On the other hand, the pentadentate $DPAPhA^{2-}$ and $DPAMA^{2-}$ form bis-aquated Mn^{2+} complexes in solution. An interesting and unexpected result obtained in this study is the likely reduction of the hydration number upon incorporating aliphatic chains into the ligand scaffold. The lipophilic derivatives form rather stable adducts with HSA, particularly when incorporating a flexible dodecyl chain. However, the relaxivity of the bound form is partially quenched due to the contribution of relatively rapid local motions.

These experimental results allow extending the number of Mn^{2+} systems that have been characterized in the search for alternative systems to the classical Gd^{3+}-based MRI contrast agents. We have shown that the relaxivities of Mn^{2+} complexes can be modulated by changing the hydration number or introducing lipophilic units in the ligand scaffold, very much like in the case of Gd^{3+} complexes. The relaxivities of the adducts formed with HSA are also comparable to those attained with lipophilic Gd^{3+} agents

Experimental Section:

Materials and Methods. All reagents and solvents were commercial and used without further purification. SiO_2 (Fluka, pore size 60 Å, 70–230 mesh) was used for preparative column chromatography. ^{1}H and ^{13}C NMR spectra were recorded at 25ºC on Bruker Avance 300 MHz and Bruker Avance 500 MHz spectrometers. High resolution ESI-TOF mass spectra were recorded using a LC-Q-q-TOF Applied Biosystems QSTAR Elite spectrometer in the positive mode. Elemental analyses were carried out on a ThermoQuest Flash EA 1112 elemental analyser. IR spectra were recorded using a Bruker Vector 22 spectrophotometer equipped with a Golden Gate attenuated total reflectance (ATR) accessory (Specac).

Equilibrium measurements. All the equilibrium measurements were conducted at a constant ionic strength maintained by 0.15 M NaCl at 298 K. For determining, the protonation constants of the ligands pH-potentiometric titrations were performed with 0.2 M NaOH using 0.002 M ligand solutions. The stability and protonation constants of Mn^{2+} complexes were determined by pH-potentiometric titrations. The metals to ligand concentration ratios were 1:1. For the calculation of the equilibrium constants the mL base – pH data were used, obtained in the pH range 1.7–12.0. The pH-potentiometric titrations were carried out using a 785 DMP Titrino titration workstation with the use of a *Metrohm- 6.0233.100* combined electrode. The titrated solution (8 mL) was thermostated at 25 °C. The samples were stirred and to avoid the effect of CO_2, N_2 gas was bubbled through the solutions. For the calibration of the pH meter, KH-phthalate (pH = 4.002) and borax (pH = 8.970) buffers were used. For the calculation of the H^+ concentration from the measured pH values, the method proposed by Irving et al. was used. [26] A 0.01 M HCl (0.15 M NaCl) solution was titrated with the 0.2 M NaOH and the difference between the measured and calculated pH values were used to calculate $[H^+]$ from the pH values determined in the titration experiments. For the calculation of the equilibrium constants the PSEQUAD program was used.[27]

^{1}H NMRD and ^{17}O NMR Measurements. The proton $1/T_1$ NMRD profiles were measured on a fast field-cycling Stelar SmartTracer relaxometer (Mede, Pv, Italy) over a continuum of magnetic field strengths from 0.00024 to 0.25 T (corresponding to 0.01-10 MHz proton Larmor frequencies). The relaxometer operates under computer control with an absolute uncertainty in $1/T_1$ of ± 1%. The temperature control was carried out using a Stelar VTC-91

airflow heater equipped with a calibrated copper–constantan thermocouple (uncertainty of ±0.1 K). Additional data points in the range 20-70 MHz were obtained on a Stelar Relaxometer equipped with a Bruker WP80 NMR electromagnet adapted to variable-field measurements (15-80 MHz proton Larmor frequency). The exact complex concentration was determined by the BMS shift method at 11.7 T. Relaxometric HSA titrations were performed on the Stelar Relaxometer at 0.47 T (20 MHz) and 25 °C on dilute aqueous solutions at neutral pH. ^{17}O NMR measurements were recorded on a Bruker Avance III spectrometer (11.7 T) equipped with a 5 mm probe and standard temperature control unit. Aqueous solution of the complexes (ca. 6-10 mM) containing 2.0% of the ^{17}O isotope (Cambridge Isotope) were used. The observed transverse relaxation rates were calculated from the signal width at half-height.

References:

1. B. Gallez, C. Baudelet, M. Geurts, *Magn. Reson. Imaging*, **1998**, 16, 1211.
2. R. Artali, Z. Baranyai, M. Botta, G. B. Giovenzana, A. Maspero, R. Negri, G. Palmisano, M. Sisti, S. Tollari, *New J. Chem.,* **2015**, 39, 539.
3. G. S. Loving, S. Mukherjee, P. Caravan, *J. Am. Chem. Soc*., **2013**, 135, 4620.
4. S. Aime, M. Botta, E. Gianolio, E. Terreno, *Angew. Chem. Int. Ed*., **2000**, 39, 747.
5. A. Nonat, P. H. Fries, J. Pecaut, M. Mazzanti, *Chem. Eur. J.,* **2007**, 13, 8489.
6. F. K. Kálmán, G. Tircsó, *Inorg. Chem.*, **2012**, 51, 10065
7. J. Sanchiz, S. Dominguez, A. Mederos, F. Brito and J. M. Arrieta, *Inorg. Chem.,* **1997**, 36, 4108.
8. A. E. Martell, R. J. Motekaitis, R. M. Smith, R. M. NIST Critically selected stability constants of metal complexes database. Version 8.0 for windows. Gaithersburg, MD: National Institute of Standards and Technology, Standard Reference Data Program, **2004**.
9. B. Drahos, J. Kotek, P. Hermann, I. Lukes, É. Tóth, *Inorg. Chem*., **2010**, 49, 3224.
10. J. S. Troughton, M. T. Greenfield, J. M. Greenwood, S. Dumas, A. J. Wiethoff, J. Wang, M. Spiller, T. J. McMurry, P. Caravan, *Inorg. Chem.*, **2004**, 43, 6313.
11. A. Bianchi, L. Calabi, C. Giorgi, P. Losi, P. Mariani, D. Palano, P. Paoli, P. Rossi, B. Valtancoli, *J. Chem. Soc., Dalton Trans.,* **2001**, 917–922.
12. B. Drahos, M. Pniok, J. Havlícková, J. Kotek, I. Císarová, P. Hermann, I. Lukes, É. Tóth, *Dalton Trans*., **2011**, 40, 10131.
13. E. Balogh, Z. He, W. Hsieh, S. Liu, É. Tóth, *Inorg. Chem.,* **2007**, 46, 238.
14. D. Esteban-Gómez, C. Cassino, M. Botta, C. Platas-Iglesias, *RSC Adv.*, **2014**, 4, 7094.
15. E. M. Gale, J. Zhu, P. Caravan, *J. Am. Chem. Soc.,* **2013**, 135, 18600
16. R. Mills, *J. Phys. Chem*., **1973**, 77, 685.
17. G. A. Rolla, C. Platas-Iglesias, M. Botta, L. Tei, L. Helm, *Inorg. Chem*., **2013**, 52, 3268.
18. M. Regueiro-Figueroa, C. Platas-Iglesias, *J. Phys. Chem.,* **2015**, 119, 6436.
19. L. Tei, G. Gugliotta, M. Fekete, F. K. Kálmán, M. Botta, *Dalton Trans*., **2011**, 40, 2025
20. A. de Sa, C. S. Bonnet, C. F. G. C. Geraldes, E. Toth, P. M. T. Ferreira and J. P. Andre, *Dalton Trans.*, **2013**, 42, 4522.
21. O. M. Evbuomwan, G. Kiefer and A. D. Sherry, *Eur. J. Inorg. Chem.*, **2012**, 2126.
22. E. M. Surender, S. Comby, S. Martyn, B. Cavanagh, T. C. Lee, D. F. Brougham and T. Gunnlaugsson, *Chem. Commun*., **2016**, 52, 10858.
23. (a) G. Lipari, S. Szabo, *J. Am. Chem. Soc*., **1982**, 104, 4546; (b) G. Lipari, S. Szabo, *J. Am. Chem. Soc.*, **1982**, 104, 4559.
24. F. Kielar, L. Tei, E. Terreno, M. Botta, *J. Am. Chem. Soc.*, **2010**, 132, 7836.
25. M. Botta, S. Avedano, G. B. Giovenzana, A. Lombardi, D. Longo, C. Cassino, L. Tei, S. Aime. *Eur. J. Inorg. Chem.* **2011**, 802–810.
26. H. M. Irving, M. G. Miles, L. Pettit, *Anal. Chim. Acta,* **1967**, 38, 475.
27. L. Zékány, I. Nagypál, In Computational Method for Determination of Formation Constants, Legett, D. J. (Ed), *Plenum*, New York, **1985**, 291.

Chapter 6

Bisamide Derivative of [Mn(1,4-DO2A)]

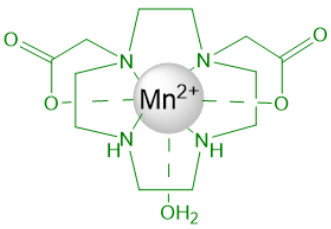

[Mn(1,4-DO2A)(H_2O)]

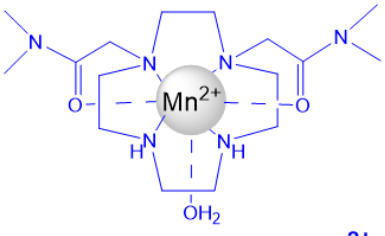

[Mn(1,4-DO2AM)(H_2O)]$^{2+}$

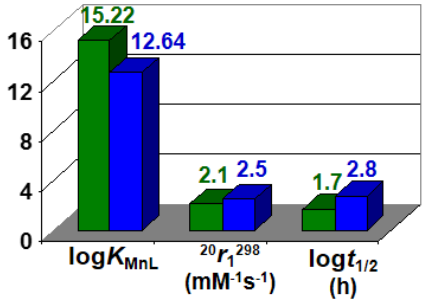

Introduction:

The number of publications on Mn^{II}-based Magnetic Resonance Imaging (MRI) contrast agents (CAs) as an alternative to those based on Gd^{III} has dramatically increased in recent years.[1,2] Several new chelators, open-chain or macrocyclic, with a variable number and typology of donor atoms have been proposed for the complexation of Mn^{2+} ions.[3,4,5,6] Unlike Gd^{III}-based contrast agents for which a large set of dissociation kinetic data is available,[7] in the case of Mn^{II} complexes this important information is often lacking and studies are less systematic. It was recently shown that macrocyclic MnNOTA and MnDOTA chelates possess considerable kinetic inertia but, in both cases, the central metal ion lacks a water molecule in its inner coordination sphere (q = 0).[8] For a water molecule to have access to the paramagnetic centre, the chelator should not have more than six donor atoms and this makes it more difficult the probe design. Studying the relationship between relaxometric properties of Mn^{II}-chelates and their thermodynamic stabilities, M. Botta and co-workers have recently reported a detailed ^{1}H and ^{17}O NMR relaxometric and computational study on a series of Mn^{II} complexes with cyclen-based (cyclen = 1,4,7,10-tetraazacyclododecane) ligands bearing one, two and three acetate pendant arms (DO1A, 1,4- and 1,7-DO2A, DO3A, respectively, Scheme 1).[9] While in aqueous solution Mn(DO3A) reproduces the behaviour of Mn(DOTA) and is a q = 0 complex, the Mn^{II} complex with the pentadentate DO1A contains one bound water molecule (q = 1). However, the most interesting result was that Mn(1,7-DO2A) is predominantly six-coordinate (q = 0) whereas Mn(1,4-DO2A) is present as a mixture of a seven- (ca. 87%) and six-coordinate species (ca. 13%) with one or no coordinated water molecule, respectively. Accordingly, the relaxivity of Mn(1,4-DO2A) is about 40% greater than that of Mn(1,7-DO2A). In order to obtain useful information about the coordination ability of different donor groups linked to the same macrocyclic scaffold, we decided to carry out the 1,4-substitution on cyclen with *N*,*N*-dimethylacetamide groups to obtain the hexadentate ligand 1,4-DO2AM (Scheme 1). The aim is the investigation of the differences in thermodynamic stability, kinetic inertness and ^{1}H and ^{17}O NMR relaxometric behaviour of the Mn^{II} complex as compared to the related carboxylate derivative Mn(1,4-DO2A). The main reason behind the choice of the *N*,*N*-dimethylacetamide pendant arms is the improved kinetic stability typically exhibited by Gd^{III} complexes with amide donor groups. In fact, it is well recognized that the replacement of acetate for amide donor groups slows down the rate of the dissociation reactions of the Ln-DOTA-like complexes.[10,11] This property has been attributed to both the decreased negative charge of the complex which hinders the protonation and then

the acid-catalysed dissociation and to the low basicity of the amide oxygen atom which makes proton transfer to the ring nitrogen very unlikely.[11] Moreover, the presence of neutral amide coordinating groups and the formation of a cationic Mn^{II} complex should impact its relaxometric properties.[12] We are particularly interested in evaluating the water exchange rate ($k_{ex} = 1/\tau_M$) of Mn(1,4-DO2AM) by ^{17}O NMR techniques in order to ascertain the influence on this key parameter of the chemical nature of the donor group. Since the $^{298}k_{ex}$ value of Mn(1,4-DO2A) is particularly high (1.1×10^9 s^{-1}),[9] 2.4 times faster than that found for $[Mn(EDTA)]^{2-}$, it is important to evaluate the effect of the amide coordination on k_{ex}. We report the synthesis of the bis-amide derivative of 1,4-DO2A and the equilibrium, kinetics and relaxometric properties of $[Mn(1,4\text{-}DO2AM)]^{2+}$ in close comparison with those of the parent Mn(1,4-DO2A).

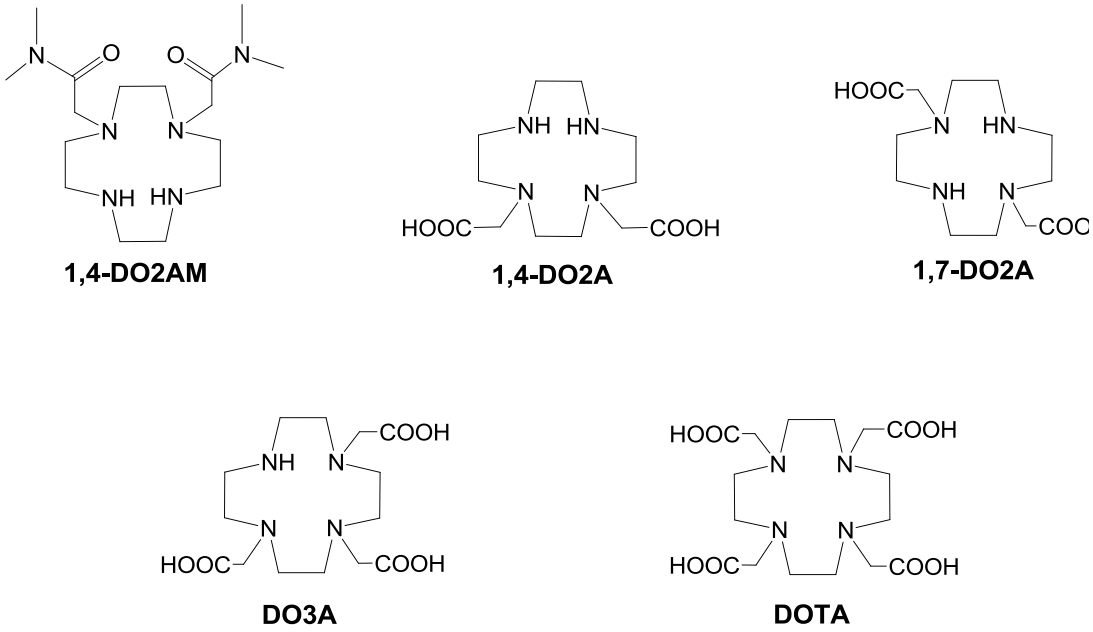

Scheme 1. The structure of 1,4-DO2AM, 1,4-DO2A, 1,7-DO2A, DO3A and DOTA ligands discussed in this chapter.

Synthesis:

1,4-DO2AM was synthesised in one step starting from 1,4,7,10-tetraazacyclododecane (cyclen) following the same protocol used for the synthesis of 1,4-DO2A (Scheme 2).[13] 1.5 equivalents of 2-chloro-*N*,*N*-dimethylacetamide were reacted with cyclen in $CHCl_3$ in the presence of excess triethylamine. The final product was obtained in about 20% yield after

semi-preparative HPLC-MS purification and was characterized by ESI-MS spectrometry and ^{1}H and ^{13}C NMR spectroscopy.

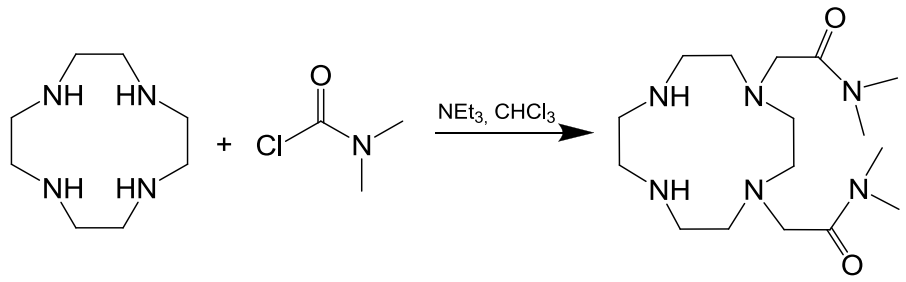

Scheme 2. Synthesis of 1,4-DO2AM

Solution equilibrium studies:

Protonation equilibria. The protonation constants of 1,4-DO2AM, defined by Eq. (1), were measured by pH-potentiometric titration and ^{1}H-NMR spectroscopy in 0.1 M KCl aqueous solution.

$$H_{i-1}L + H^{+} \rightleftharpoons H_iL$$

$$K_i^{H} = \frac{[H_iL]}{[H_{i-1}L][H^{+}]} \qquad i=1, 2,\ldots, 8. \qquad (1)$$

The protonation sequence of 1,4-DO2AM was determined by ^{1}H-NMR spectroscopy, recording the chemical shift variations of the non-labile protons as a function of pH. The ^{1}H-NMR titration curves (Figure 1) display pronounced chemical shift changes over well-defined pH ranges. These are associated with the various protonation steps of the ligand. Because the protonation/deprotonation processes are fast on the NMR time scale, the chemical shifts of the observed signals represent a weighted average of the shifts of the different species involved in a specific protonation step (Eq. (2)):[14]

$$\delta_{H(obs)} = \sum x_i \delta_H^{H_iL} \qquad (2)$$

where $\delta_{H(obs)}$ is the observed chemical shift of a given signal, x_i and $\delta_{H(obs)}^{HiL}$ are the molar fractions and the chemical shift of the involved species, respectively. The fitting of the data of Figure 1 according to Eq. (2) gave the results reported in Table 1, where the molar fractions x_i and the concentration of the different protonated species are expressed in terms of the protonation constants K_i^{H}.

In the ^{1}H-NMR spectrum of 1,4-DO2AM at pH=9.6 (Figure 1), the protons of the acetamide arms give rise to three singlets (*e*, *f*, *g*), whereas relatively broad multiplets are associated with the methylene protons of the macrocyclic ring (*a*, *b*, *c*, *d*). The addition of one equivalent of acid to the deprotonated 1,4-DO2AM results in a downfield shift of the NMR signals corresponding to *a*, *b*, *c*, *d* and *e*, whereas the chemical shift of the *N*-methyl protons *f* and *g* slightly decreases in higher pH range. The second protonation process causes the downfield shift of the peaks of *e* and ring protons (*a*-*d*), while the chemical shift values of *f* and *g* remain unchanged in the pH range 7.5 – 10. By considering the effects of the first and second protonation steps on the chemical shifts, we can safely assume that the first protonation occurs on the N_1/N_2 atoms of the macrocycle (the protonation involves partially both N-atoms). The second protonation takes place on the unsubstituted N_3 (or N_4) atom along with a shift of the former proton to afford a bis-protonated species on N_1–N_4 or N_2–N_3. This shift allows a better charge separation and is quite typical of DOTA- and DTPA-like ligands. The logK_i^H values of 1,4-DO2AM, 1,4-DO2A, 1,7-DO2A, DO3A and DOTA, are listed in Table 1. Standard deviations (3σ) are shown in parentheses.

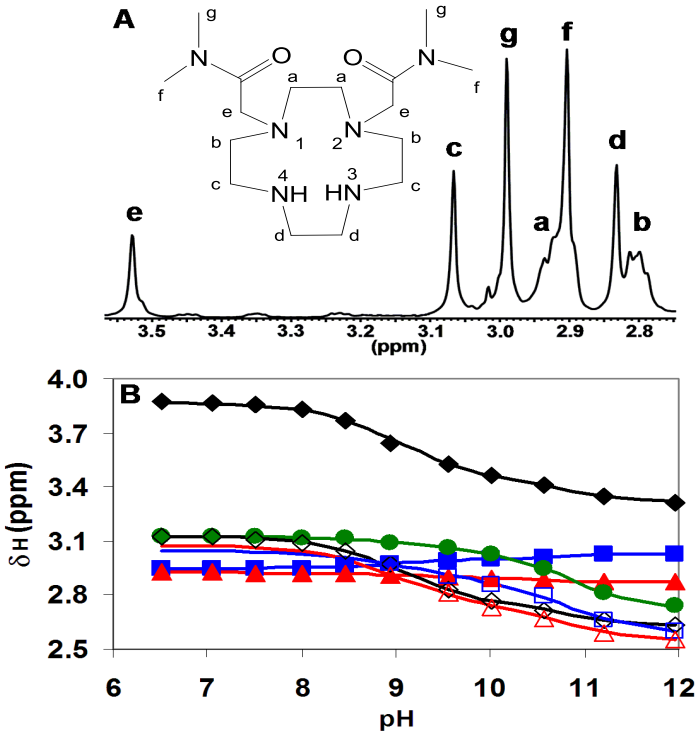

Figure 1. ^{1}H-NMR spectra of 1,4-DO2AM (**A**) at 400 MHz and the chemical shifts of the different protons as a function of pH (**B**). (A: pH=9.6; B: a (●), b (◇), c (□), d (Δ), e (♦),f (▲) and g (■), [1,4-DO2AM]=0.01 M, 0.1 M KCl, 25°C).

Table 1. Protonation constants of 1,4-DO2AM, 1,4-DO2A, 1,7-DO2A, DO3A and DOTA at 25°C in 0.1 M KCl.

	1,4-DO2AM		**1,4-DO2A[a]**	**1,7-DO2A[a]**	**DO3A[b]**	**DOTA[b]**
I	0.1 M KCl					
Method	pH-pot.	^{1}H-NMR	pH-pot.	pH-pot.	pH-pot.	pH-pot.
logK_1	10.14(2)	10.34(9)	11.40	11.66	11.99	11.41
logK_2	8.38 (4)	8.64 (4)	9.58	9.75	9.51	9.83
logK_3	-	-	3.74	4.06	4.30	4.38
logK_4	-	-	1.65	1.78	3.63	4.63
logK_5	-	-	-	-	1.84	1.92
logK_6	-	-	-	-	-	1.58
$\sum$logK_i^H	18.52	18.98	26.37	27.25	31.26	33.75

[a]Ref15. [b]Ref16

Comparison of the protonation constants of 1,4-DO2AM with those of the related ligands 1,4-DO2A, 1,7-DO2A, DO3A and DOTA indicates that the logK_1^H and logK_2^H values of 1,4-DO2AM are lower by 1.5 log$K$ unit. In general, the presence of an amide group in open-chain or macrocyclic amino-polycarboxylate ligands decreases the basicity of the amine N-atoms.[17,18] The lower protonation constants of 1,4-DO2AM can be explained by the replacement of the carboxylate pendant arms with the amide groups which form weaker H-bond with the protonated ring nitrogens. The ΣlogK_i^H value of 1,4-DO2AM is significantly lower than that of 1,4-DO2A, 1,7-DO2A, DO3A and DOTA due to the absence of protonable carboxylate groups. By taking into account the lower value of ΣlogK_i^H for 1,4-DO2AM, a lower stability for the 1,4-DO2AM complexes compared to the related 1,4-DO2A, 1,7-DO2A, DO3A and DOTA complexes is to be expected.

Complexation properties.

The stability and protonation constants (K_{ML} and K_{MHiL}, defined by Eqs. (3) and (4) with i=1, 2, 3) characterizing the formation of 1,4-DO2AM, 1,4-DO2A and 1,7-DO2A complexes with Ca^{2+}, Mn^{2+} and Zn^{2+} were calculated from the pH-potentiometric titration data obtained at 1:1 metal to ligand concentration ratios (25 ºC, 0.1M KCl).

$$K_{ML} = \frac{[ML]}{[M][L]} \qquad (3)$$

$$K_{H_iL} = \frac{[MH_iL]}{[MH_{i-1}L][H^+]} \qquad \text{with } i = 1, 2 \qquad (4)$$

Moreover, the corresponding values of K_{ML} and K_{MHiL} for the Cu^{2+} complexes were determined by UV-VIS spectrophotometry (Table 2).

Table 2. The stability ($\log K_{ML}$) and protonation ($\log K_{MHiL}$) constants of metal complexes formed with 1,4-DO2AM, 1,4-DO2A, 1,7-DO2A, DO3A and DOTA (0.1 M KCl, 25°C).

	1,4-DO2AM	**1,4-DO2A**	**1,7-DO2A**	**DO3A[a]**	**DOTA[a]**
CaL		8.62 (3)	8.86 (5)	12.57	16.11
CaHL	-	-	-	4.60	3.67
MnL	12.64 (5)	15.22 [b]	15.07 [b]	19.34	19.33
MnHL	-	4.15 (2)	4.48 (2)	3.69	4.09
MnH_2L	-	-	-	3.02	3.70
ZnL	15.59 (4)	18.03 (3)	18.86 (4)	21.57	20.21
ZnHL		3.58 (4)	4.23 (2)	3.47	4.12
ZnH_2L		1.65	1.78	2.07	3.49
CuL	21.38 (3)	24.43 (1)	24.24 (5)	25.75	24.83
CuHL	-	2.95 (3)	3.06 (6)	3.65	4.12
CuH_2L	-	-	-	1.69	3.57
CuH_3L	-	-	-	-	0.87

[a]Ref16. [b]Ref15

We calculated of the equilibrium constants. The best fitting of the experimental data (volume of KOH added vs. pH) was obtained by assuming the formation of ML complexes with 1,4-DO2AM and ML and MHL species with 1,4-DO2A and 1,7-DO2A. In the case of the Cu-complexes, the equilibrium reaction (5) was investigated over the $[H^+]$ range 0.01 – 1.0 M

([H^+]≤0.1 M; [H^+]+[K^+]=0.1 M), assuming the formation of Cu^{2+}, CuL, CuH_yL and H_xL species (1,4-DO2AM: x=2, y=0; 1,4-DO2A, 1,7-DO2A: x=3, 4; y=0, 1).

$$Cu^{2+} + H_xL \rightleftharpoons [Cu(H_yL)] + (x-y)H^+ \qquad (5)$$

Some characteristic absorption spectra and the species distribution of the Cu^{2+}-1,4-DO2AM, Cu^{2+}-1,4-DO2A and Cu^{2+}-1,7-DO2A systems with the maxima of the absorption spectra (λ_{max} values) are shown in Figures 2 and 3. Noteworthy, the metal complexes of 1,4-DO2AM show a significantly lower stability as compared to the corresponding complexes with 1,4-DO2A and 1,7-DO2A ($\Delta \log K_{ML}$ = 2.5 – 3.0). The difference with DO3A or DOTA complexes is even larger. A similar effect was reported for DOTA-tetramide complexes which are characterized by stability constants approxametly 6-7 log*K* units lower than those of the corresponding DOTA complexes.[19] The lower stability constants of the 1,4-DO2AM metal complexes can be accounted for by the significantly lower basicity ($\Sigma \log K_i^H$) of the ring N-atoms.

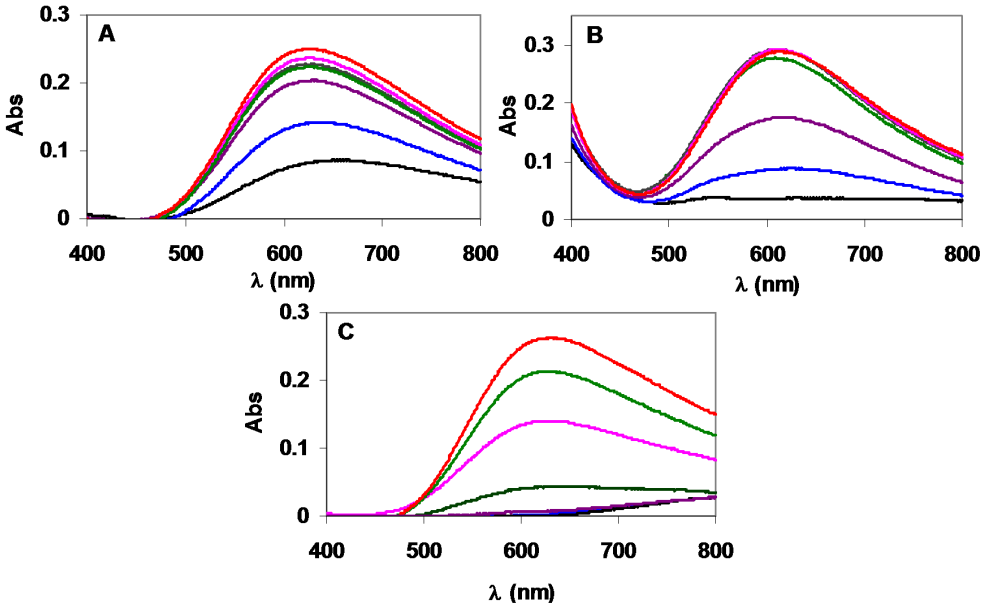

Figure 2. Absorbtion spectra of Cu^{2+}–1,4-DO2AM (A), Cu^{2+}–1,4-DO2A (B) and Cu^{2+}–1,7-DO2A systems ([Cu^{2+}]=[1,4-DO2AM]=[1,4-DO2A]=[1,7-DO2A]=1.5 mM, [H^+] = **1.0 M**, **0.60 M**, **0.31 M**, **0.10 M**, **0.050 M**, **0.025 M** and **0.01 M**, [H^+]+[K^+]=0.1 M in the last 4 samples, l=1 cm, 25 °C).

We determined the protonation constants of [Cu(1,4-DO2A)] and [Cu(1,7-DO2A)] by spectrophotometric titrations of the complexes in the pH range 1.7 – 6.0, in this pH range mono-protonated and deprotonated complexes are present. The species distribution diagram

and the maxima of the absorption spectra (λ_{max} values) of Cu^{2+}-1,4-DO2AM, Cu^{2+} - 1,4-DO2A and Cu^{2+} - 1,7-DO2A systems are shown as functions of pH in Figure 3.

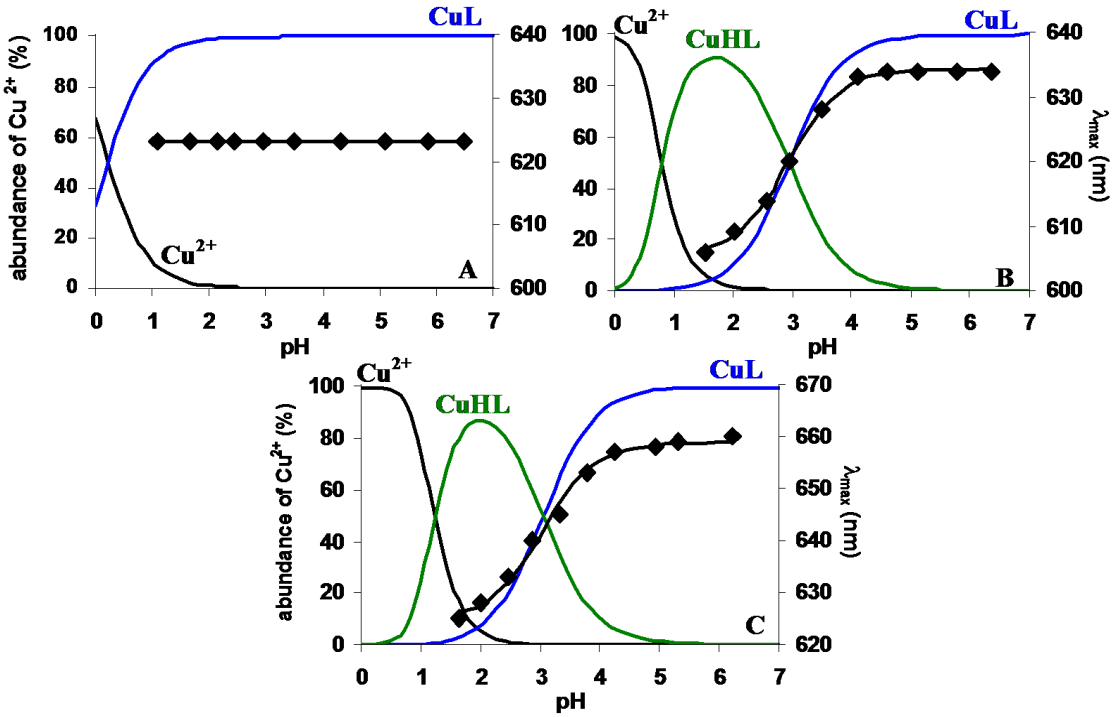

Figure 3. Species distribution and the λ_{max} values (♦) of Cu^{2+}- 1,4-DO2AM (**A**), Cu^{2+}- 1,4-DO2A (**B**) and Cu^{2+} - 1,7-DO2A (**C**) system as a function of pH. ([Cu^{2+}]=[1,4-DO2A]=[1,7-DO2A]=1.0 mM, 0,1 M KCl, 25 °C).

Transmetallation kinetics:

Because of the toxicity of free metal ions and ligands, the study of the dissociation kinetics of the metal complexes used in medical diagnosis and/or therapy has a great relevance since the products of the dissociation.[7] Typically, the dissociation of MnDOTA-like complexes is very slow and occurs via proton-assisted pathways whereas the presence of endogenous metal ions like Zn^{2+} and Cu^{2+} has a minor influence on the dissociation rates.[8,15] While the rates of the metal exchange reactions occurring between [Mn(1,4-DO2A)] and [Mn(1,7-DO2A)] and Zn^{2+} and Cu^{2+} ions were previously investigated,[3,4,5,6] in this work we studied the kinetic inertness of [Mn(1,4-DO2AM)] by focusing on the metal exchange reactions with high Zn^{2+} concentrations (10 – 40 fold excess) in order to form pseudo-first order conditions (Eq. (6)). These reactions were followed by relaxometry at 20 MHz and 25°C in the pH range 4.5 – 6.5.

$$MnL + Zn^{2+} \rightleftharpoons ZnL + Mn^{2+} \qquad (6)$$

As a pseudo-first-order process, the reaction rate is expressed by the Eq. (7) where k_d is a pseudo-first-order rate constant, $[MnL]_t$ and $[MnL]_{tot}$ are the concentrations of the MnL species at time t and the total concentration of the complex, respectively.

$$-\frac{d[MnL]_t}{dt} = k_d[MnL]_{tot} \qquad (7)$$

The calculated pseudo-first order rate constants for the transmetallation reaction of [Mn(1,4-DO2AM)]$^{2+}$ and Zn^{2+} as a function of $[H^+]$ are shown in Figure 4.

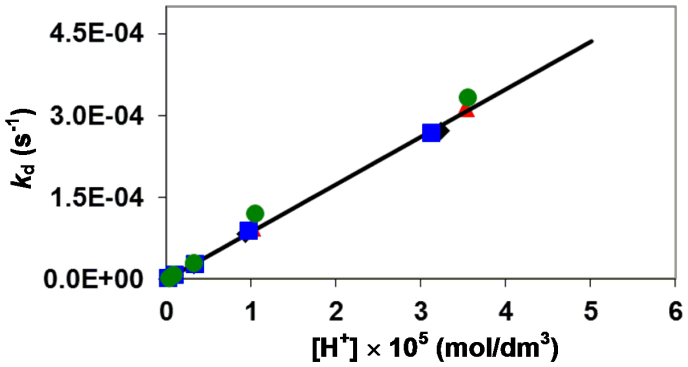

Figure 4. k_d values of the transmetallation reactions between [Mn(1,4-DO2AM)]$^{2+}$ and Zn^{2+} ([MnL]=1.0 mM, $[Zn^{2+}]$=10 mM (◆), 20 mM (■), 30 mM (▲) and 40 mM (●), 0.1 M KCl, 25°C)

The dissociation rates of [Mn(1,4-DO2AM)]$^{2+}$ are shown in Figure 4. The dissociatin rates are directly proportional to the H^+ concentration and independent of the concentration of the exchanging Zn^{2+} ions. The increase in the k_d values with increasing $[H^+]$ can be interpreted in terms of a rate determining step consisting of the proton assisted dissociation of [Mn(1,4-DO2AM)]$^{2+}$ followed by a fast reaction between the free ligand and the Zn^{2+} ion. The dependence of k_d on $[H^+]$ can be expressed as a first-order function of $[H^+]$ which indicates that the exchange can take place by proton-independent (Eq. (8)) and proton assisted (Eq. (9)) pathways.

$$MnL \xrightarrow{k_0} Mn^{2+} + H_2L \qquad (8)$$

$$MnL + H^+ \xrightarrow{k_1} Mn^{2+} + H_xL \qquad (9)$$

k_0 and k_1 are the rate constants characterizing the dissociation of $[Mn(1,4\text{-}DO2AM)]^{2+}$ through spontaneous and proton-assisted reaction pathways, respectively. By considering all the possible pathways and the rate of transmetallation of $[Mn(1,4\text{-}DO2AM)]^{2+}$ (Eq. (7)), the pseudo-first-order rate constant (k_d) can be expressed by Eq. (10).

$$-\frac{d[MnL]t}{dt} = k_0[MnL] + k_1[MnL][H^+] \qquad (10)$$

By taking into account the total concentration of the complex ($[MnL]_{tot} = [MnL]$), the pseudo-first-order rate constant (k_d) can be expressed as follows:

$$k_d = k_0 + k_1[H^+] \qquad (11)$$

The parameters k_0 and k_1 were calculated by fitting the experimental data in Figure 4 to Eq. (11). The rate constants characterizing the transmetallation reaction of $[Mn(1,4\text{-}DO2AM)]^{2+}$ with Zn^{2+} and the half-life of dissociation ($t_{1/2} = \ln 2/k_d$) of the complex calculated at pH=7.4 are listed in Table 3 and compared with the corresponding values reported for Mn(1,4-DO2A), Mn(1,7-DO2A) and Mn(DOTA).

Table 3. Rate constants and half-lives for the dissociation reactions of $[Mn(1,4\text{-}DO2AM)]^{2+}$, [Mn(1,4-DO2A)], [Mn(1,7-DO2A)] and $[Mn(DOTA)]^{2-}$ (pH=7.4; 0.1 M KCl; 25°C).

	1,4-DO2AM	**1,4-DO2A[a]**	**1,7-DO2A[a]**	**DOTA[b]**
k_0 **(s^{-1})**	-	-	-	1.8×10^{-7}
k_1 **($M^{-1}s^{-1}$)**	8.7±0.5	99	84	0.04
k_2 **($M^{-2}s^{-1}$)**	-	1.5×10^{6}	2.5×10^{6}	1.6×10^{3}
$\log K_{MnLH}$	-	4.15	4.48	4.26
k_d **(s^{-1}) pH=7.4**	3.5×10^{-7}	3.9×10^{-6}	3.3×10^{-6}	2.6×10^{-6}
$t_{1/2}$ **(h) pH=7.4**	556	49.4	58.3	1070

[a] Ref 15. [b] Ref 8

The rate constant k_0 is very small and the associated error is relatively large, to suggest that the spontaneous dissociation of [Mn(1,4-DO2AM)] does not give a sizeable contribution to the transmetallation reaction. The data presented in Table 3 also show that the k_1 value, *i.e.*

the rate of proton-assisted dissociation of [Mn(1,4-DO2AM)], is one order of magnitude lower than that of [Mn(1,4-DO2A)] or [Mn(1,7-DO2A)]. In the latter complexes, most likely the dissociation occurs by protonation at one of the carboxylate groups. After that the proton is transferred to the ring nitrogen forcing the release of Mn^{2+} from the coordination cavity. The replacement of the protonable carboxylate groups with non-protonable amide groups does not allow the formation of the protonated MnHL intermediate. Thus, it can be assumed that the proton assisted dissociation of $[Mn(1,4DO2AM)]^{2+}$ takes place by protonation of the ring N-atom followed by dissociation of the Mn^{2+} ion. Finally, the half-life ($t_{1/2}$) of dissociation of $[Mn(1,4\text{-}DO2AM)]^{2+}$ is ca. 50% lower than that measured for $[Mn(DOTA)]^{2-}$ and significantly higher than those reported for of [Mn(1,4-DO2A)] or [Mn(1,7-DO2A)]. Notably, in acidic condition the dissociation reaction of $[Gd(DOTA)]^{-}$ takes place more than 5 times faster than for $[Gd(DOTTA)]^{3+}$ (DOTTA = 1,4,7,10-tetrakis[(*N*,*N*-dimethylcarbamoyl)methyl]-1,4,7,10-tetraazacyclododecane] ($[Gd(DOTA)]^{-}$: $t_{1/2}$ = 68 h; $[Gd(DOTTA)]^{3+}$: $t_{1/2}$ = 384 h; $[HNO_3]$ = 2.5 M, 25°C), which clearly confirms that the replacement of acetate with bismethyl-amide groups improves the kinetic inertness of the metal-complexes with DOTA-like ligands.[10]

^{1}H and ^{17}O NMR relaxometric studies:

We performed the measurmnet of the proton relaxivity of $[Mn(1,4\text{-}DO2AM)]^{2+}$ as a function of pH, temperature and magnetic field strength. Together, this information allows to obtain a comprehensive picture of the relaxometric properties the complex and to understand the changes in the molecular parameters following the transformation of the carboxyl groups into amide groups. At neutral pH and 25°C, the measurement of r_{1p} at 60 MHz provides the value of 2.2 mM^{-1} s^{-1}, which compares well with the corresponding value for [Mn(1,4-DO2A)], namely 2.0 mM^{-1} s^{-1}.[9] These values are roughly intermediates between that associated with a q = 1 complex ($[Mn(EDTA)]^{2-}$) and that of a complex without water molecules in the first coordination sphere (q = 0; [Mn(1,7-DO2A)]) (Figure 5). The small difference between the values of r_{1p} of [Mn(1,4-DO2A)] and $[Mn(1,4\text{-}DO2AM)]^{2+}$ can be attributed to the small difference in their molecular masses that dictates the value of the rotational correlation time. Therefore, these findings suggest that $[Mn(1,4\text{-}DO2AM)]^{2+}$ in aqueous solution shows a behaviour very similar to [Mn(1,4-DO2A)], which is characterized by the presence of a hydration equilibrium involving q = 1 and q = 0 complex species. In our previous study we estimated an "effective" q value of 0.87 (± 0.01) for [Mn(1,4-DO2A)].[9] In the absence of further experimental evidence, we attribute the same value also to $[Mn(1,4\text{-}DO2AM)]^{2+}$.

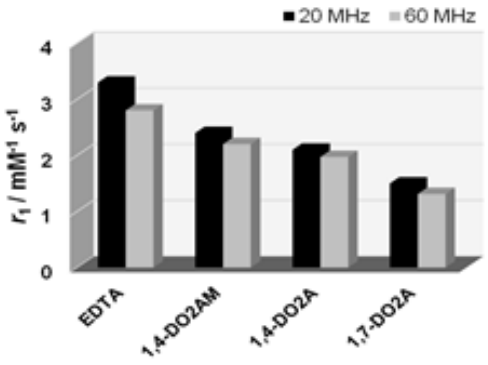

Figure 5. Plot of the ^{1}H relaxivity, r_{1p}, for selected Mn(II) complexes at 20 and 60 MHz and 298 K.

The behaviour of r_{1p} with pH reproduces quite closely the main features found for [Mn(1,4-DO2A)] and [Mn(1,7-DO2A)].[9] The relaxivity is constant over the pH range 12 to 6, where complete formation of the metal complex occurs, then it increases rather sharply to reach a new plateau at pH lower than ca. 3. Such an increase is clearly associated with the progressive release of the Mn(II) ion as a result of the protonation of the basic sites of the chelator. The lower stability of $[Mn(1,4\text{-}DO2AM)]^{2+}$ is reflected in the slightly higher pH value in which the increase of r_{1p} begins. The pH dependence of the relaxivity is reported in Figure 6, together with the species distribution diagram for the Mn^{2+}/1,4-DO2AM system.

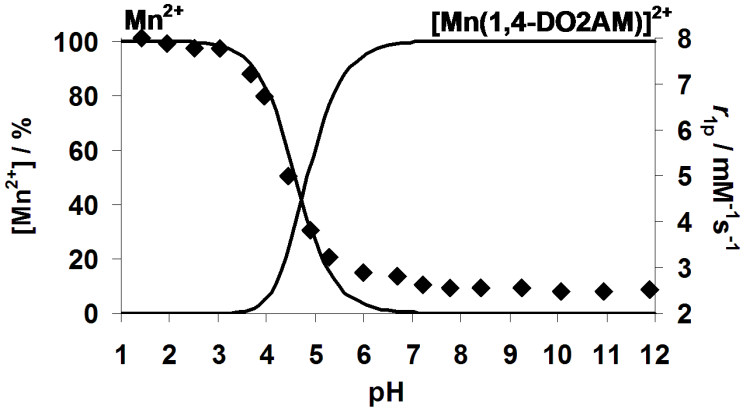

Figure 6. Plot of ^{1}H relaxivity r_{1p} at 20 MHz and 298 K for $[Mn(1,4\text{-}DO2AM)]^{2+}$ and the species distribution diagram of the Mn^{2+}/1,4-DO2AM system as a function of pH ($[Mn^{2+}]$ = [1,4-DO2AM] = 1×10^{-3} M, [KCl] = 0.1 M, 20 MHz, 25 °C).

The (NMRD) profile, has been measured at 283, 298 and 310 K over the proton Larmor frequency range 0.01-70 MHz, corresponding to magnetic field strengths varying between

2.343×10^{-4} T and 1.645 T (Figure 7A). The profiles have the typical shape of rapidly tumbling, low molecular weight complexes, featuring a region of constant relaxivity at low fields, a single dispersion around 6-8 MHz and another plateau, not well defined, in the region at high fields (> 20 MHz).[20]

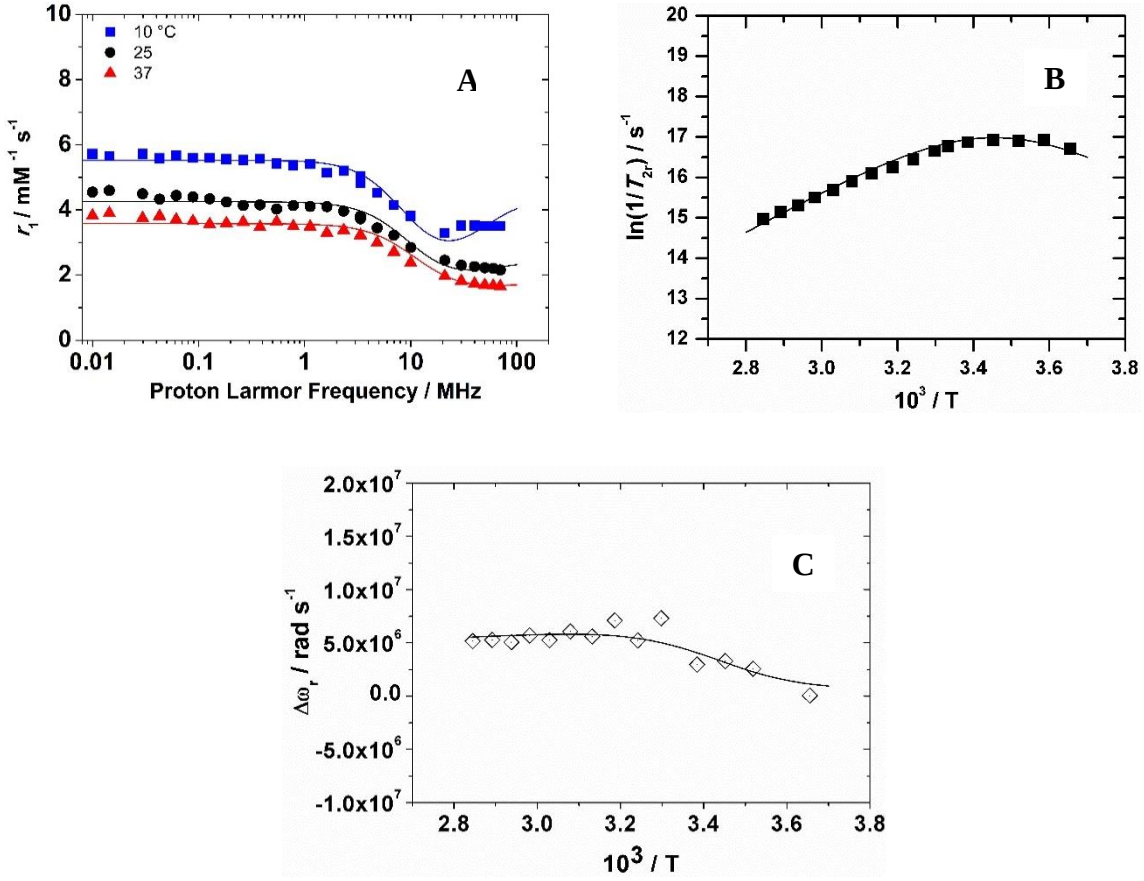

Figure 7. (A) $1/T_1$ ^{1}H NMRD profiles for $[Mn(1,4\text{-}DO2A)]^{2+}$ at pH = 7.2 and 283 K (blue squares); 298 K (black circles); 310 K (red triangles). The solid lines represent the results of the best fitting to the experimental data (Table 3). Temperature dependence of the reduced water ^{17}O NMR transverse relaxation rates (B) and chemical shifts (C) at 11.75 T and pH = 7.2 for a 4.8 mM solution.

The relaxivity decreases by increasing temperature over the entire frequency range, which indicates that water exchange ($k_{ex} = 1/\tau_M$) in and out of the coordination site does not represent a limiting factor. Rather, the fast rotation of the complex in solution determines and controls the value of the relaxivity. This is clearly shown by the temperature dependence of

r_{1p} at 20 MHz over the range 280 - 341 K. At neutral pH, the relaxivity of the complex increases exponentially with lowering temperature (Figure 8), following the behaviour of systems in the fast-exchange regime (the exchange lifetime, τ_M, is much shorter than the longitudinal relaxation time of the bound water protons, T_{1M}), such as the Mn(II) complexes of AAZTA-like ligands.[21]

Detailed information on the water exchange kinetics is obtained by measuring and analysing the temperature dependence of the ^{17}O NMR transverse relaxation rate (R_2) and paramagnetic shift ($\Delta\omega$) (Figure 7B and C).[20] The data were collected at 14.1 T on a 4.8 mM solution of the complex at neutral pH and analysed according to the well-established set of Swift-Connick equations.[22] The reduced R_2 ($1/T_{2r}$) and $\Delta\omega$ values are reported in Figure7B and %C, respectively. The increase of $1/T_{2r}$ with decreasing temperature over a wide range of values indicates the occurrence of a relatively fast rate of water exchange, as for $[Mn(EDTA)]^{2-}$.[9]

The relaxometric data, ^1H NMRD and ^{17}O NMR, were fitted simultaneously according to the established theory of paramagnetic relaxation expressed in terms of the well known Solomon-Bloembergen-Morgan[23] and Freed's[24] equations for the *inner*- (IS) and *outer sphere* (OS) proton relaxation mechanisms, respectively, and of the Swift-Connick theory for ^{17}O relaxation. The IS contribution to r_{1p} is determined by the number q of bound water molecules and their rate of exchange (k_{ex}), the molecular rotational correlation time (τ_R), and the electronic relaxation times ($T_{1,2e}$) of Mn^{II}.[17] The OS term depends on $T_{1,2e}$, the relative diffusion coefficient between the complex and the water molecules (D) and their distance of closest approach, a. The Swift-Connick equations depend on a number of parameters, among which the most relevant are:[22] i) those associated with $T_{1,2e}$, *i.e.* the trace of the square of the zero-field splitting tensor, Δ^2; the correlation time describing the modulation of the zero-field splitting, τ_V, and its activation energy, E_V; ii) the enthalpy, $\Delta H^{\#}$, of activation for the water exchange process; iii) the hyperfine $Mn\text{-}^{17}O_{water}$ coupling constant, $A/\hbar$. Given the large number of parameters, we need to fix the value of some of them according to reasonable estimates: q was fixed to 0.87; the distance between the metal ion and the protons of the bound water molecule, r, was fixed to 2.83 Å; a and D were set to 3.6 Å and 2.3×10^{-5} cm^2 s^{-1} (at 25°C), respectively; E_V was fixed to 1.0 kJ mol^{-1}. To E_R (activation energy for the rotational motion of the complex) and E_D (activation energy of D) were assigned the same values found for [Mn(1,4-DO2A)]: 19.1 and 17.3 kJ mol^{-1}, respectively. The relevant best-fit

parameters are listed in Table 4 and compared with those of related Mn(II) complexes of similar size.

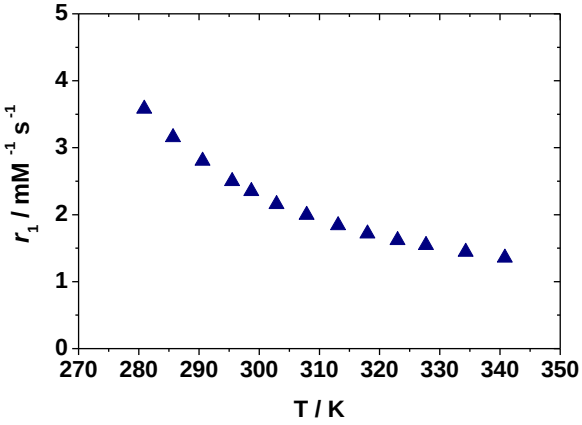

Figure 8. Temperature dependence of the longitudinal water proton relaxivity at 20 MHz and pH = 7

Table 4. Parameters obtained from the simultaneous analysis of ^{1}H NMRD profiles and ^{17}O NMR data (14.1 T) for the Mn^{2+} complexes of 1,4-DO2AM and related ligands

Parameters	**1,4-DO2AM**	**1,4-DO2A**[9]	**DO1A**[9]	**EDTA**[9]
r_1/mM^{-1}s^{-1}	2.5	2.1	2.4	3.3
$^{298}k_{ex}$ /×10^{6} s^{-1}	111 ± 6	1134	5957	471
Δ^2 /×10^{19} s^{-2}	51 ± 8	48.1	12.8	6.9
$^{298}\tau_V$ / ps	5.5 ± 0.2	4.4	13.9	27.9
$^{298}\tau_R$ / ps	53 ± 3	46	22	57
$\Delta H^{\#}$/kJ mol^{-1}	39.8 ± 0.7	29.4	17.6	33.5
$A/\hbar$/10^{6} rad s^{-1}	39.0 ± 0.4	43.0	39.4	40.5
q	0.87	0.87	1	1
r_{Mn-H} / Å	2.83	2.83	2.83	2.83

The electron relaxation parameters, Δ^2 and τ_V, are nearly identical for the both hexadentate macrocyclic complexes and this is indicative of quite similar solution structures, as expected. The rotational correlation time is slightly longer, about 15%, for $[Mn(1,4\text{-DO2AM})]^{2+}$ and in perfect agreement with its larger molecular weight. This result confirms the dominant role of

the rotational dynamics in determining the relaxivity of the small metal chelates at high magnetic field strengths. Then, the difference in the r_{1p} values between the two chelates is fully accounted for by their different τ_R values. In the case of $[Mn(EDTA)]^{2-}$ the higher values of both τ_R and q are responsible of the higher r_{1p}.[9]

The rate of water exchange is markedly lower, about one order of magnitude, thus representing the parameter most influenced by the nature of the donor groups. Accordingly, the enthalpy of activation is sensibly higher. For Gd(III) chelates the replacement of carboxylates with amides results in slower rates of water exchange due to a combination of lower steric encumbrance, decreased electron density at the metal centre and reduced overall negative charge of the complexes.[7,10,25] Likewise, these factors seem to play a significant role also for the Mn(II) chelates, being the magnitude of the resulting effect quite comparable.

Dynamic NMR study:

Some insights into the structural and dynamic properties of $[Zn(1,4\text{-DO2AM})]^{2+}$, as a diamagnetic analogue of $[Mn(1,4\text{-DO2AM})]^{2+}$, have been investigated by ^{1}H-NMR spectroscopy in aqueous solution. The solution structure of $[Zn(1,4\text{-DO2AM})]^{2+}$ is expected to be similar to that of the corresponding [Mn(1,4-DO2A)], investigated at the solid state by X-ray diffraction method and in solution by density functional theory (DFT) calculations.[9,26] Crystallographic data reveal the formation of a dimeric $[Mn(1,4\text{-DO2A})]_2$ complex in which the coordination geometry around each Mn(II) ion can be described as a distorted monocapped trigonal prism where the two triangular faces, formed by two ring N- and the carboxylate O-atoms, are nearly parallel (distortion angle is 1.8°) and the capping positions are occupied by two bridging carboxylate O donor atoms.[26] The optimized geometries of the complexes [Mn(1,4-DO2A)] and $[Mn(1,4\text{-DO2A})(H_2O)]$ obtained from DFT calculations highly resemble that found in the solid state: a trigonal prism and a monocapped trigonal prism, respectively, comprised of two parallel (distortion angle is 5.4°) triangular faces defined by two ring N- and the carboxylate O-atoms.[9]

We assume that the predominant species in solution of $[Zn(1,4\text{-DO2AM})]^{2+}$ corresponds closely to that of [Mn(1,4-DO2A)]. In the ^{1}H-NMR spectra of $[Zn(1,4\text{-DO2AM})]^{2+}$ obtained at 273 K, the signals associated with the protons of the cyclen ring give rise to unresolved multiplets, whereas an AB multiplet (-CH_2-) and two singlets (-CH_3) are attributed to the protons of the acetamide pendant arms. By increasing temperature, the bands of the AB multiplet broaden, coalesce (T = 288 K) and then merge into a single resonance (Figure 9).

This fluxional behaviour is likely to be associated with the processes of de-coordination and rotation of the acetamide arms (Scheme 3).

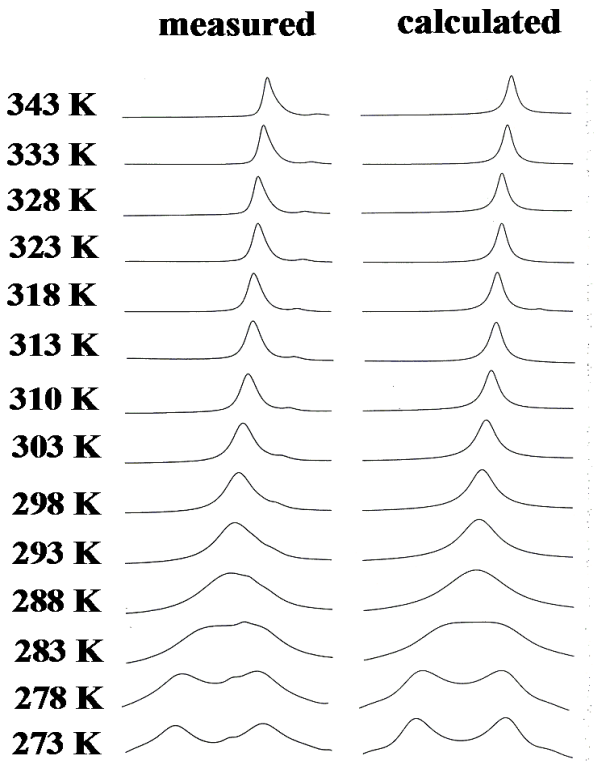

Figure 9. Experimental (left) and calculated (right) ^{1}H-NMR spectra (400 MHz) of the *e* protons in $[Zn(1,4\text{-DO2AM})]^{2+}$ as a function of temperature.

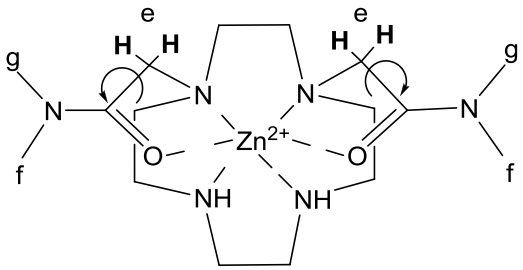

Scheme 3. Arms rotation process in $[Zn(1,4\text{-DO2AM})]^{2+}$

A complete line-shape analysis allows extracting the kinetic parameters of the dynamic process. The proton NMR spectral data were collected at eighteen different values of temperature, in the range 273-343 K (Figure 9). The limiting value of the transverse relaxation time (T_2) has been calculated from the line width of the *g* and *f* proton signals at

273 K (T_2 = 0.07 s), because of its temperature independence below 283 K. In the simulation a chemical shift difference, Δn°, between the *e* protons signals of 61.8 Hz was considered.

From the temperature dependence of the calculated rate constants ($k_{ex}=1/\tau$) characterizing the dynamic process the activation parameters were assessed using the *Eyring* equation (Figure 10). The activation parameters for $[Zn(1,4\text{-}DO2AM)]^{2+}$ are listed in Table 5.

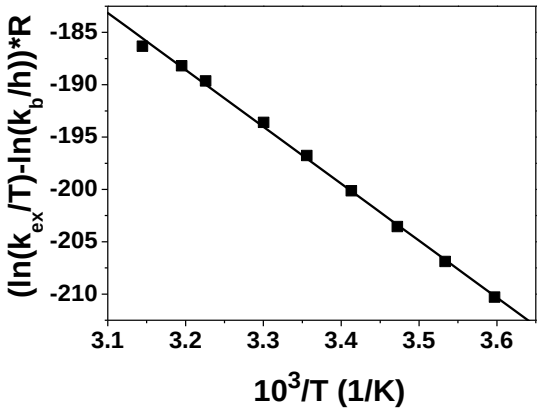

Figure 10. *Eyring* plots for determining the activation parameters of the de-coordination and the arm rotation processes in $[Zn(1,4\text{-}DO2AM)]^{2+}$

Table 5. Rate constant and activation parameters for the de-coordination and arm rotation processes of $[Zn(1,4\text{-}DO2AM)]^{2+}$ obtained from the line-shape analysis of the 1H-NMR spectra.

	$[Zn(1,4\text{-}DO2AM)]^{2+}$
$\Delta H^{\#}$ / kJ·mol^{-1}	54.4 (8)
$\Delta S^{\#}$ / J·mol^{-1}K^{-1}	-14 (2)
$\Delta G^{\#298}$ / kJ·mol^{-1}	50.2 (8)
k^{298} / s^{-1}	328 (5)

The value of $\Delta G^{\#298}$ is markedly lower than that found ($\Delta G^{\#298}$ = 68.2 kJ mol^{-1}) for the racemisation processes of the terminal N atoms in [Lu(DTPA-bis-propylamide)], in spite of a higher $\Delta H^{\#}$ value.[17] This suggests that the dynamic process occurring in $[Zn(1,4\text{-}DO2AM)]^{2+}$ might require the concerted inversion of the macrocyclic ring, which is typically characterized

by high activation enthalpies. For example, in LnDOTA-like complexes $\Delta H^{\#}$ values are ca. 59 – 69 kJ·mol^{-1}.[25]

Conclusions:

The replacement of two negatively charged acetate groups with neutral acetamide arms has a marked influence on the solution properties of the corresponding Mn^{II} chelates. The thermodynamic stability decreases by about 2.5 logK_{ML} units because of the lower basicity of the nitrogen atoms of the macrocyclic ring. On the other hand, the kinetic inertness of the cationic complex $[Mn(1,4\text{-DO2AM})]^{2+}$ is significantly greater than that of the related carboxylates analogues. The half-life for dissociation is ca. one order of magnitude longer than that measured for [Mn(1,4-DO2A)] and [Mn(1,7-DO2A)].

The relaxometric properties are only marginally influenced by the chemical modification of the ligand, with the exception of the rate of water exchange which decreases by more than one order of magnitude with respect to the value found for [Mn(1,4-DO2A)]. This effect is well known and documented in the case of Gd^{III} chelates. The relevant difference is that in the case of the Mn^{II} complexes examined in the present work the k_{ex} values never assume values as short as to limit the relaxivity. So, improved kinetic inertness of Mn^{II} chelates can be attained without a negative impact on the relaxivity. Clearly, a further effort is necessary to combine elevated kinetic inertness and relaxivity with high thermodynamic stability.

Experimental Section:

General: All chemicals were purchased from Sigma-Aldrich Co. and were used without further purification. The concentration of the $MnCl_2$, $ZnCl_2$, $CaCl_2$ and $CuCl_2$ solutions were determined by complexometric titration with standardized Na_2H_2EDTA and xylenol orange ($ZnCl_2$), murexid ($CuCl_2$), Patton-Reader ($CaCl_2$) and Eriochrome Black T ($MnCl_2$) as indicators. The concentration of the 1,4-DO2AM, 1,4-H_2DO2A[10] and 1,7-H_2DO2A[24] was determined by pH-potentiometric titration in the presence and absence of a 50 fold excess of $CaCl_2$. The pH-potentiometric titrations were made with standardized 0.2 M KOH solution. ^{1}H and ^{13}C NMR spectra were recorded on a *Bruker DRX 400* (9.39 T) and *Bruker Avance III* (11.74 T) spectrometers. Chemical shifts are reported relative to TMS and were referenced using the residual proton solvent resonances. Electrospray ionization mass spectra (ESI MS) were recorded on an *SQD 3100 Mass Detector* (Waters), operating in positive or negative ion mode, with 1% v/v HCOOH in methanol as the carrier solvent. HPLC analyses were carried

out on a 1525EF Waters liquid chromatograph equipped with Waters 2489 UV/vis and Waters SQD 3100 MS detectors and using a Waters Atlantis® T3 RPC18 column (150 mm × 4.6 mm, 5 μm). Preparative HPLC separations were carried out using a Waters Atlantis® T3 OBD RPC18 column (100 mm × 19 mm, 5 μm) and a Waters FCIII fraction collector.

Synthesis of DO2AM: Cyclen (0.3 g, 1.7 mmol) was dissolved in $CHCl_3$ (15 mL) and triethylamine (10 eq., 2.42 mL, 17.5 mmol) was added. Then, 2-chloro-*N*,*N*-dimethylacetamide (1.5 eq., 0.488 g, 2.6 mmol) dissolved in $CHCl_3$ (5 mL) was added dropwise to the solution over a period of 4 hours. After stirring overnight at room temperature, the solvent was removed using a rotary evaporator. The solid product was dissolved in CH_2Cl_2 (20 mL) and washed with water (3 x 15 mL). Finally, the aqueous phase was washed with CH_2Cl_2 (3 x 15 mL). The resulting aqueous solution was dried and the crude product was then purified by semi-preparative HPLC-MS (Solvent A: H_2O TFA 0.1%; Solvent B: MeOH; 0-2 min 5% B then gradient 5-40% B in 7 min; Flow 20 mL/min; retention time: 4.6 min) to obtain 90 mg of a pale yellow oil (0.26 mmol, 20.2% yield). Analytical HPLC: (Solvent A: H_2O TFA 0.1%; Solvent B: MeOH; 0-1 min 5% B then gradient 5-100% B in 19 min; flow 1 mL/min; retention time: 6.35 min). ESI-MS (m/z): found 343.3 [M + H^+] (calc. for $C_{16}H_{35}N_6O_2$: 343.5). ^{1}H-NMR (D_2O, 500 MHz): δ 3.81 (s, CH_2CO, 4H), 3.18-3.05 (m, NCH_2 ring, 16H), 2.88 and 2.86 (s, NCH_3, 12H); ^{13}C-NMR (D_2O, 125 MHz): δ 169.8 (C=O), 55.9 (CH_2), 55.5 (CH_2), 53.3 (CH_2), 44.5 (CH_2), 43.3 (CH_2), 37.4 (CH_3), 37.0 (CH_3).

Equilibrium measurements: The protonation constants of 1,4-DO2AM, the stability and protonation constants of the Mn^{2+}-, Ca^{2+}-, Zn^{2+}- and Cu^{2+}-complexes formed with the 1,4-DO2AM, 1,4-DO2A and 1,4-DO2A ligands have been determined by pH-potentiometry and UV-VIS-spectrophotometry. The pH-potentiometic titrations were performed at 1:1 metal-to-ligand concentration ratio (the concentration of the ligand was generally 0.002 M). In calculating the equilibrium constants, the best fitting of the 80-150 mL NaOH – pH and mL KOH - pH data pairs have been obtained by assuming the formation of ML and MHL complexes in the pH range of 1.7-12.0. The equilibrium constants were calculated with the program *PSEQUAD*.[27] For the pH measurements and titrations, a *Methrohm 888 Titrando* titration workstation and a *Metrohm 6.0233.100* combined electrode were used. Equilibrium measurements were carried out at a constant ionic strength (0.1 M KCl) in 6 mL samples at 25 °C. The solutions were stirred, and N_2 was bubbled through them. The titrations were made in the pH range of 1.7-12.0. KH-phthalate (pH=4.005) and borax (pH=9.177) buffers were used

to calibrate the pH meter. For the calculation of $[H^+]$ from the measured pH values, the method proposed by *Irving et al.* was used.[28] A 0.01M HCl solution was titrated with the standardized KOH solution in the presence of 0.1 M KCl ionic strength, respectively. The differences between the measured (pH_{read}) and calculated pH ($-\log[H^+]$) values were used to obtain the equilibrium H^+ concentration from the pH values, measured in the titration experiments. The ion product of water was determined from the same titrations (HCl/KOH) in the pH range of 11.5-12.0.The stability constants of $[Cu(1,4\text{-}DO2AM)]^{2+}$, [Cu(1,4-DO2A)] and [Cu(1,7-DO2A)] have been determined by VIS-spectrophotomtry studying the Cu^{2+} - 1,4-DO2AM, Cu^{2+} - 1,4-DO2A and Cu^{2+} - 1,7-DO2A systems at the absorption band of Cu^{2+} complexes in the $[H^+]$ range 0.01 – 1.0 M. For these experiments 7 samples were prepared (7×3 mL) in which the concentration of Cu^{2+} and ligands was identical ($[Cu^{2+}]=[L]=2.0$ mM). The total H^+ concentration was adjusted by addition of calculated amount of 2.0M HCl ($[H^+]\leq 0.1$ M, $[H^+]+[K^+]=0.1$ M). The samples were kept at 25°C for a week. The absorbance values of the samples were determined at 11 wavelengths (575, 595, 615, 635, 655, 675, 695, 715, 735, 755 and 775 nm). For the calculations of the stability and protonation constants of the $[Cu(1,4\text{-}DO2AM)]^{2+}$, [Cu(1,4-DO2A)] and [Cu(1,7-DO2A)], the molar absorptivities of Cu^{2+}, CuL and CuHL species were determined by recording the spectra of 1.5 mM, 3.0 mM and 5.0 mM solutions of $CuCl_2$, $[Cu(1,4\text{-}DO2AM)]^{2+}$, [Cu(1,4-DO2A)] and [Cu(1,7-DO2A)] in the pH range 1.5 – 6.5 (0.1M KCl, 25°C). The protonation constants of [Cu(1,4-DO2A)] and [Cu(1,7-DO2A)] complexes were also determined by pH-potentiometric titrations at 1:1 metal-to-ligand concentration ratio. The spectrophotometric experiments were performed with a Cary 1E spectrophotometer in a 1 cm quartz cuvette at 25°C.

Kinetic studies: The rates of the metal exchange reactions of $[Mn(1,4\text{-}DO2AM)]^{2+}$ with Zn^{2+} was followed by measuring the water proton relaxation rates ($1/T_1$) of the samples with a *Bruker MQ20 Minispec* spectrometer owing to the large differences in the relaxivities of $[Mn(1,4\text{-}DO2AM)]^{2+}$ ($r_{1p}=2.51$ $mM^{-1}s^{-1}$) and that of free Mn^{2+} ($r_{1p}=8.0$ $mM^{-1}s^{-1}$) at 20 MHz and 25 °C. The longitudinal relaxation times were measured by the '*inversion recovery*' method (180° - τ- 90°) by using 8 different τ values. The measurements were made with 2.0 mM $[Mn(1,4\text{-}DO2AM)]^{2+}$ solution in the presence of 10 to 40 fold excess of Zn^{2+}. The temperature was maintained at 25 °C and the ionic strength of the solutions was kept constant (0.15 M NaCl and 0.1 M KCl). For keeping the pH values constant, *N*-methylpiperazine (pH range of 4.1 – 5.2) and piperazine (pH range of 4.7 – 6.6) buffers (0.01 M) were used. The pseudo-first-order rate constants (k_d) were calculated with the use of the Eq. (12)

$$R_I^t = (R_I^0 - R_I^e)\mathrm{e}^{-k_d t} + R_I^e \qquad (12)$$

where R_1^0, R_1^t, and R_1^e are the relaxation rate ($1/T_1$) values at the start, at time t, and at equilibrium of the reactions, respectively. The calculations were performed using the computer program *Micromath Scientist*, version 2.0 (Salt Lake City, UT, USA).

NMR measurements: ^{1}H-NMR measurements were performed by a *Bruker DRX 400* spectrometer (9.4 T) equipped with *Bruker VT-1000* thermocontroller and a BB inverse *z* gradient probe (5mm). The protonation processes of the 1,4-DO2AM ligand were followed by ^{1}H- NMR spectroscopy. A 0.01 M solution of the ligand in H_2O was prepared for these experiments (D_2O was added to the samples in capillary). The pH was adjusted by stepwise addition of KOH and/or HCl solutions (both prepared in H_2O). The structural behaviour and the dynamic processes of the $[Zn(1,4\text{-}DO2AM)]^{2+}$ complexes were followed by 1D (^{1}H and ^{13}C) and 2D (COSY, NOESY and HSQC) NMR spectroscopy. In ^{13}C-NMR spectroscopy proton decoupling was used with an inverse gated decoupling pulse program. The $[Zn(1,4\text{-}DO2AM)]^{2+}$ complexes were prepared in D_2O ([ZnL]=0.01 M, pD=7.4). The COSY, NOESY, HSQC and HMBC spectra were collected by using gradient pulses in the *z* direction with the standard *Bruker* pulse programs. For NOESY spectra the mixing time (D8) was 300 ms. Spectra were analysed with *Bruker WinNMR* software package.

^{1}H and ^{17}O NMR relaxometric measurements: The proton $1/T_1$ NMRD profiles of $[Mn(1,4\text{-}DO2AM)]^{2+}$ aqueous solutions ([MnL] ~ 1.0 mM) were measured on a fast field-cycling *Stelar SmartTracer* relaxometer over a continuum of magnetic field strengths from 0.00024 to 0.25 T (corresponding to 0.01-10 MHz proton Larmor frequencies). Additional data points in the range 15-70 MHz were obtained on a *Bruker WP80 NMR* electromagnet adapted to variable-field measurements (15-80 MHz proton Larmor frequency) Stelar Relaxometer. Variable-temperature ^{17}O NMR measurements were recorded on a *Bruker Avance III* (11.7 T) spectrometer equipped with a 5 mm probe and standard temperature control units. Aqueous solution of the $[Mn(1,4\text{-}DO2AM)]^{2+}$ complex (~5 mM) containing 2.0% of the ^{17}O isotope (Cambridge Isotope) were used. The observed transverse relaxation rates were calculated from the signal width at half-height.

References:

1. (a) M. Kueny-Stotz, A. Garofalo, D. Felder-Flesch, *Eur. J. Inorg. Chem.*, **2012**, 1987-2005. (b) D. Pan, A. H. Schmieder, S. A. Wickline, G. M. Lanza, *Tetrahedron* **2011**, 67, 8431.
2. B. Drahoš, I. Lukeš, É. Tóth, *Eur. J. Inorg. Chem.,* **2012**, 1975.
3. B. Drahos, J. Kotek, I. Císarová, P. Hermann, L. Helm, I. Lukes, É. Tóth, *Inorg. Chem.* **2011**, 50, 12785.
4. J. Zhu, E. M. Gale, I. Atanasova, T. A. Rietz, P. Caravan, *Chem. Eur. J.* **2014**, 20, 14507.
5. G. S. Loving, S. Mukherjee, P. Caravan, *J. Am. Chem. Soc*. **2013**, 135, 4620.
6. L. Tei, G. Gugliotta, M. Fekete, F. K. Kálmán, M. Botta, *Dalton Trans.* **2011**, 40, 2025.
7. E. Brücher, G. Tircsó, Z. Baranyai, Z. Kovács, A. D. Sherry, In The Chemistry of Contrast Agents in Medical Magnetic Resonance Imaging; 2nd Edition (Eds.: A. E. Merbach, L. Helm, É. Tóth); John Wiley & Sons Ltd. **2013**, 157.
8. B. Drahos, V. Kubicek, C. S. Bonnet, P. Hermann, I. Lukes, E. Toth, *Dalton Trans.,* **2011**, 40, 1945.
9. G. A. Rolla, C. Platas-Iglesias, M. Botta, L. Tei, L. Helm, *Inorg. Chem*., **2013**, 52, 3268.
10. S. Aime, A. Barge, J. I. Bruce, M. Botta, J. A. K. Howard, J. M. Moloney, D. Parker, A. S. de Sousa, M. Woods, *J. Am. Chem. Soc.* **1991**, 121, 5762.
11. A. Pasha, G. Tircsó, E. T. Benyo, E. Brucher, A. D. Sherry, Eur. *J. Inorg. Chem.*, **2007**, 4340.
12. S. Zhang, Z. Kovacs, S. Burgess, S. Aime, E. Terreno, A. D. Sherry, *Chem. Eur. J.* **2001**, 7, 288.
13. C. Li, W.-T. Wong, *J. Org. Chem.* **2003**, 68, 2956.
14. A. S. Mildvan, M. Cohn, *Biochemistry,* **1963**, 2, 910.
15. Z. Garda, A. Forgács, F. K. Kálmán, S. Timári, I. Tóth, Z. Baranyai, L. Tei, Z. Kovács,, G. Tircsó, *Inorg. Chem*., **2016**, 163, 206.
16. A. Takacs, R. Napolitano, M. Purgel, A. C. Benyei, L. Zekany, E. Brucher, I. Toth, Z. Baranyai, S. Aime, *Inorg. Chem.*, **2014**, 53, 2858
17. C. F. G. C. Geraldes, A. M. Urbano, M. C. Alpoim, A. D. Sherry, K.-T. Kuan, R. Rajagopalan, F. Maton, R. N. Muller, *Magn. Reson. Imaging*, **1995**, *13*, 401.
18. H. Imura, G. R. Choppin, W. P. Chacheris, L. A. de Learie, T. J. Dunn, D. H. White, *Inorg. Chim. Acta*, **1997**, *258*, 227.
19. Z. Baranyai, E. Brücher, T. Iványi, R. Király, I. Lázár, L. Zékány, *Helv. Chim. Acta*, **2005**, 88, 604.
20. S. Aime, M. Botta and E. Terreno, Adv. *Inorg. Chem.,* **2005**, 57, 173.
21. L. Tei, G. Gugliotta, M. Fekete, F. K. Kálmán, M. Botta, *Dalton Trans.*, **2011**, 40, 2025
22. T. J. Swift, R. Connick, *E. J. Chem. Phys.* **1962**, 37, 307.
23. N. Bloembergen, L. O. Morgan, *J. Chem. Phys.,* **1961** 34, 842.
24. J. H. Freed, *J. Chem. Phys.* **1978**, 68, 4034.
25. C. Platas-Iglesias, *Eur. J. Inorg Chem.* **2012**, 2023.
26. A. Bianchi, L. Calabi, C. Giorgi, P. Losi, P. Mariani, D. Palano, P. Paoli, P. Rossi, B. Valtancoli, *J. Chem. Soc., Dalton Trans.*, **2001**, 917.
27. L. Zékány, I. Nagypál, In Computational Method for Determination of Formation Constants, Legett, D. J. (Ed), Plenum, New York, **1985**, 291.
28. H. M. Irving, M. G. Miles, L. Pettit, *Anal. Chim. Acta* **1967**, 38, 475.

Chapter 7

Hexadentate Macrocyclic Ligands for Mn(II) Complexation

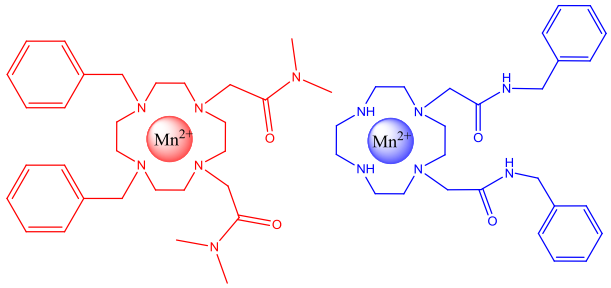

$[Mn(1,4\text{-}BzDO2AM)]^{2+}$ $[Mn(1,4\text{-}DO2AMBz)]^{2+}$

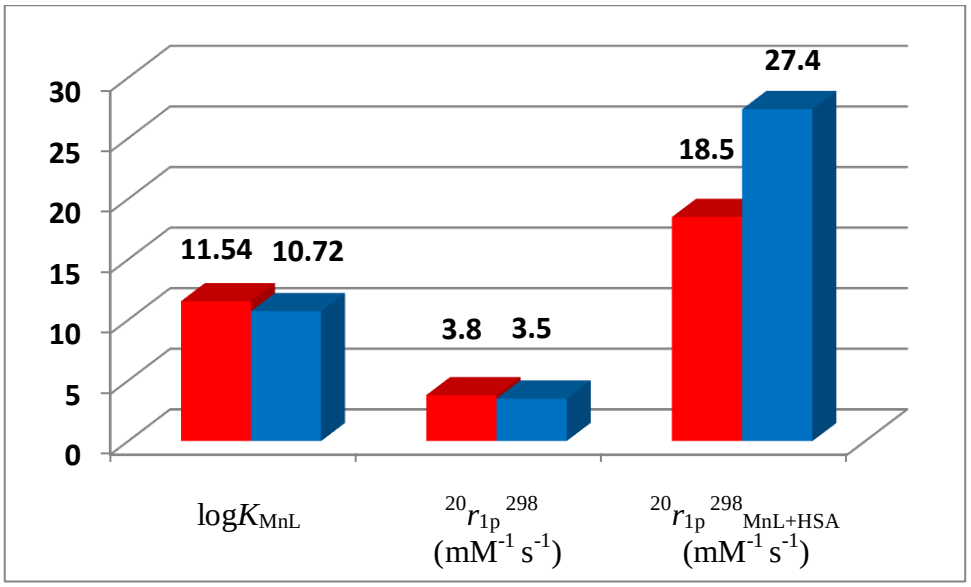

Introduction:

Many ligands based upon 1,4,7,10-tetraazacyclododecane (cyclen) and containing different types and numbers of pendant coordinating functionalities were investigated in the last decades, due to several successful applications of their metal complexes.[1] For example, lanthanide complexes of such ligands have proved useful as magnetic resonance imaging (MRI) contrast agents, [2] NMR shift reagents,[3] in vivo temperature reporters,[4] and catalysts in RNA cleavage.[5] The properties of these complexes are mainly connected with the chemical properties and number of pendant groups. The acetic acid group ($-CH_2CO_2H$) is probably the most common functionality, since cyclen-based ligands containing similar groups form metal complexes characterized by high thermodynamic stability and marked kinetic inertness towards dissociation, hence favouring their use for in vivo applications.[6] The formation of manganese(II) complexes with polyaminopolycarboxylic ligands based upon 1,4,7,10-tetraazacyclododecane (cyclen) has been studied in aqueous solution by means of potentiometric and microcalorimetric techniques affording log*K*, $\Delta H°$ and $T\Delta S°$ values for the complexation reactions. The ML complexes present high stability constants, due to both favourable enthalpic and entropic contributions; with the unique exception of DOTA (1,4,7,10-tetraazacyclododecane-1,4,7,10-tetraacetic acid), the entropic term is prevalent. The 1,4-DO2A (1,4,7,10-tetraazacyclododecane-1,4-diacetic acid) forms a more stable complex than the 1,7-DO2A isomer.[7]

In this chapter we discuss two newly synthesized ligands and we investigate in detail their Mn(II) complexes. We performed thermodynamic, kinetic studies and we report their ability to enhance water (^1H and ^{17}O) relaxation times. Our plan was to synthesize two new ligands maintaining the thermodynamic and kinetic stability properties of the $[Mn(1,4\text{-}DO2AM)]^{2+}$ (Chapter 6), while increasing its relaxivity by suitable modification of the molecular structure. We have introduced two benzyl groups either on the amino groups of cyclen (1,4-BzDO2AM) or on the two acetamide pendant arms (1,4-DO2AMBz). The presence of two hydrophobic moieties favors the formation of adducts with Human Serum Albumin (HSA)[8] through non-covalent interactions. We know that such macromolecular adducts are characterized by large enhancement in the relaxivity thanks to the reduced rotational tumbling in solution.[1a] Of course we need to make sure the chemical modification does not change the hydration state of the complexes (*q*).

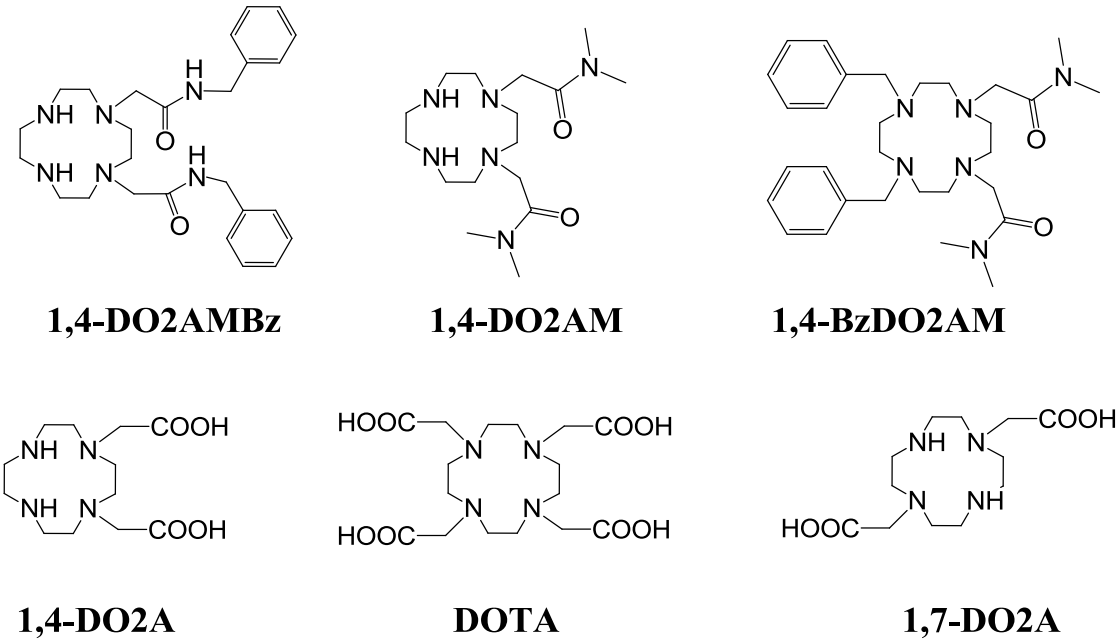

Scheme 1. The structure of the ligands 1,4-DO2AMBz, 1,4-DO2AM, 1,4-BzDO2AM, 1,4-DO2A, DOTA and 1,7-DO2A, discussed in this chapter.

Synthesis:

The 1,4-DO2AMBz was synthesized in a two-step reaction. First, the sidearm was synthesized from 2-bromoacetyl bromide and benzyl amine [9], after that, the sidearm was added to cyclen. The final product was obtained in about 20% yield after semi preparative HPLC-MS purification and was characterized by ESI-MS spectrometry and ^{1}H and ^{13}C NMR spectroscopy. The 1,4-BzDO2AM was synthesized starting from 1,4,7,10-tetraazacyclododecane (cyclen) following the same protocol used for the synthesis of 1,4-dibenzyl-1,4,8,11-tetraazacyclotetradecane [10], after that the intermediates and *N*,*N*-dimethyl 2-chloroacetamides reaction led to the final product in about 20% yield.

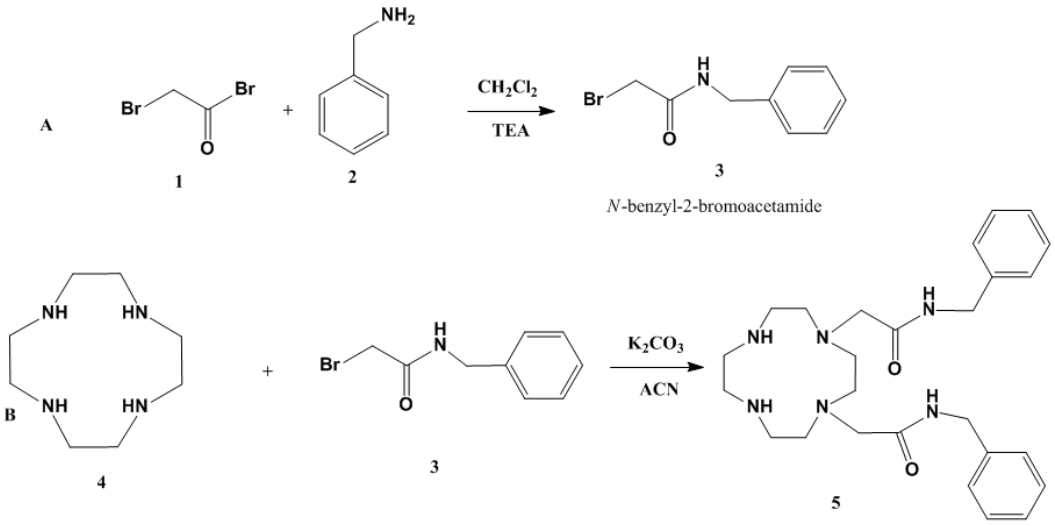

Scheme 2. Synthesis of 1,4-DO2AMBz

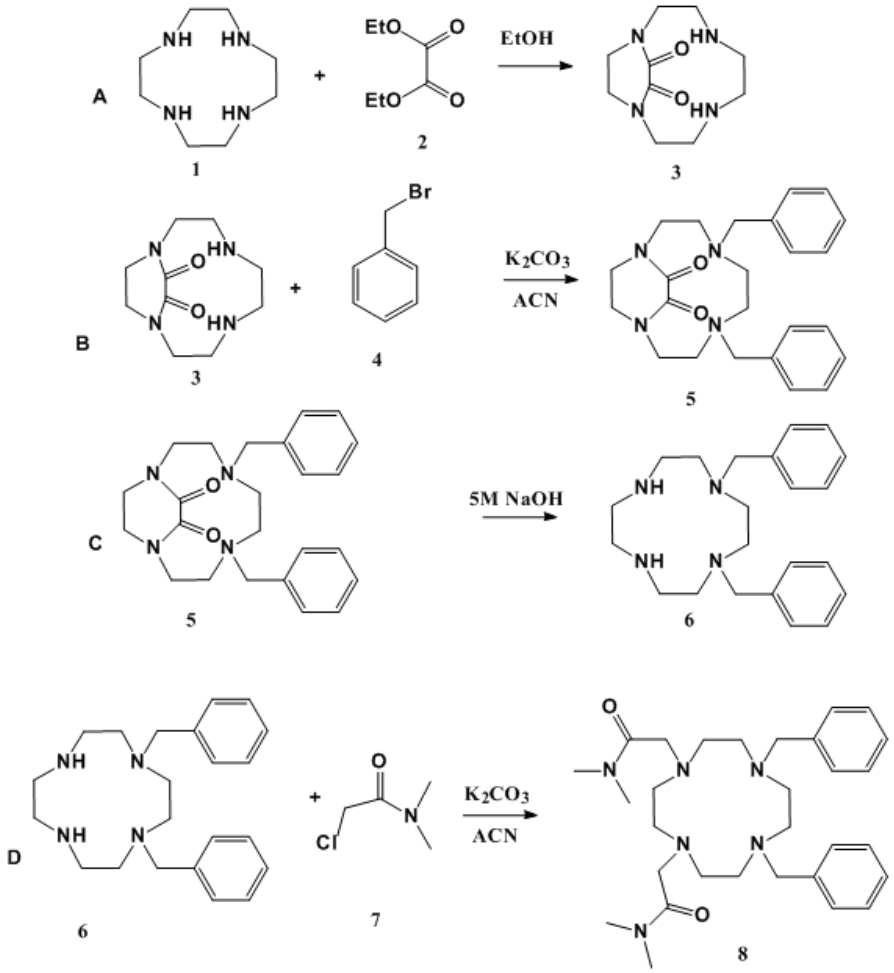

Scheme 3. Synthesis of 1,4-BzDO2AM

Solution equilibrium studies:

Protonation equilibria. The protonation constants of 1,4-DO2AMBz and 1,4-BzDO2AM ligands, defined by Eq. (1), were determined by pH-potentiometry in 0.1 M KCl aqueous solution. The $\log K_i^H$ values of 1,4-DO2AMBz and 1,4-BzDO2AM ligands are listed and compared with those of 1,4-DO2AM, 1,4-DO2A, 1,7-DO2A, DO3A and DOTA in Table 1. Standard deviations (3σ) are shown in parentheses.

$$H_{i-1}L + H^+ \rightleftharpoons H_iL$$

$$K_i^H = \frac{[H_iL]}{[H_{i-1}L][H^+]} \qquad i=1, 2,\ldots, 8. \qquad (1)$$

Table 1. Protonation constants of 1,4-BzDO2AM, 1,4-DO2AMBz, 1,4-DO2AM, 1,4-DO2A, 1,7-DO2A, and DOTA at 25°C in 0.1 M KCl

	1,4-BzDO2AM	**1,4-DO2AMBz**	**1,4-DO2AM[a]**	**1,4-DO2A[b]**	**1,7-DO2A[b]**	**DOTA[c]**
	0.1 M KCl					
$\log K_1$	11.11(1)	9.62(3)	10.14	11.40	11.66	11.41
$\log K_2$	8.22(4)	6.90(5)	8.38	9.58	9.75	9.83
$\log K_3$			-	3.74	4.06	4.38
$\log K_4$			-	1.65	1.78	4.63
$\log K_5$			-	-	-	1.92
$\log K_6$			-	-	-	1.58
$\sum \log K_i^H$	19.33	16.52	18.52	26.37	27.25	33.75

[a] Ref 11 [b] Ref 12 [c]Ref 13

The protonation scheme of DO2AM ligand is well known and it has been fully characterized with both ^{1}H-NMR spectroscopy and pH-potentiometry methods. Because of the similarities of 1,4-BzDO2AM, 1,4-DO2AMBz and 1,4-DO2AM, we may assume that the first protonation occurs on the N_1/N_2 atoms of the macrocycle (the protonation involves partially both N-atoms). The second protonation takes place on the un-substituted (1,4-DO2AMBz) or benzyl-substituted (1,4-BzDO2AM) N_3 (or N_4) atom along with a shift of the former proton to

afford a bis-protonated species on N_1–N_4 or N_2–N_3. This shift of protons allows a larger charge separation, which is well known to occur during the protonation of tetraaza macrocyclic ligands.

Comparison of the protonation constants of 1,4-BzDO2AM and 1,4-DO2AMBz with those of the 1,4-DO2AM indicates that the $\log K_1^H$ value of 1,4-BzDO2AM is slightly higher, whereas the $\log K_1^H$ and $\log K_2^H$ values of 1,4-DO2AMBz are significantly lower than those of the 1,4-DO2AM. In general, the nature of the substituents on the amide group of macrocyclic amino-polycarboxylate ligands can influence the basicity of the ring N-atoms.[14] The lower protonation constants of 1,4-DO2AMBz can be explained by the electron withdrawal effect of the benzyl group on the amide pendant arm results in the lower basicity of the ring nitrogens. The total basicity ($\Sigma \log K_i^H$) of 1,4-BzDO2AMBz is comparable whereas the $\Sigma \log K_i^H$ value of 1,4-DO2AMBz is significantly lower than that of 1,4-DO2AM ligand. By taking into account the $\Sigma \log K_i^H$ values, a lower stability for the 1,4-DO2AMBz complexes can be expected in the comparison with the related complexes of 1,4-DO2AM ligand.

Complexation properties:

The stability constants of the Mn^{II}-complexes formed with 1,4-BzDO2AM and 1,4-DO2AMBz ligands are defined by Eq. (2).

$$K_{ML} = \frac{[ML]}{[M][L]} \qquad (2)$$

The stability constants of the 1,4-BzDO2AM and 1,4-DO2AMBz complexes have been calculated from the titration curves obtained at 1:1 metal to ligand concentration ratios. The best fitting of the experimental data (volume of KOH added vs. pH) was obtained by using the model which includes the formation of ML species in equilibrium. However, the titration data of the Mn^{2+} - 1,4-BzDO2AM and Mn^{2+} - 1,4-DO2AMBz systems indicate base consuming process at pH>8.5. This process characterized by K_{MLH-1} equilibrium constants, can be interpreted by assuming the hydrolysis of the metal ion (the coordination of OH^- ion to Mn^{II} center) according to Eq. *(3)*.

$$K_{MLH_{-1}} = \frac{[ML]}{[ML H_{-1}][H^+]} \qquad (3)$$

The logK_{MnL} and logK_{MnLH-1} values of Mn(1,4-BzDO2AM), Mn(1,4-DO2AMBz) complexes obtained by pH-potentiometry are listed and compared with those of Mn(1,4-DO2AM), Mn(1,4-DO2A), Mn(1,7-DO2A), Mn(DO3A) and Mn(DOTA) in Table 2.

Table 2. The stability (logK_{ML}) and protonation (logK_{MLH-1}) constants Mn^{II}-complexes formed with 1,4-BzDO2AM, 1,4-DO2AMBz, 1,4-DO2AM, 1,4-DO2A, 1,7-DO2A, DO3A and DOTA (0.1 M KCl, 25°C).

	1,4-BzDO2AM	**1,4-DO2AMBz**	**1,4-DO2AM[a]**	**1,4-DO2A[b]**	**1,7-DO2A[b]**	**DOTA[c]**
MnL	11.54 (4)	10.72(3)	12.64	15.22[b]	15.07[b]	19.33
MnHL	-	-	-	4.15[b]	4.48[b]	4.09
MnH_2L	-	-	-	-	-	3.70
$MnLH_{-1}$	10.44(5)	9.44(7)	-	-	-	-

[a] Ref 11 [b] Ref 12 [c]Ref 13

The stability constants of the Mn^{II}-complexes formed with the 1,4-BzDO2AM and 1,4-DO2AMBz are about 1 and 2 orders of magnitude lower than that of Mn(1,4-DO2AM), respectively. The lower logK_{ML} value determined for Mn(1,4-DO2AMBz) complex is not surprising, since the total basicity of 1,4-DO2AMBz is lower by 2 log$K$ unit than that of 1,4-DO2AM ligand. However, the stability constant of Mn(1,4-BzDO2AM) complex is significantly lower than it can be expected by taking into account the $\Sigma\log K_i^H$ values presented in Table 1. Because of the similar basicity of the N donor atoms in 1,4-BzDO2AM and 1,4-DO2AM ligands, it can be assumed that the presence of the bulky benzyl substituents on the N_2 and N_3 sterically hinder the optimal arrangement of two amide oxygen and four ring nitrogen donor atoms around the relatively small Mn^{II}-ion (82 pm). Because of the lower stability of Mn(1,4-BzDO2AM) and Mn(1,4-DO2AMBz) complexes, the hydrolysis of Mn^{II}-ion takes place by the formation of $MnLH_{-1}$ species (Eq. (3)) at basic pH range.

It should be noted that MnL complexes formed with 1,4-BzDO2AM, 1,4-DO2AMBz and 1,4-DO2AM ligands are characterized with significantly lower stability than Mn(1,4-DO2A), Mn(1,7-DO2A), Mn(DO3A) and Mn(DOTA) complexes. The lower logK_{ML} values of the Mn^{II}-complexes formed with 1,4-DO2A-bisamide ligands can be explained by the significantly lower basicity ($\Sigma\log K_i^H$) of the ring N-atoms due to the replacement of the charged carboxylate groups with the non-charged amide pendant arms.

Transmetallation kinetics

The metal-complexes used *in vivo*, must have high kinetic inertness, because the products of their dissociation, both the free metal ion and the ligand are toxic.[15] Nowadays it has been realized that, in the *in vivo* applications of metal-complexes, the kinetic stability is more important that the stability constant.[16] Body fluids are very complex systems and the *in vivo* study of the rate of dissociation reactions of metal-complexes would be difficult. However, the results of *in vitro* studies may provide important information concerning the kinetic behavior of the complexes under *in vivo* conditions. The kinetic stabilities of complexes are characterized either by the rates of their dissociation measured in 0.1 M HCl or by the rates of transmetallation reaction, occurring in solutions with Zn^{2+} or Cu^{2+}.[11,12,17] Generally, the dissociation of MnDOTA-like complexes take place slowly via the proton-assisted dissociation of Mn^{II}-complexes whereas the presence of endogenous metal ions like Zn^{2+} and Cu^{2+} has essentially no effect on the dissociation rates.[11,12,18] The rates of the metal exchange reactions of [Mn(1,4-DO2AM)], [Mn(1,4-DO2A)] and [Mn(1,7-DO2A)] with Zn^{2+} and Cu^{2+} ions were previously investigated.[11,12] For the direct comparison of the kinetic properties of [Mn(1,4-BzDO2AM] and [Mn(1,4-DO2AMBz)] with those of [Mn(1,4-DO2AM)], [Mn(1,4-DO2A)] and [Mn(1,7-DO2A)], the same method and identical conditions were used as in the study of [Mn(1,4-DO2AM)], [Mn(1,4-DO2A)] and [Mn(1,7-DO2A)].[11,12] The rates of the transmetallation reactions of [Mn(1,4-BzDO2AM] and [Mn(1,4-DO2AMBz)] with the use of Zn^{2+} as exchanging metal ion (Eq. (4)) were studied by relaxometry at 20 MHz and 25°C in the pH range 4.5 – 6.5.

$$MnL + Zn^{2+} \rightleftharpoons ZnL + H_2L^{2+} \qquad (4)$$

In the presence of 10 and 20 fold excess of the Zn^{2+}-ion the transmetallation can be treated as a pseudo-first-order process and the rate of reactions can be expressed with the Eq. (5).

$$-\frac{d[MnL]_t}{dt} = k_d[MnL]_{tot} \qquad (5)$$

where k_d is a pseudo-first-order rate constant and $[MnL]_t$ and $[MnL]_{tot}$ are the concentrations of the MnL species at time t and the total concentration of the complex, respectively. The calculated pseudo-first order rate constants for the transmetallation reaction of $[Mn(1,4\text{-}BzDO2AM)]^{2+}$, $[Mn(1,4\text{-}DO2AMBz)]^{2+}$ and Zn^{2+} as a function of $[H^+]$ are shown in Figure 1.

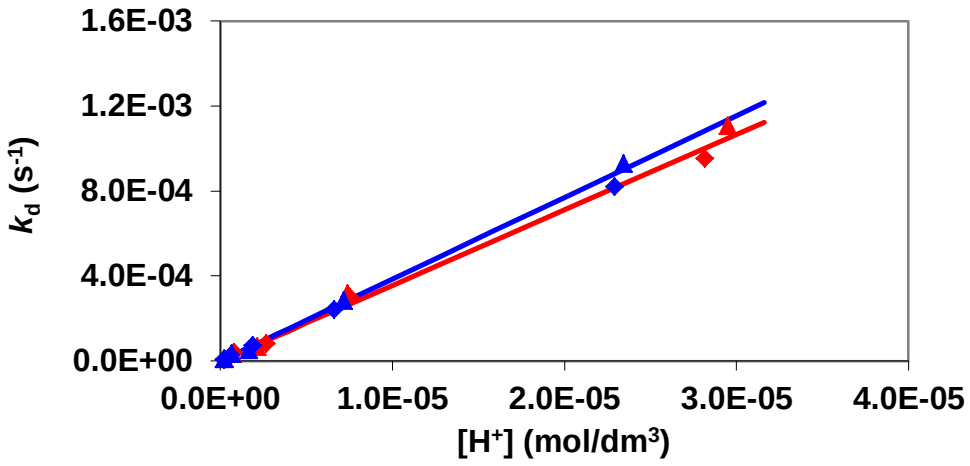

Figure 1. k_d values of the transmetallation reactions of **[Mn(1,4-BzDO2AM)]$^{2+}$** and **[Mn(1,4-DO2AMBz)]$^{2+}$** with Zn^{2+} ([MnL]=0.5 mM, [Zn^{2+}]=10 mM (◆) and 20 mM (▲); 0.1 M KCl, 25°C)

As it can be seen in Figure 1, the transmetallation rates of [Mn(1,4-BzDO2AM)]$^{2+}$ and [Mn(1,4-DO2AMBz)]$^{2+}$ are directly proportional to the H^+ concentration and independent of the [Zn^{2+}]. The increase in the k_d values with increasing [H^+] can be interpreted in terms of the relatively slow proton assisted dissociation of [Mn(1,4-BzDO2AM)]$^{2+}$ and [Mn(1,4-DO2AMBz)]$^{2+}$, followed by a fast reaction between the free ligand and the exchanging Zn^{2+} ions. The dependence of k_d on the [H^+] can be expressed as a first-order function of [H^+] by taking into account the proton-independent (Eq. (6)) and proton assisted (Eq. (7)) pathways.

$$MnL \xrightarrow{k_0} Mn^{2+} + H_2L \qquad (6)$$

$$MnL + H^+ \xrightarrow{k_1} Mn^{2+} + H_xL \qquad (7)$$

k_0 and k_1 are the rate constants characterizing the spontaneous and proto-assisted dissociation of [Mn(1,4-BzDO2AM)]$^{2+}$ and [Mn(1,4-DO2AMBz)]$^{2+}$, respectively. By considering all the possible pathways and the rate of transmetallation of [Mn(1,4-BzDO2AM)]$^{2+}$ and [Mn(1,4-DO2AMBz)]$^{2+}$ (Eq. (5)), the pseudo-first-order rate constant (k_d) can be expressed by Eq. (8).

$$-\frac{d[MnL]_t}{dt} = k_0[MnL] + k_1[MnL][H^+] \qquad (8)$$

By taking into account the total concentration of the complex ($[MnL]_{tot} = [MnL]$), the pseudo-first-order rate constant (k_d) can be expressed as follows:

$$k_d = k_0 + k_1[H^+] \quad (9)$$

The k_0 and k_1 rate constants were calculated by fitting the experimental data presented in Figure 1 to Eq. (9). The rate constants and the dissociation half-lives at pH=7.4 ($t_{1/2} = \ln 2/k_d$) characterizing the transmetallation reaction of $[Mn(1,4\text{-BzDO2AM})]^{2+}$ and $[Mn(1,4\text{-DO2AMBz})]^{2+}$ with Zn^{2+} are listed and compared with the corresponding values reported for $[Mn(1,4\text{-DO2AM})]^{2+}$, [Mn(1,4-DO2A)], [Mn(1,7-DO2A)] and [Mn(DOTA)] in Table 3.

Table 3. Rate constants and half-lives at pH=7.4 for the dissociation reactions of $[Mn(1,4\text{-BzDO2AM})]^{2+}$, $[Mn(1,4\text{-DO2AMBz})]^{2+}$, $[Mn(1,4\text{-DO2AM})]^{2+}$, [Mn(1,4-DO2A)], [Mn(1,7-DO2A)] and $[Mn(DOTA)]^{2-}$ complexes (0.1 M KCl, 25°C).

	Mn(1,4-BzDO2AM)	**Mn(1,4-DO2AMBz)**	**Mn(1,4-DO2AM)[a]**	**Mn(1,4-DO2A)[b]**	**Mn(1,7-DO2A)[b]**	**Mn(DOTA)[c]**
k_0 ($M^{-1}s^{-1}$)	$(-9\pm8)\times10^{-6}$	$(-1\pm5)\times10^{-7}$	-6×10^{-7}	–	–	1.8×10^{-7}
k_1 ($M^{-1}s^{-1}$)	36 ± 2	38 ± 2	8.7	99	84	0.04
k_2 ($M^{-2}s^{-1}$)	–	–	–	1.5×10^6	2.5×10^6	1.6×10^3
$\log K_{MnLH}$	–	–	–	4.15	4.48	4.26
k_d (s^{-1}) pH=7.4	1.4×10^{-6}	1.5×10^{-6}	3.5×10^{-7}	3.9×10^{-6}	3.3×10^{-6}	2.6×10^{-6}
$t_{1/2}$ (h) pH=7.4	136	126	556	49.4	58.3	1070

[a] Ref 11 [b] Ref 12 [c]Ref 18

The data presented in Table 3 also show that the obtained k_0 values are very low and the error in them is very high, indicating the unimportance of the spontaneous dissociation of the $[Mn(1,4\text{-BzDO2AM})]^{2+}$ and $[Mn(1,4\text{-DO2AMBz})]^{2+}$. The k_1 rate constants characterizing the proton-assisted dissociation of the $Mn(1,4\text{-BzDO2AM})]^{2+}$ and $[Mn(1,4\text{-DO2AMBz})]^{2+}$ complexes are about 4 times higher than that of the $[Mn(1,4\text{-DO2AM})]^{2+}$ and about three times smaller than those of [Mn(1,4-DO2A)] and [Mn(1,7-DO2A)] complexes. It is generally accepted that the proton assisted dissociation of Mn^{II}-complexes of DOTA-like ligands possessed by carboxylate pendant arms takes place by the protonation at one of the carboxylate group, which is more likely followed by the transfer of proton to the ring nitrogen with the release of Mn^{2+} from the coordination cavity.[12,18] Since the replacement of the protonable carboxylate groups with non-protonable amide groups does not allow the

formation of the protonated MnHL intermediate, it can be assumed that the proton assisted dissociation of Mn^{II}-complexes formed with DO2A-bisamides takes place by protonation of the ring N-atom followed by dissociation of the Mn^{2+} ion. By taking into account the k_1 values of $Mn(1,4\text{-BzDO2AM})]^{2+}$, $[Mn(1,4\text{-DO2AMBz})]^{2+}$ and $[Mn(1,4\text{-DO2AM})]^{2+}$, it can be assumed that the protonation of the ring N-atom in $[Mn(1,4\text{-BzDO2AM})]^{2+}$ and $[Mn(1,4\text{-DO2AMBz})]^{2+}$ occur more easily, which might be explained by the weak interactions between the donor atoms of 1,4-BzDO2AM and 1,4-DO2AMBz ligands and Mn^{II}-ion. This hypothesis has been confirmed by the lower stability constants of $[Mn(1,4\text{-BzDO2AM})]^{2+}$ and $[Mn(1,4\text{-DO2AMBz})]^{2+}$ complexes (Table 2). The half-life ($t_{1/2}$) of dissociation of $[Mn(1,4\text{-BzDO2AM})]^{2+}$ and $[Mn(1,4\text{-DO2AMBz})]^{2+}$ calculated for pH=7.4 is about four times lower than that measured for $[Mn(1,4\text{-DO2AM})]^{2+}$ but remain significantly higher than those reported for of [Mn(1,4-DO2A)] or [Mn(1,7-DO2A)].

^{1}H and ^{17}O NMR relaxometric studies.

The relaxometric characterization of the two complexes begins with the measure of the pH dependency of the relaxivity. The overall behaviour follows quite closely that observed for $[Mn(1,4\text{-DO2AM})]^{2+}$. The relaxivity is constant over the pH range 12 to 5, where complete formation of the metal complex occurs, and then it shows a sharp increase up to pH ca. 3-4, where another range of constant r_{1p} is formed. These results confirm that the introduction of the benzyl groups either on the macrocycle or on the pendant arms does not alter significantly the stability of the complexes. The pH dependence of the relaxivity for both complexes is reported in Figure 2.

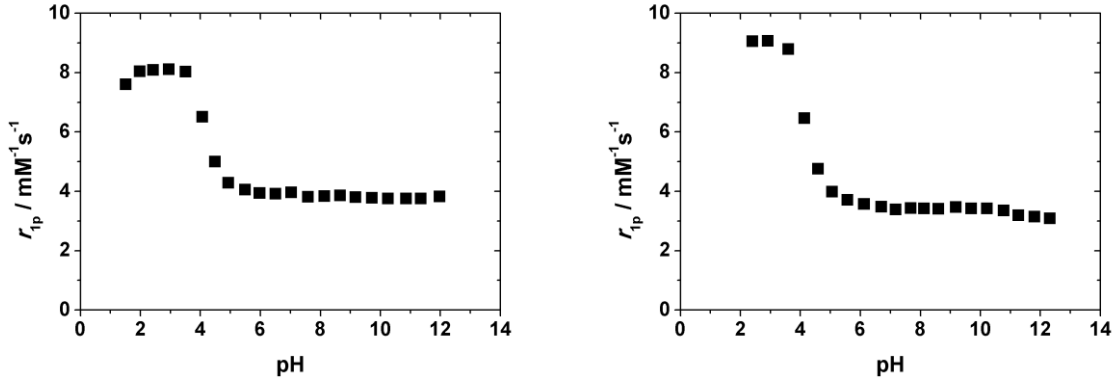

Figure 2. Plot of the relaxivity (20 MHz; 25 ºC) of the $[Mn(1,4\text{-BzDO2AM})]^{2+}$ (left) and $[Mn(1,4\text{-DO2AMBz})]^{2+}$ (right) complexes as a function of pH.

The r_{1p} values of $[Mn(1,4\text{-BzDO2AM})]^{2+}$ and $[Mn(1,4\text{-DO2AMBz})]^{2+}$ as measured at 25°C, 20 MHz and neutral pH are 3.8 and 3.5 mM^{-1} s^{-1}, respectively. These values are considerably higher than that of [Mn(1,4-DO2A)] and $[Mn(1,4\text{-DO2AM})]^{2+}$, suggesting that both complexes feature one coordinated water molecule and an enhanced inner sphere relaxivity associated with their larger size (longer τ_R).

The NMRD profiles have been measured at 298 and 310 K over the proton Larmor frequency range 0.01-70 MHz, corresponding to magnetic field strengths varying between 2.343×10^{-4} T and 1.645 T (Figure 3). As typical for low molecular weight complexes, the profiles have a rather simple functional form consisting of a region of constant relaxivity at low fields, a simple dispersion around 6-8 MHz, and another region at high fields (> 20 MHz) where the relaxivity tends to flatten out.

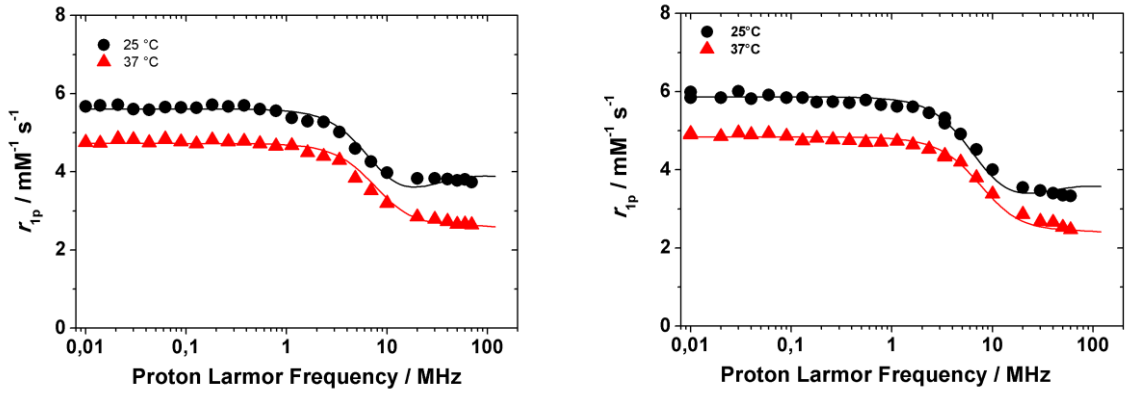

Figure 3. ^{1}H NMRD profiles recorded at different temperatures for $[Mn(1,4\text{-BzDO2AM})]^{2+}$ (left) and $[Mn(1,4\text{-DO2AMBz})]^{2+}$ (right). The lines represent the fit of the data as explained in the text.

As for the parent complex, also in this case the relaxivity decreases by increasing temperature over the entire frequency range, clearly indicating that both Mn(II) chelates are in the fast-exchange regime and that r_{1p} is only limited by the rotational correlation time.

Also in this case a quantitative assessment of the water exchange kinetics has been gained through the measurements and analyses of the temperature dependence of the ^{17}O NMR transverse relaxation rate (R_2) and paramagnetic shift ($\Delta\omega$) (Figure 4 A and B). The experimental data were measured on a high-resolution NMR spectrometer, operating at 14.1 T, on aqueous solutions of the complexes (2-7 mM) at neutral pH. The data were then analysed according to the well-established set of Swift-Connick equations. The reduced R_2 ($1/T_{2r}$) and $\Delta\omega$ values are reported in Figure 4A and 4B, respectively. As for the parent

complex (see Chapter 6), the increase of $1/T_{2r}$ with decreasing temperature over a wide range of values represents a clear indication of a fast rate of exchange for the coordinated water molecule, in agreement with the qualitative conclusions obtained from the analysis of the T-dependent NMRD profiles.

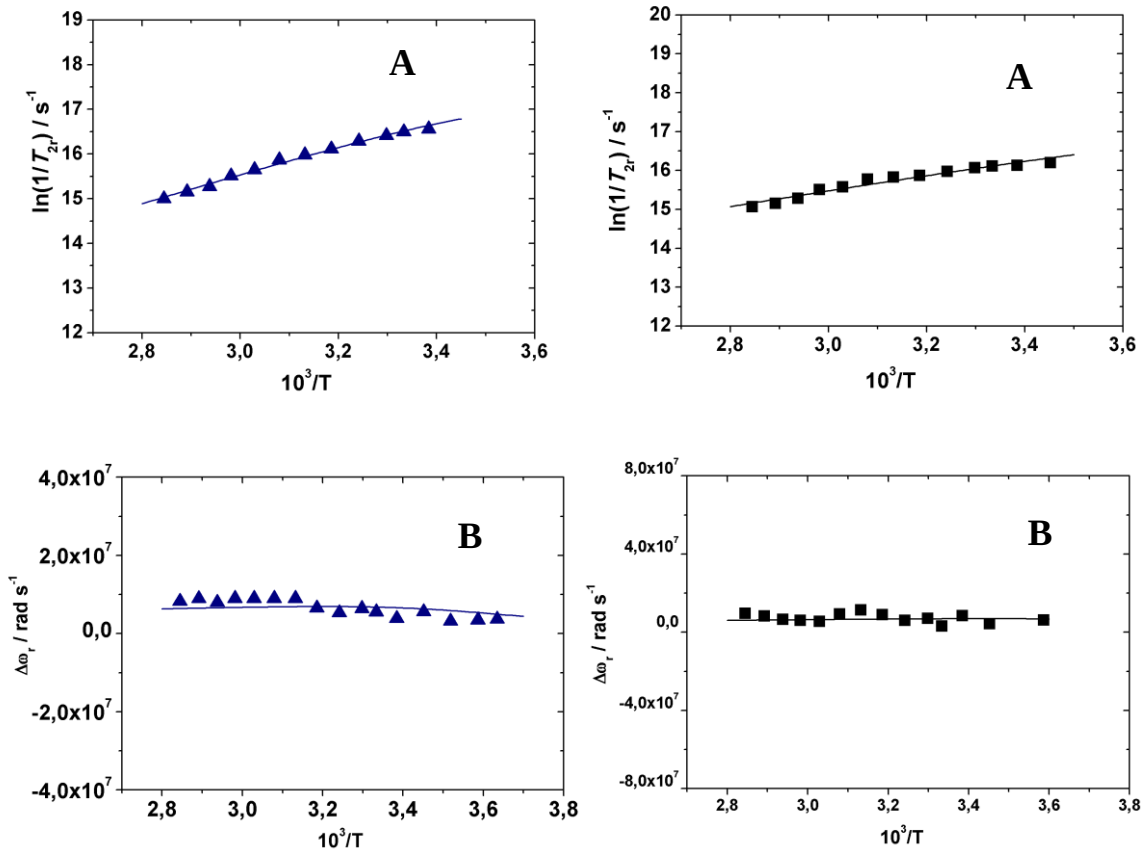

Figure 4. Reduced transverse (A) ^{17}O NMR relaxation rates and ^{17}O NMR chemical shifts (B) measured for[Mn(1,4-DO2AMBz)]$^{2+}$ (left) and [Mn(1,4-BzDO2AM)]$^{2+}$ (right) at 11.74 T. The lines represent the fit of the data as explained in the text

The ^{1}H NMRD and ^{17}O NMR data were fitted simultaneously according to the established theory of paramagnetic relaxation expressed in terms of the Solomon-Bloembergen-Morgan[19] and Freed's[20] equations for the *inner-* (IS) and *outer sphere* (OS) proton relaxation mechanisms, respectively, and of the Swift-Connick theory for the ^{17}O relaxation. Following a well-established practice, due to the large number of relaxation parameters some of them were fixed to reasonable values: q was fixed to 1; the distance between the metal ion and the protons of the bound water molecule, r, was fixed to 2.83 Å; a and D were set to 3.6 Å and 2.3×10^{-5} cm^2 s^{-1} (at 25°C), respectively; E_V was fixed to 1.0 kJ mol^{-1}. To E_R (activation energy for the rotational motion of the complex) and E_D (activation energy of D) were

assigned the same values found for [Mn(1,4-DO2A)]: 19.1 and 17.3 *k*J mol^{-1}, respectively. The relevant best-fit parameters are listed in Table 4 and compared with those of related macrocyclic Mn(II) complexes.

Table 4. Parameters obtained from the simultaneous analysis of ^{17}O NMR and ^{1}H NMRD data.

Parameters	1,4-BzDO2AM	1,4-DO2AMBz	1,4-DO2AM	1,4-DO2A[21]
r_1 / mM^{-1} s^{-1}	3.8	3.5	2.5	2.1
$^{298}k_{ex}$ /×10^6 s^{-1}	253 ± 9	175 ± 5	111 ± 6	1134
Δ^2 /×10^{19} s^{-2}	20 ± 2	20 ± 1	51 ± 8	48.1
$^{298}\tau_V$ / ps	13 ± 1	11 ± 1	5.5 ± 0.2	4.4
$^{298}\tau_R$ / ps	96 ± 2	85 ± 3	53 ± 3	46
$\Delta H^{\#}$ / *k*J mol^{-1}	14.4 ± 1.1	24.6 ± 0.8	39.8 ± 0.7	29.4
$A/\hbar$ / 10^6 rad s^{-1}	31.0 ± 0.4	33.0 ± 0.3	39.0 ± 0.4	43.0
q	1*	1*	0.87	0.87
r_{Mn-H} / Å*	2.83	2.83	2.83	2.83
a / Å*	3.6	3.6	3.6	3.6

* fixed during the fit

The electron relaxation parameters, Δ^2 and τ_V, are very similar for the both macrocyclic complexes and similar to the values for the parent complex. This represents a strong indication of the occurrence of strictly analogous solution structures for the three complexes. The rotational correlation time τ_R assumes the value of 96 and 85 ps for [Mn(1,4-BzDO2AM)]$^{2+}$ and [Mn(1,4-DO2AMBz)]$^{2+}$, respectively. This nicely reflects the increased molecular mass of the benzylic derivatives over the parent complex and confirms the limiting role of the rotational dynamics to the relaxivity of the complexes. In addition, the difference in the r_{1p} and τ_R values between the two chelates is well accounted for by their slightly different molecular masses.

The rates of water exchange are about are about two times higher than for [Mn(1,4-DO2AM)]$^{2+}$ and approximately half that of [Mn(EDTA)]$^{2-}$. So, the introduction of hydrophobic substituents impacts not only the rotational dynamics but also the water exchange dynamics of the complexes, likely by influencing the relative energy values of their six- and seven-coordinate states.

Human Serum Albumin (HSA) binding studies.

The presence of hydrophobic groups allows the complexes to bind HSA. The binding interaction has been investigated through the well-established proton relaxation enhancement (PRE) technique that consists in measuring the increase of the water proton longitudinal relaxation rate (R_1) as a function of increasing concentration of the protein at 20 MHz and 298 K (Figure 5). R_1 is enhanced by the increase of the fraction of bound complex, characterized by a decreased reorientational motion. The fitting of the experimental data to the theoretical values calculated based on the established theory provides the values of the thermodynamic association constant, K_A, the number of the equivalent and independent binding sites, n, and the relaxivity of the resulting paramagnetic metallo-protein, r_1^{bound}. All the data were fitted to a 1:1 binding isotherm even though the presence of multiple affinity sites on HSA cannot be excluded for these complexes. The affinity of the complexes for the protein is influenced by the position of the pendant hydrophobic moieties: K_A is ca. 3.9×10^3 M^{-1} for $[Mn(1,4\text{-}BzDO2AM)]^{2+}$ and 1.9×10^3 M^{-1} for $[Mn(1,4\text{-}DO2AMBz)]^{2+}$.

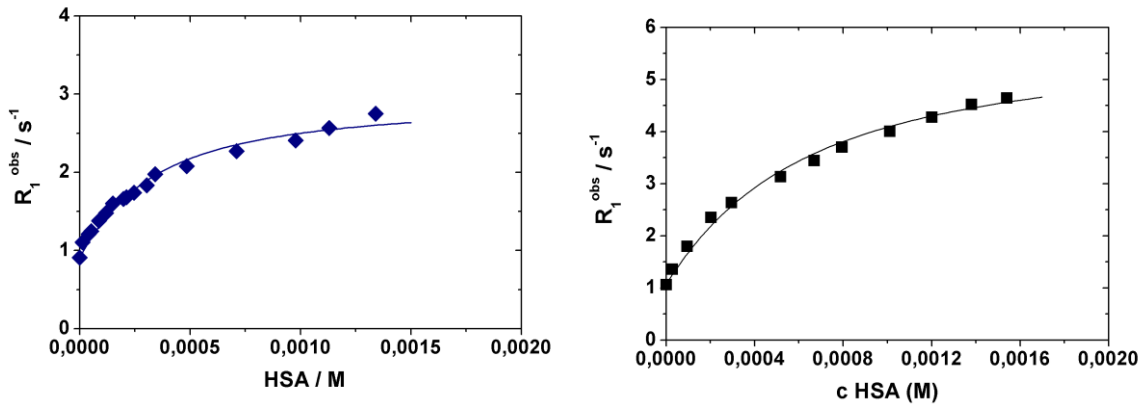

Figure 5. Changes in the observed longitudinal relaxation rates of water protons observed upon addition of HSA to solutions of the $[Mn(BzDO2AM)]^{2+}$ (0.139 mM) and $[Mn(DO2AMBz)]^{2+}$ (0.199 mM) complexes. The solid lines represent the least-squares fits of the data according to a 1:1 binding isotherm.

Table 5. Best-fit parameters obtained from the analysis of the ^1H relaxometric titrations (20 MHz; 298 K) of the Mn^{2+} complexes with HSA.

	$[Mn(1,4\text{-}DO2AMBz)]^{2+}$	$[Mn(1,4\text{-}BzDO2AM)]^{2+}$
$n\cdot K_A$ (M^{-1})	1964 ± 342	3909 ± 583
r_{1p}^b (mM^{-1} s^{-1})	27.4 ± 1.4	18.5 ± 0.7
r_{1p}^f (mM^{-1} s^{-1})	3.5	3.8

These values are 2-3 times higher than similar data reported for Gd(III) complexes bearing analogous targeting groups.[22] However, the Gd-chelates (anionic) and these Mn(II) complexes (cationic) differ for the overall charge. The r_{1p}^{bound} (20 MHz and 298 K) values show a difference: 18.5 mM^{-1} s^{-1} for $[Mn(1,4\text{-}BzDO2AM)]^{2+}$ and 27.4 mM^{-1} s^{-1} for $[Mn(1,4\text{-}DO2AMBz)]^{2+}$ (Table 5). Clearly, the relative position of the benzylic groups in the two complexes influences the motional coupling between the paramagnetic unit and the protein. One hypothesis is that the presence of the two hydrophobic groups on the coordinating acetamide moieties limits the degree of local motions involving the coordination cage (longer effective rotational correlation time) and thus increases relaxivity.

Conclusions:

The chemical modification of the basic structure of DO2AM, with the introduction of two benzyl groups either on the macrocycle or on the pendant arms, has strong effect on various properties of the corresponding Mn(II) complexes.

- Both complexes show higher r_{1p} values. The increase of molecular mass seems to be translated entirely into a corresponding increase of relaxivity, thus suggesting a rather compact structure characterized by an isotropic tumbling motion.
- The high relaxivity values suggest the presence of one bound water molecule, although we cannot exclude the presence of a small population of the q=0 isomer. In any case, the hydration state of the parent complex did not decrease upon the chemical modification.
- The rate of water exchange has increased by a factor of ca. two as compared to the value of MnDO2AM. This is not easy to explain without additional information on the mechanism of exchange, because the overall charge of the complexes and their coordination geometries did not change. Probably, steric interactions between the hydrophobic substituents and the coordinated water molecule might be involved.
- As for the corresponding Gd(III) chelates, the presence of the hydrophobic pendant groups enables the formation of non-covalent adducts with HSA. The affinity constants and the relaxivity values of the adducts are quite comparable to those typical of the analogous Gd(III) complexes.
- The thermodynamic stability constants decreased by nearly one log$K$. Moreover, the kinetic inertness of the modified complexes sensibly reduced, as shown by the $t_{1/2}$ values, ca. 5 times lower than for MnDO2AM.

This last point is quite disappointing because the lower stability of the complexes attenuates to some extent the advantages obtained in terms of relaxation efficiency. Clearly, more efforts are necessary to find a better compromise between safety and efficiency for the Mn-based MRI probes.

Experimental Section:

General: All chemicals were purchased from Sigma-Aldrich Co. and were used without further purification. The concentration of the $MnCl_2$, and $ZnCl_2$ solutions were determined by complexometric titration with standardized Na_2H_2EDTA and xylenol orange ($ZnCl_2$), and Eriochrome Black T ($MnCl_2$) as indicators. The concentration of the 1,4-BzDO2AM, and 1,4-DO2AMBz was determined by pH-potentiometric titration in the presence and absence of a 50 fold excess of $CaCl_2$. The pH-potentiometric titrations were made with standardized 0.2 M KOH solution. ^{1}H and ^{13}C NMR spectra were recorded on a *Bruker DRX 400* (9.39 T) and *Bruker Avance III* (11.74 T) spectrometers. Chemical shifts are reported relative to TMS and were referenced using the residual proton solvent resonances. Electrospray ionization mass spectra (ESI MS) were recorded on an *SQD 3100 Mass Detector* (Waters), operating in positive or negative ion mode, with 1% v/v HCOOH in methanol as the carrier solvent. HPLC analyses were carried out on a 1525EF Waters liquid chromatograph equipped with Waters 2489 UV/vis and Waters SQD 3100 MS detectors and using a Waters Atlantis® T3 RPC18 column (150 mm × 4.6 mm, 5 μm). Preparative HPLC separations were carried out using a Waters Atlantis® T3 OBD RPC18 column (100 mm × 19 mm, 5 μm) and a Waters FCIII fraction collector.

Synthesis of 1,4-DO2AMBz:2-bromoacetyl bromide (1 mL, 11.5 mmol) and benzyl amine (1.14mL, 10.4 mmol) were dissolved in CH_2Cl_2 (10 mL) and triethylamine (0.88 mL, 6.26 mmol) was added at 0 °C. The reaction mixture was stirred at 0 ^{o}C for 1 h, and then allowed to warm to room temperature. 15 ml of water was added and the aqueous layer was extracted with 4x 15 ml CH_2Cl_2. The combined organic layer was washed with 50 ml 5% HCl, water, 50 ml saturated $NaHCO_3$, and brine. The organic layer was dried over $MgSO_4$ and then filtered. The solvent was removed in vacuum and the product **3** was purified by flash chromatography Petroleum ether 7:3 Ethyl acetate on silica gel. ESI-MS (m/z): found 228.0 [M + H^+]. We used the sidearm without other characterization.[23] After that cyclen (0.28 g 1.6 mmol) and K_2CO_3 (0.33 g 2.4 mmol) was dissolved in ACN (15 ml) and the product **3** (0.74 g

3.3 mmol) was added dropwise. The mixture was heated to reflux for 24 h. The resulting aqueous solution was dried and the crude product was then purified by semi-preparative HPLC-MS (Solvent A: H_2O TFA 0.1%; Solvent B: MeOH; 0-2 min 10% B then gradient 10-100% B in 18 min; Flow 20 mL/min; retention time: 6.3 min) to obtain 140 mg of an orange oil **5** (0.26 mmol, 18.2% yield). ESI-MS (m/z): found 467.5 [M + H^+] (calc. for $C_{26}H_{38}N_6O_2$: 466.5). ^{1}H-NMR (D_2O, 500 MHz): δ 3.22 (σ CH_2NH 4H) 3.05 (s, CH_2CO, 4H), 2.85-2.65 (m, NCH_2 ring, 16H), 7.51-7.41 (m, CHAr, 10H); ^{13}C-NMR (D_2O, 125 MHz): δ 171.4 (C=O), 131.0 (CH), 129.1 (CH), 57.7 (CH_2), 53.5 (CH_2), 53.0 (CH_2), 50.0 (CH_2), 48.9 (CH_2), 36.6 (CH_2)

Synthesis of 1,4-BzDO2AM: Cyclen (0.5 g 2.9 mmol) was dissolved in ethanol (15 ml) and diethyl oxalate (585 μL 4.3 mmol) was added dropwise. The mixture was heated to reflux for 24 h and then the solvent was removed in vacuum. We characterized the intermediate with mass chromatography: ESI-MS (m/z): found 227.2 [M + H^+]. The product **3** (0.64 g 2.8 mmol) was dissolved in ACN (15 ml) and benzyl bromide (840 μL 7.0 mmol) and K_2CO_3 (2.35 g 17 mmol) were added to the mixture. The mixture was heated to reflux for 24 h and then the solvent was removed in vacuum. The crude product **5** was dissolved in CH_2Cl_2 (20 ml) and washed with water (3x15 ml). The product was purified by flash chromatography (DCM 98:2 MeOH, silica gel). ESI-MS (m/z): found 407.5 [M + H^+]. The product **5** was dissolved in 5 M NaOH (20 ml) and was stirred on 100 °C for 24 h. The solvents volume was rotavaporated to smaller amount (10 ml) and washed with CH_2Cl_2 (3x20 ml); after that the organic phase was washed with water (3x20 ml). The organic layer was dried over $MgSO_4$ and then filtered. The organic solvent was then removed in vacuum. ESI-MS (m/z): found 353.5 [M + H^+]. The intermediate was used without any further characterization.[24]The product **6** (0.17 g 0.5 mmol) and K_2CO_3 (0.63 g, 4.5 mmol) were suspended in ACN (10 ml) and *N*,*N*-dimethyl 2-chloroacetamide (105 μL 1.01 mmol) was added dropwise. The mixture was stirred for 24 h and then the solvent was removed in vacuo. The crude product **8** was purified by flash chromatography (DCM:MeOH 99:1, silica gel) to obtain a pale yellow oil. (0.46 mmol, 15.9 % yield).). ESI-MS (m/z): found 523.5 [M + H^+] (calc. for $C_{30}H_{46}N_6O_2$: 522.5). ^{1}H-NMR (D_2O, 500 MHz): δ 4.31 (σ CH_2 4H) 3.18 (s, CH_2CO, 4H), 3.51 (s CH_3 12H) 2.01-2.28 (m, NCH_2 ring, 16H), 7.30-7.37 (m, CHAr, 10H); ^{13}C-NMR (D_2O, 125 MHz): δ 172.5 (C=O), 137.8 (CH), 126.5.0 (CH), 127.0 (CH), 127.6 (CH) 49.5 (CH_2), 50.1 (CH_2), 50.6 (CH_2), 51.2 (CH_2), 51.9 (CH_2), 55.0 (CH_2) 41.9 (CH_3)

Equilibrium measurements: The protonation constants of 1,4-BzDO2AM and 1,4-DO2AMBz the stability and protonation constants of the Mn^{2+}-complexes formed with the 1,4-BzDO2AM and 1,4-DO2AMBz ligands have been determined by pH-potentiometry. The pH-potentiometic titrations were performed at 1:1 metal-to-ligand concentration ratio (the concentration of the ligand was generally 0.002 M). For the calculation of the equilibrium constants the mL base – pH data were used, obtained in the pH range 1.7–12.0.. The equilibrium constants were calculated with the program *PSEQUAD*.[25] For the pH measurements and titrations, a *Methrohm 888 Titrando* titration workstation and a *Metrohm 6.0233.100* combined electrode were used. Equilibrium measurements were carried out at a constant ionic strength (0.1 M KCl) in 8 mL samples at 25 °C. The solutions were stirred, and N_2 was bubbled through them. The titrations were made in the pH range of 1.7-12.0. KH-phthalate (pH=4.005) and borax (pH=9.177) buffers were used to calibrate the pH meter. For the calculation of $[H^+]$ from the measured pH values, the method proposed by *Irving et al.* was used.[26] A 0.01M HCl solution was titrated with the standardized KOH solution in the presence of 0.1 M KCl ionic strength, respectively. The differences between the measured (pH_{read}) and calculated pH ($-\log[H^+]$) values were used to obtain the equilibrium H^+ concentration from the pH values, measured in the titration experiments. The ion product of water was determined from the same titrations (HCl/KOH) in the pH range of 11.5-12.0.

Kinetic studies: The kinetic inertness of $[Mn(1,4\text{-}BzDO2AM)]^{2+}$ and $[Mn(1,4\text{-}DO2AMBz)]^{2+}$ were characterized by the rates of the exchange reactions taking place between the MnL complexes and Zn^{2+}. The rates of the metal exchange reactions of $[Mn(1,4\text{-}BzDO2AM)]^{2+}$ and $[Mn(1,4\text{-}DO2AMBz)]^{2+}$ with Zn^{2+} was followed by measuring the water proton relaxation rates ($1/T_1$) of the samples with a Stelar Relaxometer equipped with a Bruker WP80 NMR electromagnet adapted to variable-field measurements (15-80 MHz proton Larmor frequency. The kinetic measurements were performed on the Stelar Relaxometer at 0.47 T (20 MHz) and 25 °C owing to the large differences in the relaxivities $[Mn(1,4\text{-}BzDO2AM)]^{2+}$ (r_{1p}=3.83 $mM^{-1}s^{-1}$) and $[Mn(1,4\text{-}DO2AMBz)]^{2+}$ (r_{1p}=3.47 $mM^{-1}s^{-1}$) and that of free Mn^{2+} (r_{1p}=8.0 $mM^{-1}s^{-1}$). The longitudinal relaxation times were measured by the '*inversion recovery*' method (180° - τ- 90°) by using 8 different τ values. The measurements were made with 1.0 mM of $[Mn(1,4\text{-}BzDO2AM)]^{2+}$ and $[Mn(1,4\text{-}DO2AMBz)]^{2+}$ solution in the presence of 10 to 20 fold excess of Zn^{2+}. The temperature was maintained at 25 °C and the ionic strength of the solutions was kept constant (0.15 M NaCl and 0.1 M KCl). For keeping the pH values constant, *N*-methylpiperazine (pH range of 4.1 –

5.2) and piperazine (pH range of 4.7 – 6.6) buffers (0.01 M) were used. The pseudo-first-order rate constants (k_d) were calculated with the use of the Eq. (10)

$$R_1^t = (R_1^0 - R_1^e)e^{-k_d t} + R_1^e \qquad (10)$$

where R_1^0, R_1^t, and R_1^e are the relaxation rate ($1/T_1$) values at the start, at time t, and at equilibrium of the reactions, respectively. The calculations were performed using the computer program *Micromath Scientist*, version 2.0 (Salt Lake City, UT, USA).

^{1}H NMRD and ^{17}O NMR measurements. The water proton longitudinal relaxation rates as a function of pH (20 MHz) were measured with a Stelar Spinmaster Spectrometer FFC–2000 (Mede, PV, Italy) on about 0.6-2.0 mM aqueous solutions in non-deuterated water. The exact concentrations of Mn^{2+} ions were determined by measurement of bulk magnetic susceptibility shifts of a *t*BuOH signal on a Bruker Avance III spectrometer (11.7 T). The ^{1}H T_1 relaxation times were acquired by the standard inversion recovery method with typical 90° pulse width of 3.5 μs, 16 experiments of 4 scans. The reproducibility of the T_1 data was ±5%. The temperature was controlled with a Stelar VTC-91 airflow heater equipped with a calibrated copper–constantan thermocouple (uncertainty of ±0.1 °C). The proton $1/T_1$ NMRD profiles were measured on a fast field-cycling Stelar SmartTracer relaxometer over a continuum of magnetic field strengths from 0.00024–0.25 T (corresponding to 0.01–10 MHz proton Larmor frequencies). The relaxometer operates under computer control with an absolute uncertainty in $1/T_1$ of ±1%. Additional data points in the range 15–70 MHz were obtained on a Stelar Relaxometer equipped with a Bruker WP80 NMR electromagnet adapted to variable-field measurements (15–80 MHz proton Larmor frequency).

Variable-temperature ^{17}O NMR measurements were recorded on a Bruker Avance III spectrometer (11.7 T) equipped with a 5 mm probe and standard temperature control unit. An aqueous solution of the complex (4 mM) containing 2.0% of the ^{17}O isotope (Cambridge Isotope) was used. The observed transverse relaxation rates were calculated from the signal width at half-height.

References:

1. (a) R. B. Lauffer, *Chem. Rev*., **1987**, 87, 901. (b) J. C. G. Bünzli, G. R. Choppin, *Elsevier, Amsterdam*, **1989**. (c) A. D. J. Sherry, *J. Less-Common Met.*, **1989**, 149, 133. (d) S. Aime, M. Botta, M. Fasano, E. Terreno, *Chem. Soc. Rev.,* **1998**, 27, 19.
2. (a) J. C. Bousquet, S. Saini, D. D. Stark, P. F. Hahn, M. Nigam, M. F. Wittemberg J. Ferrucci, *Radiology*, **1988**, 166, 693. (b) M. F. Tweedle, G. T. Gaughan, J. H. U. S. Hagan, *US Pat.* **1987,** 4, 885, 363.
3. (a) D. C. Buster, M. M. C. A. Castro, C. F. G. C. Geraldes, C. R. Malloy, A. D. Sherry, T. C. Siemers, *Magn. Reson. Med.,* **1990**, 15, 25. (b) C. R. Malloy, D. C. Buster, M. M. C. A. Castro, C. F. G. C. Geraldes, F. M. H. Jeffrey and A. D. Sherry, *Magn. Reson. Med.*, **1990**, 15, 33.
4. (a) S. Aime, M. Botta, M. Fasano, E. Terreno, P. Kinchesh, L. Calabi, L. Paleari, *Magn. Reson. Imag.*, **1996**, 35, 648. (b) T. Frenzel, K. Roth, S. Kobler, B. Raduchel, H. Bauer, J. Platzek, H. Weinmann, *Magn. Reson. Med.*, **1996**, 35, 648. (c) C. S. Zuo, J. L. Bowers, K. R. Metz, T. Nosaka, A. D. Sherry, M. E. Clouse, *Magn. Reson. Med.*, **1996**, 36, 955.
5. S. Aime, J. R. Morrow, C. R. Lake, M. R. Churchill, *Angew. Chem., Int. Ed. Engl.*, **1994**, 33, 773.
6. (a) W. P. Cacheris, S. K. Nickle, A. D. Sherry, *Inorg. Chem.*, **1987**, 26, 958. (b) E. Brucher, A. D. Sherry, *Inorg. Chem.*, **1990**, 29, 1555. (c) D. D. Dischino, E Delaney, J. E. Emswiler, G. T. Gaughan, J. S. Prasad, S. K. Srivastava, M. F. Tweedle, *Inorg. Chem.,* **1991**, 30, 1265. (d) E. T. Clarke, A. E. Martell, *Inorg. Chim. Acta*, **1991**, 190, 37. (e) S. Aime, P. L Anelli, M. Botta, F. Fedeli, M. Grandi, P. Paoli, F. Uggeri, *Inorg. Chem.*, **1992**, 31, 2422. (f) X. Wang, T. Jin, V. Combin, A. Lopez-Mut, E. Merciny J. F. Desreux, *Inorg. Chem.,* **1992**, 31, 1095. (g) K. Kumar, T. Jin, X. Wang, J. F. Desreux, M. F. Tweedle, *Inorg. Chem.*, **1994**, 33, 3823. (h) S. Aime, M. Botta, M. Fasano, S. Paoletti, P. L. Anelli, F. Uggeri, M. Virtuani, *Inorg. Chem.*, **1994**, 33, 4707. (i) F. Uggeri, S. Aime, P. L. Anelli, M. Botta, M. Brocchetta, C. de Haën, G. Ermondi, M. Grandi, P. Paoli, *Inorg. Chem.*, **1995**, 34, 633. (j) S. Aime, M. Botta, D. Parker, J. A. G. Williams, *J. Chem. Soc., Dalton Trans,* **1996**, 17. (k) S. Aime, M. Botta, D. Parker, J. A. G. Williams, *J. Chem. Soc., Dalton Trans,* **1996**, 3613. (l) J. Huskens, D. A. Torres, Z. Kovacs, J. P. André, C. F. G. C. Geraldes, A. D. Sherry, *Inorg. Chem.*, **1997**, 36, 1495. (m) A. Bianchi, L. Calabi, C. Giorgi, P. Losi, P. Mariani, P. Paoli, P. Rossi, B. Valtancoli, M. Virtuani, *J. Chem. Soc., Dalton Trans.*, **2000**, 697. (n) J. M. Weeks, M. R. Taylor, K. P. Wainwright, *J. Chem. Soc., Dalton Trans.*, **1997**, 317.
7. A. Bianchi, L. Calabi, C. Giorgi, P. Losi, P. Mariani, D. Palano, P. Paoli, P. Rossi, B. Valtancoli, *J. Chem. Soc., Dalton Trans*. **2001**, 917.
8. S. Aime, M. Botta, M. Fasano, S. Geninatti Crich, E. Terreno, *J. Biol. Inorg. Chem.*, **1996**, 1, 312.
9. H. Xie, D. Ng, S. N. Savinov, B. Dey, P. D. Kwong, R. Wyatt, A. B. Smith, W. A. Hendrickson. *J. Med. Chem.,* **2007**, 4898.
10. F. Bellouard, F. Chuburu, N. Kervarec, L. Toupet, S. Triki, Y. Le Mest and H. Handel. *J. Chem. Soc.*, *Perkin Trans.* 1, **1999**, 3499.
11. A. Forgács, L. Tei, Z. Baranyai, I. Tóth, L. Zékány, M. Botta. *Eur. J. Inorg. Chem.*, **2016**: 1165.
12. Z. Garda, A. Forgács, F. K. Kálmán, S. Timári, I. Tóth, Z. Baranyai, L. Tei, Z. Kovács, G. Tircsó. *Inorg. Chem. J. Inorg. Biochem* **2016** 163, 206.
13. A. Takacs, R. Napolitano, M. Purgel, A. C. Benyei, L. Zekany, E. Brucher, I. Toth, Z. Baranyai, S. Aime, *Inorg. Chem.,* **2014**, 53, 2858.
14. A. Pasha, Gy. Tircsó, E. T. Benyo, E. Brucher, A. D. Sherry, *Eur. J. Inorg. Chem.,* **2007**, 4340.
15. P. Caravan, J. J. Ellison, T. J. McMurry, R. B. Lauffer, *Chemical Reviews* **1999**, 99, 2293.

16. E. Brücher, G. Tircsó, Z. Baranyai, Z. Kovács, A. D. Sherry *Stability and Toxicity of Contrast Agents, Vol. John Wiley & Sons, Ltd*, **2013**, 157.
17. P. Wedeking, K. Kumar, M. F. Tweedle, *Magn. Reson. Imaging,* **1992**, 10, 641.
18. B. Drahos, V. Kubicek, C. S. Bonnet, P. Hermann, I. Lukes, É. Tóth, *Dalton Trans*., **2011**, 40, 1945.
19. N. Bloembergen, L. O. Morgan, *J. Chem. Phys.,* **1961** 34, 842.
20. J. H. Freed, *J. Chem. Phys.* **1978**, 68, 4034.
21. G. A. Rolla, C. Platas-Iglesias, M. Botta, L. Tei, L. Helm, *Inorg. Chem*., **2013**, 52, 3268.
22. S. Aime, M. Botta, M. Fasano, S. Geninatti Crich, E. Terreno, *JBIC,* **1996** 1, 312.
23. H. Xie, D. Ng, S. N. Savinov, B. Dey , P. D. Kwong, R. Wyatt, A. B. Smith, W. A. Hendrickson, J. Med. Chem., 2007, 50, 4898.
24. F. Bellouard, F. Chuburu, N. Kervarec, L. Toupet, S. Triki, Y. Le Mest, H. Handel *J. Chem. Soc., Perkin Trans.,***1999**, 1, 3499.
25. L. Zékány, I. Nagypál, In Computational Method for Determination of Formation Constants, Legett, D. J. (Ed), Plenum, New York, **1985**, 291.
26. H. M. Irving, M. G. Miles, L. Pettit, *Anal. Chim. Acta* **1967**, 38, 475.

Summary

The main objective of this thesis was the detailed characterization of homogeneous series of Mn(II) complexes to assess the possibility of using Mn-based systems as an alternative to Gd (III)-based MRI probes. There is a need to expand the available limited library of compounds so far investigated to achieve better and more reliable information on the correlation between solution structure and molecular relaxation parameters. This is key to enhance the efficacy (relaxivity) of the probes. Moreover, it is very important to obtain accurate information relating to thermodynamic stability and kinetic inertia of the complexes. This is key to develop safe probes for *in vivo* use.

A contrast agent for MRI must have the ability to catalyze efficiently the T_1 and/or T_2 relaxation in tissues at low (μM to mM) concentrations and with acceptable tolerance. The following points summarize the most important features of paramagnetic MRI contrast agents.

- high relaxivity
- high kinetic and thermodynamic stability
- rapid clearance
- low toxicity
- specific biodistribution/accumulation
- low osmolality and viscosity

Our studies focused on the first two points: thermodynamic and kinetic measurements combined with detailed ^{1}H and ^{17}O NMR relaxometric investigations.

Two main classes of complexes were addressed in the thesis.

1) The first is represented by the Mn(II) complexes containing the acyclic pentadentate coordinating unit 6,6-((methylazanediyl)bis(methylene))dipicolinic acid (H_2dpama).

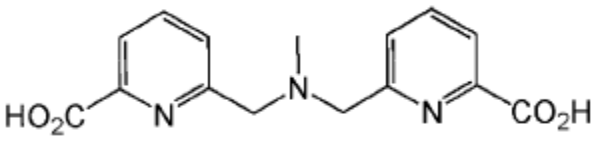

H_2dpama

I investigated mono-, bi- and trinuclear bis-hydrated complexes. Furthermore, several other derivatives bearing different pendant moieties were considered and analyzed.

2) The second general class of complexes I dealt with are those based on the macrocyclic scaffold of cyclen (1,4,7,10-tetraazacyclododecane). In particular, I focused on the exadentate ligands containing two acetamide side arms (1,4-DO2AM) and their derivatives containing hydrophobic pendant groups.

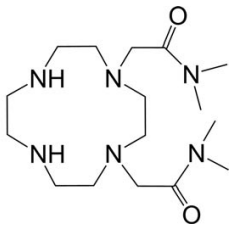

1,4-DO2AM

Chapter 4 reports the characterization of the Mn(II)-complexes of $dpama^{2-}$, $mX(dpama)_2^{4-}$, $mX(dpama)_3^{6-}$ and $bcpe^{2-}$. The ligands contain the pentadentate coordinating unit designed for pentagonal bipyramidal coordination around Mn^{2+} thanks to the presence of two coordinated water molecules. The high hydration number (q=2) imparts remarkably high relaxivities to the Mn^{2+} complexes. Furthermore, these relaxivities are further improved by interaction with HSA, particularly in the case of the bi- and trinuclear complexes. These multimeric complexes show that it is possible to develop low molecular weight Mn^{2+} chelates that may represent viable alternatives to Gd-based MRI probes. Their relaxometric properties, in both the free form and bound to HSA, are fully comparable or better than those shown by the Gd^{3+} complexes commonly used in the clinical practice.

The Mn^{2+} complexes formed with this family of ligands present moderate thermodynamic stabilities. Although this may not be a very serious limitation due to the far better safety profile of Mn^{2+} compared to Gd^{3+}, it is still relevant to continue the search for complexes that exhibit improved characteristics of kinetic inertness with respect to complex dissociation.

In **Chapter 5** we expanded the family of ligands containing the picolinate group by considering the pentadentate ligand H_2DPAPhA and the hexadentate derivative H_3DPAA. Furthermore, we also investigated two lipophilic derivatives of H_2DPAMA and H_2PhDPAMA, which contain a dodecyl side chain attached to the amine nitrogen atom of H_2DPAMA or a hexyl chain at the aniline function of H_2DPAPhA, respectively. These lipophilic can be incorporated into micelles or liposomes, for the preparation of lipid magnetic nanoprobes. These complexes are also able to bind HSA in a non-covalent manner. The hexadentate ligand $DPAA^{3-}$ forms a complex with Mn^{2+} with stability and relaxivity

comparable to that of $[Mn(EDTA)(H_2O)]^2$. On the other hand, the pentadentate ligands $DPAPhA^{2-}$ and $DPAMA^{2-}$ form bis-aquated Mn^{2+} complexes in solution. The r_{1p} value of 6.7 mM^{-1} s^{-1} measured for [Mn(DPAPhA)] at pH 7.4 (25 ºC, 20 MHz) is considerably high, which indicates the presence of two coordinated water molecules. The results obtained have shown that the relaxivities of Mn^{2+} complexes can be modulated by changing the hydration number or introducing lipophilic units in the ligand scaffold, very much like in the case of Gd^{3+} complexes. The adducts formed with HSA have also relaxivities comparable to those attained with lipophilic Gd^{3+} agents.

In **Chapter 6** I discussed the synthesis and characterization of the hexadentate ligand 1,4-DO2AM and its Mn(II) complex. The replacement of two negatively charged acetate groups with neutral acetamide arms has a marked influence on the solution properties of the corresponding Mn^{II} chelates. The thermodynamic stability decreases by about 2.5 logK_{ML} units because of the lower basicity of the nitrogen atoms of the macrocyclic ring. On the other hand, the kinetic inertness of the cationic complex $[Mn(1,4\text{-}DO2AM)]^{2+}$ is significantly greater than that of the related carboxylates analogues. The half-life for dissociation is ca. one order of magnitude longer than that measured for [Mn(1,4-DO2A)] and [Mn(1,7-DO2A)]. The relaxometric properties are only marginally influenced by the chemical modification of the ligand, with the exception of the rate of water exchange which decreases by more than one order of magnitude with respect to the value found for [Mn(1,4-DO2A)].
The main conclusion from this study is that the kinetic inertness of Mn^{II} chelates can be improved without a negative impact on the relaxivity. Clearly, further efforts are necessary to combine the elevated kinetic inertness and relaxivity with high thermodynamic stability. We hope that the results of this study can provide some clues to achieve this ambitious goal.

Chapter 7 presents the results of the synthesis and complete characterization of two novel ligands bearing benzyl pendant groups: 1,4-BzDO2AM, and 1,4-DO2AMBz. We performed thermodynamic, kinetic and relaxometric (^1H and ^{17}O) studies. The chemical modification of the basic structure of 1,4-DO2AM did not changed significantly the thermodynamic stability and also the kinetic stability remains relatively high, with a the half-life ($t_{1/2}$) of dissociation significantly higher than that reported for [Mn(1,4-DO2A)] and [Mn(1,7-DO2A)]. The r_{1p} values of the two complexes are considerably higher than those of [Mn(1,4-DO2A)] and $[Mn(1,4\text{-}DO2AM)]^{2+}$, arising from the presence of one coordinated water molecule associated with a larger molecular size (longer τ_R). The presence of hydrophobic groups allows the

complexes to bind HSA. The affinity of the complexes for the protein is influenced by the position of the pendant hydrophobic moieties: K_A is ca. 3.9×10^3 M^{-1} for [Mn(1,4-BzDO2AM)]$^{2+}$ and 1.9×10^3 M^{-1} for [Mn(1,4-DO2AMBz)]$^{2+}$. Both the affinity constants and the relaxivity values of the adducts are quite comparable to those typical of the analogous Gd(III) complexes. Unfortunately, the thermodynamic stability constants decreased by nearly one log*K*. Moreover, the kinetic inertness of the modified complexes sensibly reduced, as shown by the $t_{1/2}$ values, ca. 5 times lower than for MnDO2AM.

All the r_{1p} and logK_{MnL} values of the Mn(II)-complexes investigated in this thesis are plotted in Figure 1 and 2. In the logK_{MnL} table we also show the stability values of the [Mn(1,4-DO2A)], [Mn(1,7-DO2A)] and [Mn(EDTA)]$^{2-}$ for comparison.

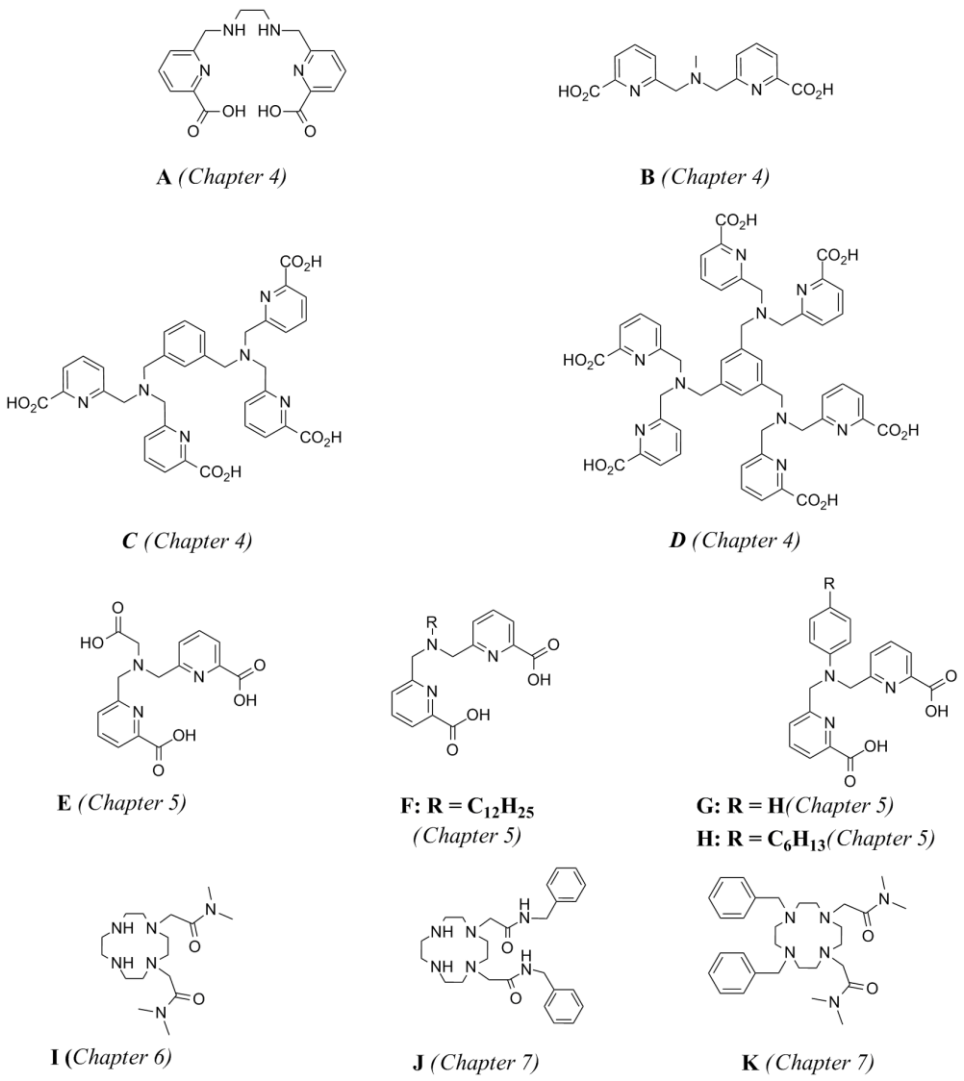

Scheme 1. Structures of the ligands shown in Figure 1.

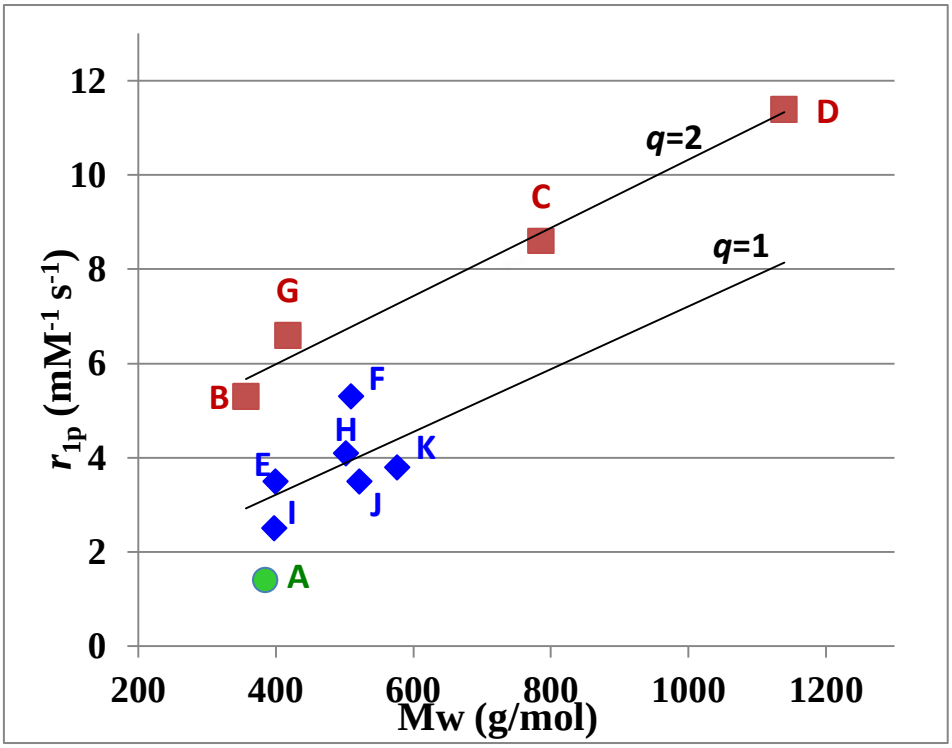

Figure 1. r_{1p} values at 25 °C of the investigated Mn(II)-complexes as a function of their molecular weight.

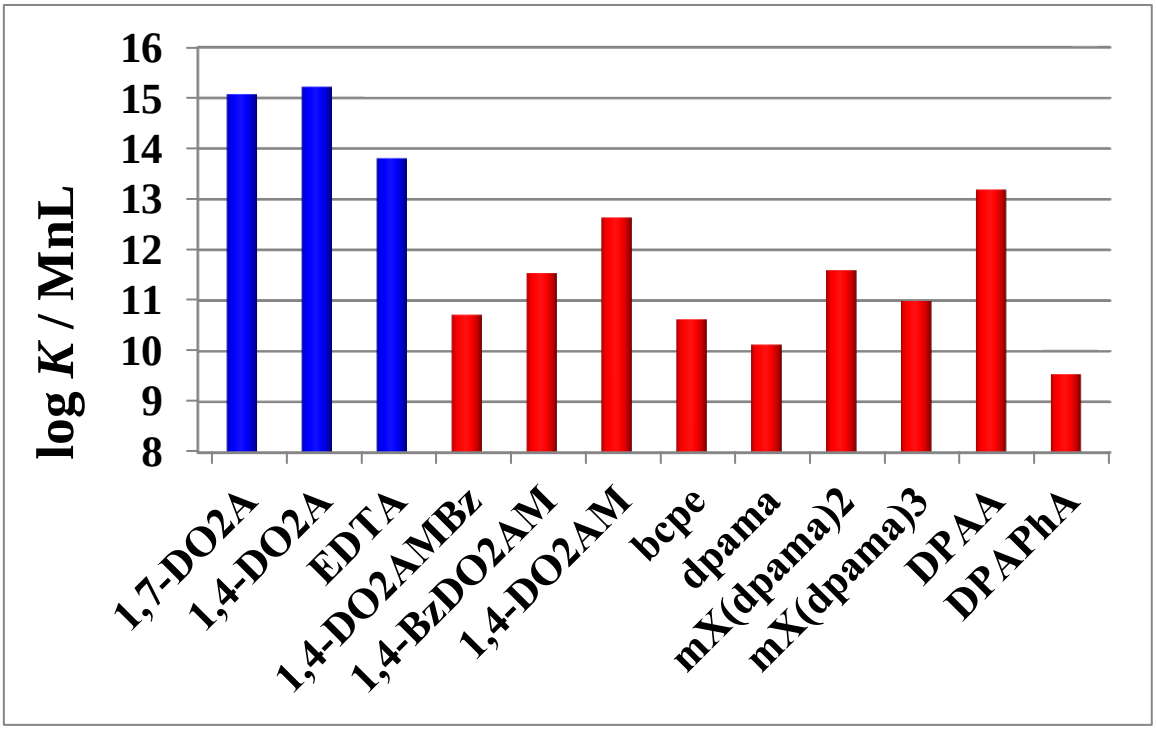

Figure 2. logK_{MnL} values of the complexes investigated during the doctoral thesis.

Acknowledgements:

First of all I would like to thank to Prof. Mauro Botta for his supervision. He invited me back to Italy after I could spent 3 months during my master studies and do my PhD studies at the *Università degli Studi del Piemonte Orientale "Amedeo Avogadro*". I would like to thank his continuous support in my work, his useful advices to solve problems in the lab during the last few years and his help in the adaptation in the new country.

I wish to express my gratitude to Prof. Imre Tóth for the possibility of working in Debrecen. In the „Rare-earth" research group I sincerely thank to Dr. Zsolt Baranyai, who was my "supervisor" during the time what I spent in Debrecen, and he also helped me in the thermodynamic, kinetic studies and also during the phase of writing the thesis.

A special acknowledgement goes to Prof. Carlos Platas-Iglesias, who made the synthesis of the ligands in Chapters 4 and 5, and performed DFT calculations and X-ray diffraction analyses.

I would like to thank also to Prof. Lorenzo Tei, who introduced me to the organic work in the lab, and helped me during the synthesis in my work. I would like to thank also the Dr. Claudio Cassino and Dr. Fabio Carniato for their help in the ^{17}O and ^{1}H-NMR studies.

In the Debrecen group I would like to thank to Katalin Takács for her technical help, and to László Zékány for his help in the dynamic NMR studies, and to everyone else in both groups who helped me to realize my thesis.

List of Publications

1) Attila Forgács, Martín Regueiro-Figueroa, José Luis Barriada, David Esteban-Gómez, Andrés de Blas, Teresa Rodríguez-Blas, Mauro Botta, and Carlos Platas-Iglesias **Mono-, Bi-, and Trinuclear Bis-Hydrated Mn^{2+} Complexes as Potential MRI Contrast Agents**, *Inorg. Chem.*, **2015**, 54, 9576. DOI: 10.1021/acs.inorgchem.5b01677

2) Lorenzo Tei, Zsolt Baranyai, Luca Gaino, Attila Forgács, Adrienn Vágner, Mauro Botta, **Thermodynamic stability, kinetic inertness and relaxometric properties of monoamide derivatives of lanthanide(III) DOTA complexes.** *Dalton Trans.,* **2015**, *44*, 5467. DOI: 10.1039/c4dt03939d

3) Attila. Forgács, Lorenzo. Tei, Zsolt. Baranyai, Imre. Tóth, László. Zékány, Mauro Botta. **Bisamide Derivative of [Mn(1,4-DO2A)]: Solution Thermodynamic, Kinetic and NMR Relaxometric Studies**. *Eur. J. Inorg. Chem.*, **2016**, 1165. DOI: 10.1002/ejic.201501415

4) Zoltán. Garda, Attila. Forgács, Ferenc. Kálmán. Kálmán, Sarolta. Timári, Imre. Tóth, Zsolt. Baranyai, Lorenzo. Tei, Zoltán. Kovács, Gyula. Tircsó**. Physico-chemical properties of Mn^{II} complexes formed with cis- and trans-DO2A: thermodynamic, electrochemical and kinetic studies.** *J. Inorg. Biochem.,* **2016,** 163, 206**.** DOI: 10.1016/j.jinorgbio.2016,07.018.

5) Attila Forgács, Rosa Pujales-Paradela, Martín Regueiro-Figueroa, Laura Valencia, David Esteban-Gómez, Mauro Botta and Carlos Platas-Iglesias **Developing the Family of Picolinate Ligands for Mn^{2+} Complexation,** *Dalton Trans.,* **2017** (accepted)

Oral Presentation:

Attila Forgács, Zsolt Baranyai, Lorenzo Tei, Imre Tóth, Mauro Botta. Solution thermodinamic, kinetic and relaxometric studies of the DO2A-bisamide Mn(II) complex. Hungarian Chemical Society. 49th Complex Chemistry Colloquium. Siófok, Hungary 28 May 2015.

Posters:

1. Attila Forgács, Mauro Botta, Carlos Platas-Iglesias. *Multinuclear NMR Relaxometric Study of Picolinate Containing Mn^{II} Complexes*. XLIII National Congress on Magnetic Resonance, Bari. 22-24 September 2014.
2. Attila Forgács, Lorenzo Tei, Zsolt Baranyai, Tóth Imre, Mauro Botta. *Solution thermodynamic, kinetic and relaxometric studies of the DO2A-bisamide Mn(II) complex*. COST TD1004 Final Annual Meeting, Belgrade, Serbia. 10-11 September 2015.
3. Attila Forgács, Mauro Botta, and Carlos Platas-Iglesias. *Bis-Hydrated Mn^{II} Complexes as MRI probes: a ^{1}H and ^{17}O NMR Study*. XLV National Congress on Magnetic Resonance, Modena. 5-7 September 2016.